Fabrication and Characterization of Carbon Nanotubes on Ceramic and Silicon Substrates for High Temperature Electronic Device Applications

by

Baha Yakupoglu

A dissertation submitted to the Graduate Faculty of
Auburn University
in partial fulfillment of the
requirements for the Degree of
Doctor of Philosophy

Auburn, Alabama
May 5, 2018

Keywords: Carbon Nanotubes, CNTs, Ceramic Substrates, Field Emission, Fowler Nordheim Curves, High Temperature Electronic Applications

Approved by

Hulya Kirkici, Chair, Professor of Electrical & Computer Engineering
Thomas Baginski, Professor Emeritus of Electrical & Computer Engineering
Robert Dean, McWane Endowed Professor of Electrical & Computer Engineering
Bogdan Wilamowski, Professor of Electrical & Computer Engineering
Minseo Park, J T Walter Professor of Physics

Abstract

This dissertation focuses on characterization and fabrication of multi-wall carbon nanotubes (CNTs) by DC plasma sputtering and thermal chemical vapor deposition techniques (CVD) on silicon (Si) and ceramic (Al_2O_3) substrates. CNTs have been attracting interest in research due to their electrical, chemical, and mechanical properties. They are considered as ideal field emission materials due to their high aspect ratio of diameter to length. They also possess excellent thermal conductivity and significantly high field emission stability. In this research we investigated their field emission characteristics by measuring current density vs field strength. We also studied their field emission properties when they are deposited on different substrates. The measurements were taken from room temperatures to 300^{o}C. Furthermore, Fowler-Nordheim plots which are commonly used to describe the quantum mechanical tunneling process, of the fabricated CNTs are investigated in this study.

In this work we have grown selective and non-selective CNTs by using traditional microfabrication technology on silicon and ceramic substrates. Catalyst layers of iron (Fe), tungsten (W), and graphite are deposited onto the substrates using a DC plasma sputtering system. In some cases W is used as the electrical contact of the sample on ceramic. After the metal film deposition, the substrate with the catalyst layers is transferred to the thermal CVD chamber for CNT growth.

One of the driving forces behind using ceramic substrates to synthesize CNTs is to use CNTs in high temperature applications and extreme conditions. Due to the thermal properties of

both CNTs and ceramic, this implementation is very promising for high temperature electronics applications.

In the last chapter of the dissertation, possible CNT applications are discussed. We also included our experimental results of a CNT-based diode, where CNTs act as electron emitters supplying the seed electrons to turn it on and the preliminary results of the diode acting as an RFID tag, to this chapter.

Acknowledgments

I had a great time in Auburn and had an opportunity to work with great faculty, administration, and exceptional circle of friends. They all turned my graduate studies to a productive and fun environment that I will always remember with smiling. I would like to acknowledge all of these very nice and skillful scientists' positive impact on my academic life and personal career.

Fore and foremost, Dr. Hulya Kirkici is not only an advisor to me, but a motherly figure who always supported my work and personal development, and took me a step ahead. I'll always be looking for her inspirational and valuable comments, encouraging influence, and guidance through my career and personal life. My biggest and deepest thanks go to Dr. Hulya Kirkici for being on my side in this journey.

My many thanks also goes to my academic committee members Dr. Thomas Baginski, Dr. Robert Dean, and Dr. Bogdan Wilamowski who not only provided me feedback on my dissertation, but also added their invaluable input and guidance through my research and career during my graduate study. I enjoyed having them as instructors in multiple classes that expanded my knowledge in the technical areas as well. I also am grateful for having Dr. Minseo Park as my outside committee member and also thank him for letting me to use his laboratory and Raman spectroscopy for my characterization experiments.

I express my gratitude to our department chair, Dr. Mark Nelms for believing in me and giving me the opportunity to teach classes as an instructor during my doctoral degree. I am also thankful to Dr. James Groccia for being my teaching mentor and showing me the interactive teaching styles and making it possible for me to create an inclusive learning environment in my classes. I thank Biggio Center namely Dr. Lindsay Doukopoulos and Dr. Diane Boyd for the transformative learning discussions and preparing future faculty classes.

I am deeply thankful to Dr. Michael Miller for teaching me to use SEM, Dr. Wei Zhan for letting me to use his AFM, and Qi Cui for assisting me in AFM measurements. I thank Dr. Michael Bozack for letting me to use his digital optical microscope and profilometer, and Erica Snipes for helping me to use them. I thank Dr. Ming-Kuo Lee for letting me to use his XRF, and Brian Miller for assisting me to use it. I thank Min Khanal and Vahid Mirkhani for teaching me the Origin software and Raman spectroscopy measurements.

I thank my GA supervisor Marcia Boosinger and all the library reference department for their endless support and creating a wonderful work environment. I thank our research group members and all my labmates, officemates, and graduate peers namely Dr. Haitao Zhao, Dr. Huirong Li, Roger Tsai, Michael Jung, Michael Moxley and many others for their involvement, discussion, and friendship. I thank all our departmental staff namely John Tenant, Drew Sellers, Dr. Charles Ellis, William Baugh, Autry May, Linda Allgood, Mary Lloyd, and Laura Pattillo for their support and help with all the laboratory equipment and paperwork.

I thank and convey my deepest gratitude and appreciation to my parents Suheyla and Cevat Yakupoglu, and to my uncle Semih Ozkurtaran for all their unconditional love, support, and

teaching me what is important in this life. I also thank my aunts Suna, Seyhan, and Ayse Ozkurtaran and my grandparents Zekiye and Recep Ozkurtaran, and Rukiye and Tahir Yakupoglu for all their support, prayers, and having my best interest in their hearts during all my life.

Lastly, I thank my wife Funda Yakupoglu. I love you and am very grateful for your patience, commitment and sacrifice during my doctoral studies. Thanks for sharing all the ups and downs and making this journey possible.

Dedication

to my mom, Suheyla
my wife, Funda
and my daughter, Ceyda

Table of Contents

List of Tables

List of Figures

Chapter 1

Introduction

Carbon Nanotubes (CNTs) are the members of the fullerene structural family [1]. One can think of CNTs as graphene sheets of honeycomb network that are rolled over and form a tube shape. They are first discovered by Dr. Iijima in 1991 who was working on ultra-fine particles on an arc-discharge evaporation setup and characterization of these particles with a high resolution electron microscope without air exposure [2]. The first found CNTs were consisted of multi-wall tubes that were structured in concentric style and single-wall carbon nanotubes (SWCNTs) were discovered two years later in 1993 [3]. The simplest multi-wall carbon nanotubes (MWCNTs) consist of only two layers and are called double-wall carbon nanotubes (DWCNTs). Figure 1.1 shows the atomic structure layers of CNTs [4].

The wrapping angle of this honeycomb network structure affect the CNTs density and conductivity that determines if they possess properties as metals or semiconductors [5]. This categorization is described by chiral vectors explained in Chapter 2. Another classification of CNTs is fabrication methods. There are three main techniques to fabricate CNTs namely arc–discharge [6], laser–ablation [7], and chemical vapor deposition (CVD) [8]. Arc–discharge and laser ablation techniques are mainly used to produce SWCNTs and lead purer samples, where CVD is used mainly for MWCNTs and produces CNTs with some defects affecting material properties [9]. Figure 1.2 compares transmission electron microscope (TEM) and atomic force microscope (AFM) pictures of CNTs that are fabricated with arc-discharge and CVD techniques

[10]. Although, CVD method produces those defects, when compared to the other two techniques, it is widely preferred due to the ease of the fabrication steps as well as the capability of bulk size fabrication of CNTs. The cost is also relatively cheap and all these advantages makes it favorable for possible industrial production. There are many assisted techniques for CVD such as thermal CVD, plasma enhanced CVD (PECVD), hot filament CVD, water assisted CVD, radio frequency CVD, microwave CVD, oxygen assisted CVD, and others described in the literature [11].

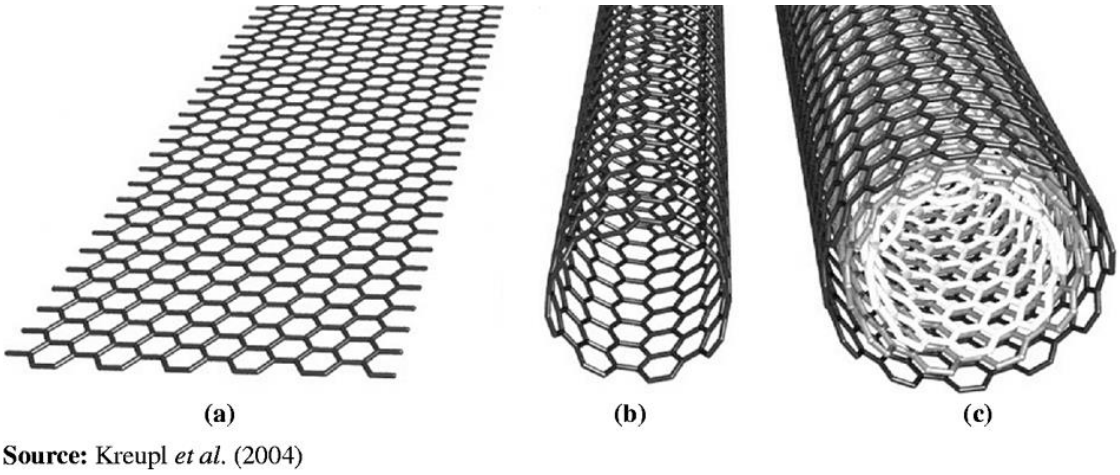

Source: Kreupl *et al.* (2004)

Fig. 1.1 Atomic structure of carbon nanotubes a) Graphite lattice b) Single – walled CNT c) Multi – Walled CNT [4]

The carbon nanotubes market is valued at US$1.6 billion at the end of 2016 and it is expected to have US$6.8 billion value with a 22.1% increase by 2023 [12]. MWCNTs have better thermal conductivity and mechanical strength compared to SWCNTs and have a higher demand in the market due to these characteristics. CNTs can have up to 100 MA/cm^2 current densities [13] and thermal conductivity up to 3000 W/mK [14]. Those unique properties also make CNTs a strong candidate in multiple and wide–range of applications such as field–effect transistors [15], [16],

[17], [18], single electron transistors [19], radar-absorbing coatings, structural composite materials [20], atomic force microscope (AFM) tips [21], biosensors and conductive plastics [22], better lifetime batteries [23], super capacitors [24] and field emitters [25], [26]. Among these, in this study we fabricated a CNT vacuum-diode in-house [27] and demonstrated its operation as a radio frequency identification (RFID) device [28], [29]. CNTs' significant share in electronics market will continue to grow and gradually increase with improved production capacity and lower cost [30].

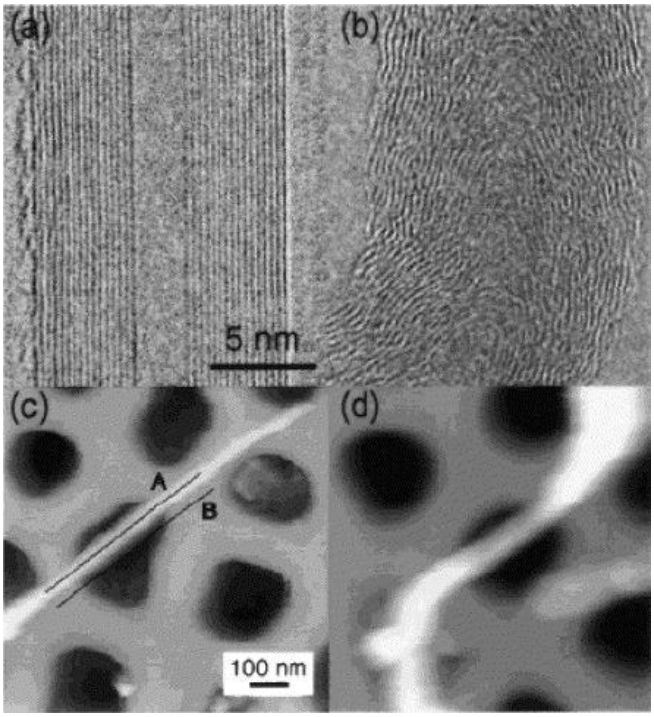

Fig. 1.2 a) arc – discharge MWCNT TEM image b) CVD MWCNT TEM image c) arc – discharge MWCNT AFM image d) CVD MWCNT AFM image [10]

CNTs normally grown on silicon substrates. One of the driving forces to use ceramic as a substrate to grow nanotubes is to use CNTs in high temperature applications and extreme

conditions. Silicon substrates limit the use of CNTs in electronic devices operating in temperatures over ~300^{o}C, because the electronic properties of silicon change significantly at high temperatures [31]. On the other hand, ceramic is an insulator and electrical properties of ceramic remains the same at temperatures up to 2000^{o}C [32]. Furthermore, in thermal CVD process, CNTs are synthesized at 700-800^{o}C, so it's possible to achieve practical and commercial products that operate at high temperatures when CNTs are grown on ceramic substrates. Chapter 2 is a review of CNTs related research in the literature

In this work, we fabricated some of the samples with tungsten under layer and used this under-layer as contact point. Tungsten has always been in high demand as a conductive material in integrated circuit (IC) design and microfabrication due to its unique thermal-expansion coefficient, electro migration and electrical resistance characteristics [33]. Iron is used as the catalyst for CNT growth. We deposited a thin catalyst Fe film on top of the W under layer, when tungsten is used, by DC magnetron sputtering and transferred the samples to thermal CVD chamber. The details of these processes are discussed in Chapter 3. The next chapter discusses CNT structures; electrical, chemical, and mechanical properties; synthesize techniques; and characterization methods in more detail. Both Chapter 3 and Chapter 4 of this dissertation discuss the field emission data and Fowler-Nordheim plots of those samples that are fabricated in our laboratory.

The high temperature field emission testing of the successfully grown CNT samples are conducted at 5x10^{-6} Torr pressure and the temperature is manually controlled and raised up to 300^{o}C by a Kurt J. Lesker M.A.P.S. HTR series temperature controller and power supply. The current values at various voltage points are collected via a Keithley picoammeter and a MATLAB

program is used to record current-voltage data of the samples. The details of the high temperature data experiments are discussed in Chapter 4.

A comparison of field emission test results and Fowler-Nordheim plots of CNTs grown on Si substrates and on ceramic substrates also discussed in Chapter 4. CNT applications, future work, and conclusions are discussed in Chapter 5.

REFERENCES

[1] S. Iijima, "Helical microtubules of graphitic carbon," Nature, vol. 354, pp. 56 – 58, Nov. 1991. doi:10.1038/354056a0

[2] "The Discovery of Carbon Nanotubes - Basle, 22.11.2007", Balzan.org, 2017. [Online]. Available: http://www.balzan.org/en/prizewinners/sumio-iijima/the-discovery-of-carbon-nanotubes-iijima

[3] S. Iijima, "Single-shell carbon nanotubes of 1-nm diameter," Nature, vol. 363, pp. 603 – 605, June 1993. doi: 10.1038/363603a0

[4] Y. S. Duksh, B. K. Kaushik, S. Sarkar, R. Singh, "Performance comparison of carbon nanotube, nickel silicide nanowire and copper VLSI interconnects: Perspectives and challenges ahead", J. of Eng., Design and Technology, vol. 8, no. 3, pp. 334 – 353, 2010.

[5] R. Saito, G. Dresselhaus, M. S. Dresselhaus, Physical properties of carbon nanotubes, World scientific, 1998.

[6] Z. Shi, et al., "Mass-production of single-wall carbon nanotubes by arc discharge method," Carbon, vol. 37, no. 9, pp. 1449 – 1453, 1999.

[7] W. K. Maser, et al., "Production of high-density single-walled nanotube material by a simple laser-ablation method," Chemical Physics Lett., vol. 292, no. 4, pp. 587 – 593, 1998.

[8] G. Che, et al., "Chemical vapor deposition based synthesis of carbon nanotubes and nanofibers using a template method," Chemistry of Materials, vol. 10, no. 1, pp. 260-267, 1998.

[9] J.P. Salvetat, et al., "Elastic modulus of ordered and disordered multi – walled carbon nanotubes," Advanced Materials, vol. 11, no. 2, pp. 161 – 165, 1999.

[10] J.N. Coleman, et al., "Small but strong: A review of the mechanical properties of carbon nanotube-polymer compsites," Carbon, vol. 44, no. 9, pp. 1624-1652, 2006.

[11] J. Prasek, et al., "Methods for carbon nanotubes synthesis-review," J. of Materials Chemistry, vol. 21, no. 40, pp. 15872 – 15884, 2011.

[12] Carbon Nanotubes Market - Global Industry Analysis, Growth, Trends And Forecast 2015–2023; Transparencymarketresearch.com, 2017. [Online]. Available: www.transparency marketresearch.com/carbon-nano-tubes-market.html

[13] B.Q. Wei, R. Vajtai, P.M. Ajayan, "Reliability and current carrying capacity of carbon nanotubes," Appl. Physics Lett., vol. 79, no. 8, pp. 1172 – 1174, 2001.

[14] P. Kim, L. Shi, A. Majumdar, P.L. McEuen, "Thermal transport measurements of individual multi – walled nanotubes," Physical Review Lett., vol. 87, pp. 215502–216606, 2001.

[15] A. Javey, J. Guo, Q. Wang, M. Lundstrom, H. J. Dai, "Ballistic carbon nanotube field – effect transistor," Nature, vol. 424, pp. 654 – 657, 2003.

[16] C. Lu, Q. Fu, S. Huang, and J. Liu, "Polymer Electrolyte – Gated carbon nanotube field – effect transistor," Nano Lett., vol. 4, pp. 623 – 627, 2004.

[17] S. J. Tan, et al., “Individual single wall carbon nanotubes as quantum wires”, Nature (London), vol. 386, pp. 474 – 477, 1997.

[18] M. Bockrath, D. H. Cobden, P. L. Mc Euen, "Individual Single-Wall Carbon Nanotubes As Quantum Wires," Science, vol. 290, pp. 1552-1555, 2000.

[19] S. J. Tans, A. R. M. Verschueren, and C. Dekker, “Room – temperature transistor based on a single carbon nanotube,” Nature (London), vol. 393, pp. 49, 1998.

[20] Z. Fan, et al., "Electromagnetic and microwave absorbing properties of multi-walled carbon nanotubes/polymer composites," Materials Sci. and Eng.: B, vol. 132, no. 1, pp. 85-89, 2006.

[21] H. J. Dai, et al., “Nanotubes as Nanoprobes in scanning probe microscopy,” Nature (London), vol. 384, pp. 147 – 150, 1996.

[22] J. Kong, et al., “Nanotube molecular wires as chemical sensors,” Sci., vol. 287, pp. 622 – 625, 2000.

[23] S. W. Lee, et al., "High-power lithium batteries from functionalized carbon-nanotube electrodes," Nature Nanotechnology vol. 5, no. 7, pp. 531-537, 2010.

[24] W. Lu and L. Dai, Carbon nanotube supercapacitors, INTECH Open Access Publisher, 2010.

[25] W. A. deHeer, A. Chatelain, and D. Ugarte, “A carbon nanotube field – emission electron source,” Sci., vol. 270, pp. 1179 – 1180, 1995.

[26] W. Zhu, C. Bower, G.P. Kochankski, and S. Jin, “Electron field emission from nanostructured diamond and carbon nanotubes,” Solid – State Electronics, vol. 45, pp. 921 – 928, 2001.

[27] B. Yakupoglu and H. Kirkici, "Fabrication and operating characteristics of carbon nanotube diode,″ 2014 IEEE Int. Power Modulator and High Voltage Conf. (IPMHVC), Santa Fe, NM, 2014, pp. 337-339.

[28] B. Yakupoglu, M. Moxley and H. Kirkici, "Characterization and fabrication of carbon nanotubes grown on ceramic substrates for high temperature RFID applications," 2016 IEEE Int. Power Modulator and High Voltage Conf. (IPMHVC), San Francisco, CA, 2016, to be published.

[29] M. Jung, T. Baginski and H. Kirkici, "Test-bed of pulsed radio frequency (RF) signal used with a diode made of carbon nanotubes (CNTs),″ 2014 IEEE Int. Power Modulator and High Voltage Conf. (IPMHVC), Santa Fe, NM, 2014, pp. 599-602.

[30] R. Das, "Carbon Nanotubes (CNT) for Electronics & Electrics 2013-2023: Forecasts, Applications, Technologies", IDTechEx, 2017. [Online] Available: http://www.idtechex.com/ research/reports/carbon-nanotubes-cnt-for-electronics-and-electrics-2013-2023-forecasts-applications-technologies-000342.asp.

[31] P. G. Neudeck, R. S. Okojie and Liang-Yu Chen, "High-temperature electronics - a role for wide bandgap semiconductors?," in *Proceedings of the IEEE*, vol. 90, no. 6, pp. 1065-1076, Jun 2002. doi: 10.1109/JPROC.2002.1021571

[32] J. D. Cressler and H. A. Mantooth, Eds. Extreme environment electronics, CRC Press, 2012.

[33] S. V. Plyushcheva, et al., "Tungsten thin-film deposition on a silicon wafer: The formation of silicides at W-Si interface," Inorganic Materials, vol. 45, no. 2, pp. 140-144, 2009.

Chapter 2

Literature Review

Carbonaceous materials become more important and popular with the developing nanotechnology. Effects of different structures and synthesis methods are widely investigated by research groups. In this chapter, we will discuss the structures and synthesize techniques of CNTs, as well as some purification, characterization, and growth mechanisms that are reported in the literature.

Carbon materials can be found in nature in three different forms of allotropes: diamond, graphite, and fullerene. Diamond is an electrical insulator and a very hard substance with three-dimensional lattice. It is used in a variety of applications from jewelry to cutting tools in natural or lab created forms. It is possible to turn graphite structure to lab created diamond by breaking the strong bonds under extreme high pressures and temperatures around $3000^{O}C$ [1]. Graphite is the most commonly used form of carbon structure and comprises of graphene layers that are consist of six ring-shape C atoms with 120^{O} angle in between on every planar layer [2]. Graphite can also be produced in the lab as well as found in nature in two different shapes: rhombohedral and hexagonal [3]. The rhombohedral form is called beta and the hexagonal one is called alpha, which is used in the lab to create graphite [4]. The last naturally occurred allotropes of carbon are fullerene and carbon nanotubes. Buckminsterfullerene belongs to this family. Fullerenes are a one-dimensional structure and consists of molecular crystals, while diamond and graphite consist of atomistic ones [5]. Figure 2.1 shows the naturally occurring allotropes of Carbon [6].

Buckminsterfullerene is also known as buckyballs due to their circular shape and is formed by 60 carbon atoms, hence the molecular formula is C_{60}. It was discovered in 1985 [7], six years earlier than carbon nanotubes (CNTs) reporting [8], and the research attention to fullerenes has hyperbolically grown since then. Especially, research on CNTs keep getting more attention and continuing worldwide. Figure 2.2 shows this trend with journal and total publication numbers of nanotubes that had been done in the last eight years [9].

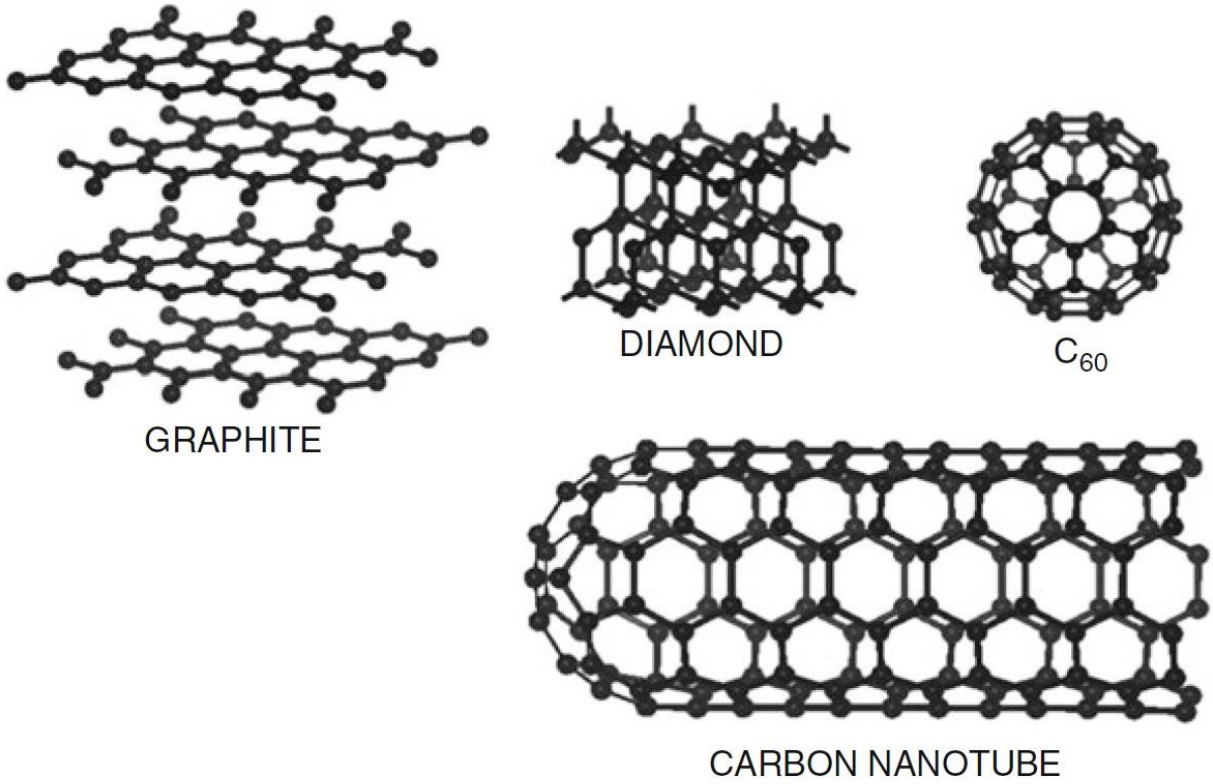

Fig. 2.1 Main carbon allotropes (graphite, diamond, and fullerene) that are naturally occurring and a side view of a defect-free single-wall CNT [6]

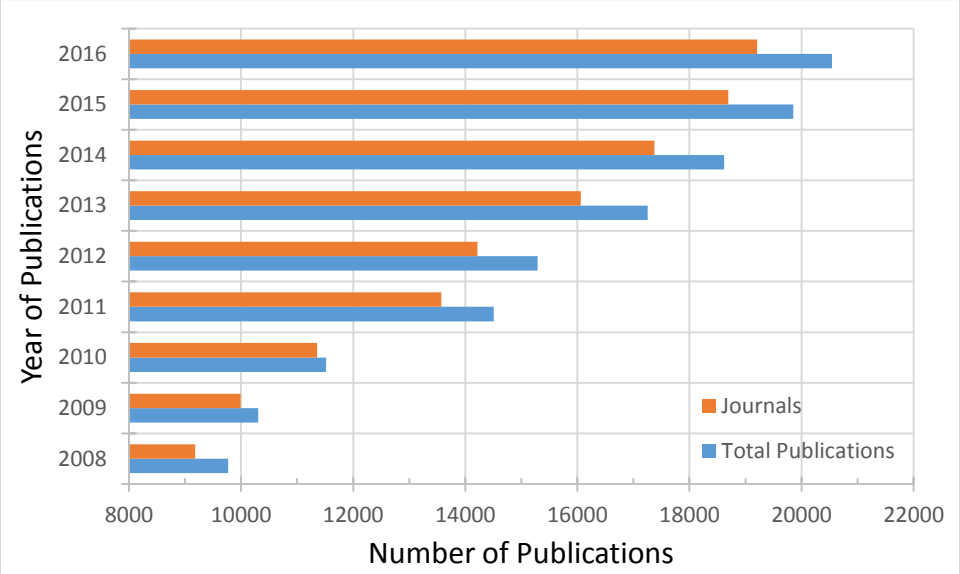

Fig. 2.2 Number of journal and total publications on nanotubes per year.
Graph is generated from WOS (Web of Science) Results Analysis. In the search window, a term of "nanotube" was used.

2.1 CNT Structures

The properties of CNTs can change depending on defects, diameter, and different wrapping angles which are defined as zig-zag, chiral (there are several non-standard forms), and armchair [10]. The wrapping angle can also define if CNTs behave as semiconductor or metallic [11]. The chiral vector defines how CNTs are wrapped, and the equation for chiral vector is $R = na_1 + ma_2$ where n and m stands for integers. The chirality convention should meet the condition of $n \geq |m| \geq 0$, so it can be used to define CNT properties.

Let us start describing the tube axis by drawing two green lines on hexagonal lattice as it is shown in Figure 2.3. A is an arbitrarily chosen point that is on one of the lines. Next step is

drawing the armchair line, which is shown in yellow here. The armchair line is drawn between two green tube axis lines and divides the honeycomb lattice in to two equal halves. The second chosen point on the other green axis tube line is called B. It is the closest point to the yellow armchair line and corresponds to a carbon atom. Our chiral vector R will be the red line that connects point A to point B. The angle between the yellow armchair line and red chiral vector is defined as the wrapping angle and shown as ϕ. If the wrapping angle $\phi = 0^o$, then the chiral vector R is on the yellow armchair line. In this case the tube type is named as armchair. In the situations where the wrapping angle $\phi = 30^o$, the tube type is named zig-zag. For the any other circumstances, $0^0 < \phi < 30^0$, the tube generates a type of chiral form. Here the values of the integers n and m take roles to influence the chirality of the tube that effect the density and the conductivity. The following equation can be used to describe the diameter of the tube with these integers:

$$d = \frac{\vec{R}}{\pi} = \frac{a\sqrt{m^2 + mn + n^2}}{\pi}$$

The wrapping angle, $\emptyset$ can also be written in form of m and n:

$$\cos\phi = \frac{\vec{R}\vec{a}_1}{\left|\vec{R}\right|\left|\vec{a}_1\right|} = \frac{2n + m}{2\sqrt{m^2 + mn + n^2}}$$

The effects of m and n integers are also used to classify the tubes as metallic and semiconducting. If the difference between n and m is an integer, when it is divided by 3, then the tubes are expected to act as metallic (if $\frac{n-m}{3}$ = integer then CNTus metallic) for other situations CNTs are considered as semiconducting. Hence, it is safe to say that the formed tubes could be expected to act as 2/3 semiconducting and 1/3 metallic no matter what random values n and m have [12].

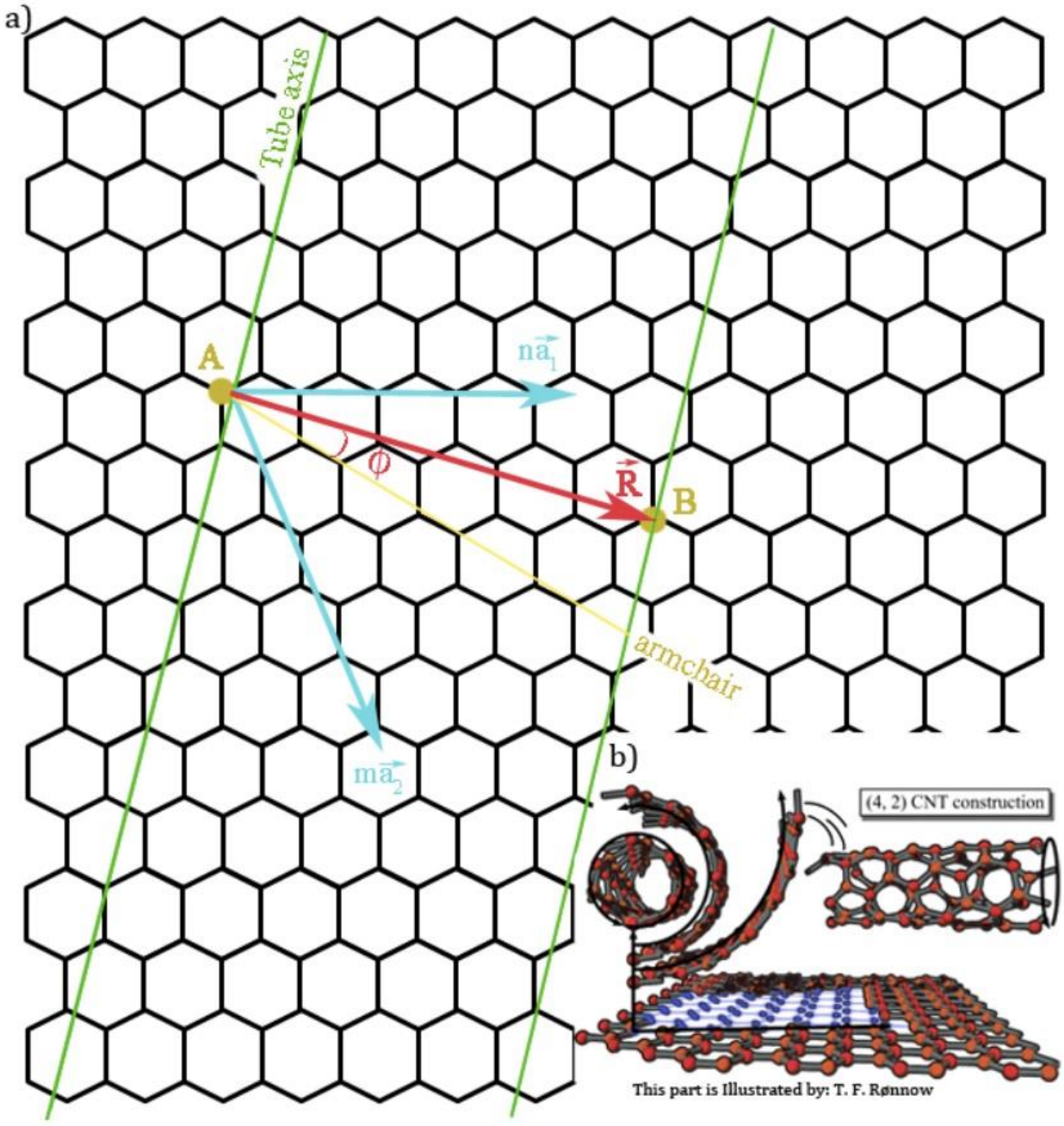

Fig. 2.3 a) A two-dimensional honeycomb lattice two show different types of tubules can be formed, and defined by chiral vectors [13] b) An example of (4,2) CNT construction [14]

2.2 CNT Properties

The unique electrical, mechanical, and chemical properties that has been revealed by multiple research groups are one of the main reasons of the increased CNT experiments and publications as mentioned above and hence the efforts to implement CNTs to current and future applications. We will be reviewing these three main properties below with some of the techniques that has been used to characterize the tubes.

2.2.1 Electrical Properties

There are multiple techniques and purification methods to determine and characterize CNTs' electrical properties. The most prominent electrical features of the tubes are resistivity and conductivity. MWCNT resistivity reported in the literature spans from 5.1×10^{-6} Ω-cm to 1.2×10^{-4} Ω-cm [13]. We also measured our in-house fabricated MWCNTs's surface resistivity and reported it in the following chapters of this dissertation. SWCNT resistivity that is reported in the literature is from 0.34×10^{-6} Ω-cm to 1×10^{-6} Ω-cm [14]. These measurements are conducted using four-point probe technique. The other popular techniques used for determining the properties of CNTs are electron spin resonance (ESR) [15], X-Ray diffraction (XRD) [16], X-Ray photoelectron spectroscopy (XPS) [17], atomic force microscopy (AFM) [18], scanning tunneling microscopy (STM) [19], electron energy loss spectroscopy (EELS) [20], and Raman spectroscopy [21].

2.2.2 Chemical Properties

CNTs are very low reactive materials chemically, but since we are focusing on some high temperature data and possible applications in this dissertation, it should be noted that oxidation is considerably effective on CNTs over high temperatures about $750^{O}C$ [23]. Oxidation starts from the tips of CNTs and when MWCNTs are considered, it goes from the outside layers to the inner layers step by step. Different oxide groups that changes CNT tips and diameter, could also be used to change properties, openings, and etc. of CNTs [23].

Cancer therapy [24] and drug delivery [25], as well as biosensors [26] and DNA detection [27] are the other popular areas that uses CNTs due to their chemical inertness, non-covalent force molecular absorption, and ultra-sensitivity levels. Moreover, the most recent studies focuses on solar-cell implementation of CNTs, since they are one of the synthesizable darkest materials [28].

2.2.3 Mechanical Properties

CNTs mechanical properties are calculated and compared with the other materials in terms of Young's modulus [29], tensile strength [30], and density [31]. MWCNTs have higher Young's modulus than SWCNTs as expected due to the multiple graphene layers and numbers of Van der Walls forces [32]. The famous saying of "Ten times stronger than steel" for CNTs also comes from Young's modulus calculations since the average value of CNTs are calculated as 1.8 TPa where the steels' modulus is 0.186 TPa [33]. Table 2.2.1 compares the MWCNT and SWCNT Young's modulus, tensile strength, and density with the other materials [34].

Material	Young's Modulus (GPa)	Tensile Strength (GPa)	Density (g/cm^3)
MWCNT	1200	150	2.6
SWCNT	1054	150	1.3
SWCNT Bundle	563	150	1.3
Graphite (in – plane)	350	2.5	2.6
Steel	208	0.4	7.8
Epoxy	3.5	0.005	1.25
Wood	16	0.008	0.6

Table 2.2.1 MWCNT, SWCNT, and the other materials comparison in terms of Young's modulus, tensile strength, and density [34]

2.2.4 Characterization of CNTs

Figure 2.4 shows an example of Raman spectroscopy results of in-house grown MWCNT samples gathered by ion laser excitation at two different wavelengths: 514 nm visible and 785 nm near infrared, respectively. The silicon, D, G, and G' lines can easily be observed in the figure, which shows the characteristic features of the tubes. Metallic tubes tend to have an asymmetric and wider G' lines, while semiconducting ones yield to sharper and narrower G' lines [22]. We can say that our samples carry semiconducting properties looking to G and G' lines from Figure 2.4. Also, it can be said that the second sample has more defects than the first one looking to the intensity of D line over the intensity of G line ratio (I_D/I_G). The more detailed analysis of Raman spectroscopy characterization on CNT samples is given in Chapter 3.

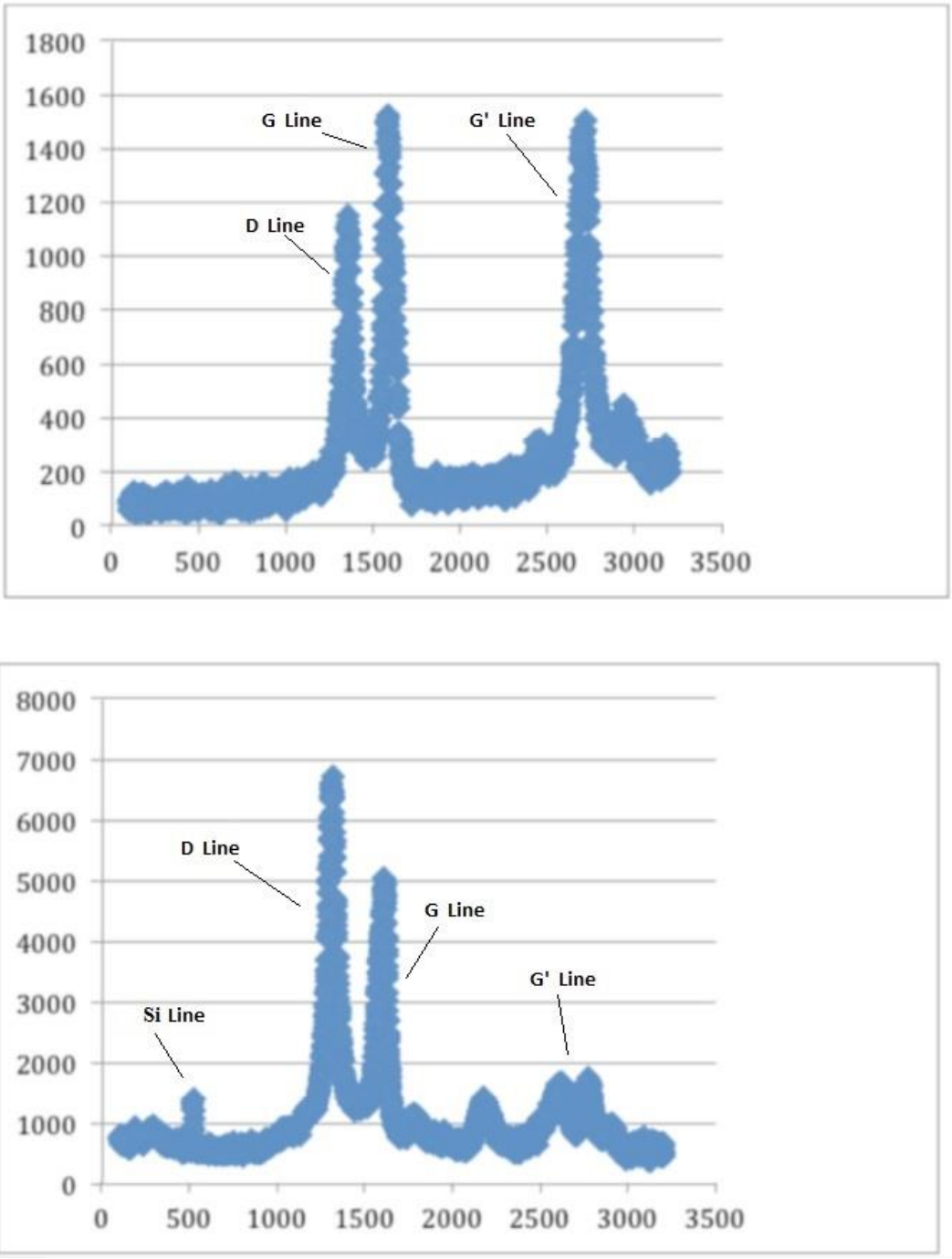

Fig. 2.4 Raman spectroscopy of a MWCNT samples at 514 nm visible (above) and 785 nm near infrared (below) wavelengths (the MWCNT samples are grown on Si substrate by thermal CVD technique with sputtered Fe and C thin film layers)

2.3 Synthesis Techniques of CNTs

There are many methods to synthesize CNTs and only the three main ones are reviewed in this work. We also discuss the advantages and disadvantages of these three main synthesis methods namely arc-discharge, laser ablation, and chemical vapor deposition.

2.3.1 Arc-Discharge Method

Arc-discharge is the method that has been used by Iijima to produce single wall nanotubes in 1991 with CH_4 and Ar gases and iron-graphite electrodes [35]. CNTs are formed with arc vaporization between two graphite rods, which are acting as an anode and a cathode. They are placed end-to-end and usually separated by and stabilized at ~1 mm [36]. The CNT quality and structure depend on the gas pressure (~500 Torr, inert gases like argon, helium are used during the process), deposit temperature (usually it is very high about 3000-4000 K) of the electrode [37], and the plasma uniformity. Arc discharge is an expensive method for CNT fabrication since it needs high purity graphite electrodes and Helium or Argon gases. Figure 2.5 shows an example of an arc-discharge apparatus schematic and a picture that is taken during the experiment [38].

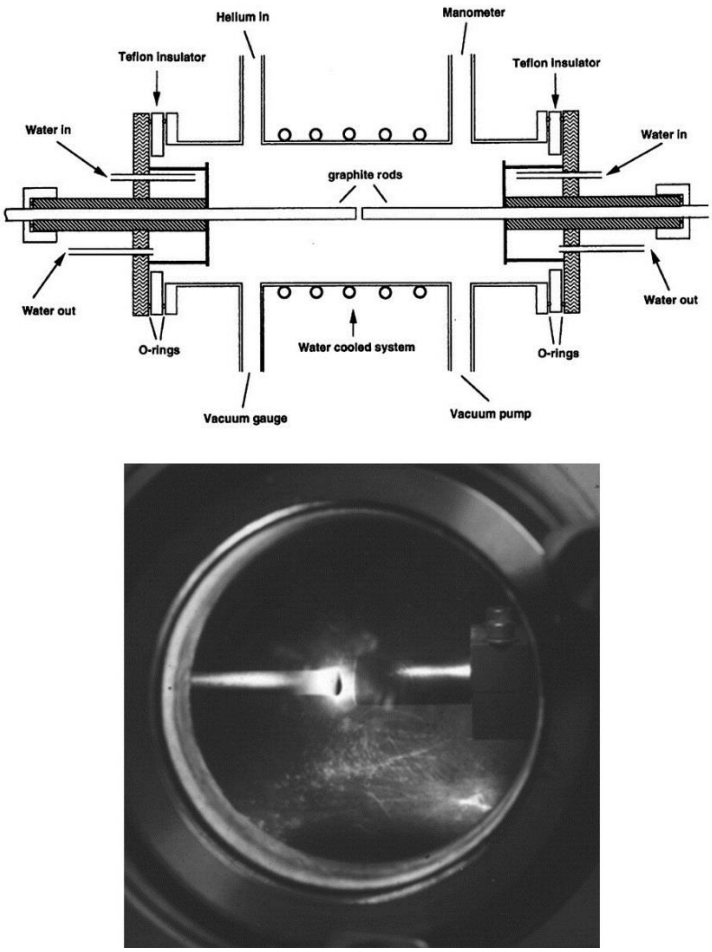

Fig. 2.5 Above is the arc discharge apparatus schematic for CNT and fullerene production and below is an image of the rods and in between that is taken during the experiment (courtesy of P. Redlich) [38]

2.3.2 Laser Ablation Method

It is also possible to synthesize pure and high quality CNTs with laser ablation method, which uses carbon target vaporization technique. The similarities with arc-discharge are the inert gas pressure, the target material structure (nickel and cobalt that frequently used as catalyst materials), and the temperature. Moreover, fabricated CNTs are also effected with the laser

properties [39]. Laser ablation method is first used by Smalley et al to synthesize CNTs and produce fullerene [40]. Different than the arc-discharge technique, the laser beam (mostly YAG or CO_2 lasers are used) provides the energy to hit the graphite target that is located in the oven. Then, inert gas (mostly high-temperature Ar buffer gas) flow helps the synthesized CNTs to pass the quartz chamber in order to be collected on the cold finger-copper collector side. One of the advantages of laser ablation technique is high quality production of SWCNTs with diameter control ability by changing the temperature (an increased temperature yields single-walled tubes with larger diameters) [41], flow rate [42], catalyst materials [43], and/or laser power (an increased laser power yields single-walled tubes with smaller diameters) [44]. The biggest disadvantage of this technique is being not economical. Laser ablation needs high quality graphite rods and the laser source needs high power. Furthermore, CNT production yield is not as higher as CVD and some other techniques. Figure 2.6 shows the schematic of laser ablation technique [45].

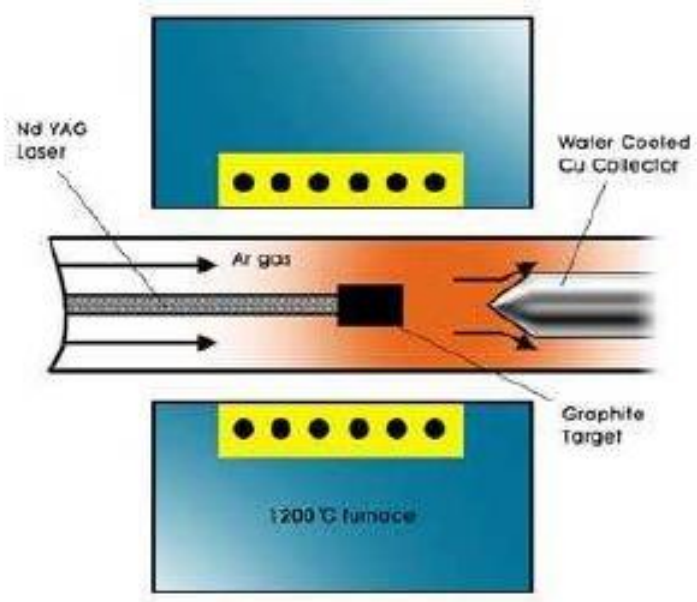

Fig. 2.6 Schematic of laser ablation technique [45]

2.3.3 Chemical Vapor Deposition Method

Chemical vapor deposition technique is the most commonly used method to synthesize CNTs and is commercially available for large-scale fabrication of both SWCNTs [46] and MWCNTs [47]. CVD is popular due to the easier control of the growth parameters, relatively less expensive than the other techniques, and most importantly the possibility of the bulk fabrication of CNTs [48]. There are four main parameters that effect CNT growth in CVD method: catalyst type and preparation (most commonly used transition metals are iron, nickel, and cobalt) [49], carbon source (hydrocarbons such as acetylene, methane, ethylene, propylene etc.), pressure, and temperature of the gas (where 500^{o}C to 900^{o}C results with multi-wall tubes and 900^{o}C to 1200^{o}C results with single wall tubes) [50], [51]. Catalyst type, preparation and the thickness have significant influence on the growth. Most commonly, Iron (Fe) is used as catalyst, but some studies used transition metal alloys and got 10 to 100 times denser SWCNTs than using pure Fe as the catalyst [52]. When catalyst is deposited on the surface of the substrate, a thin film of metallic layer is formed. This film in reality is composed of metallic islands [53] that are referred as particles. Some other studies found that it is possible to control the CNT diameter with catalyst particle size [54], and lastly some others showed that although large size catalyst particles yield MWCNTs, too large catalyst particles could end up with filaments and carbon fibers [55].

Figure 2.7 shows a thermal catalytic CVD schematic diagram [56]. The other common but not limited to CVD methods are hot filament, water assisted, and oxygen assisted CVDs. Thermal catalytic CVD method is the one we used in order to fabricate our samples in this dissertation. Thermal CVD uses pyrolysis of carbon gases with reaching to desired synthesis temperature by using conventional heat sources. Infrared lambs, resistive and/or inductive filaments can be used as heat sources. Our chamber consists of a 2 inches diameter quartz tube and is capable of going

up to 1200°C. We used acetylene (C_2H_2) as the gaseous hydrocarbon and Ar as the buffer inert gas. Experiments ran for this dissertation took place at 700°C and 70 Torr pressure. Further details of our CVD growth process are given in the next chapter of this dissertation.

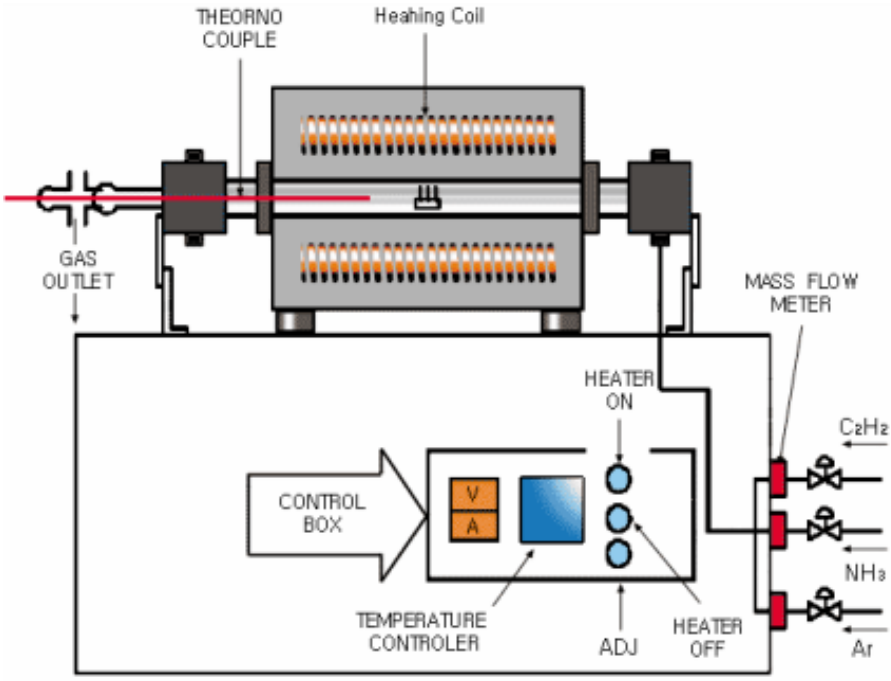

Fig. 2.7 Thermal CVD schematic diagrams to growth CNTs [56]

2.3.4 Plasma Enhanced Chemical Vapor Deposition Method

In plasma-enhanced chemical vapor deposition (PECVD) technique, a high voltage and/or high frequency is applied to both electrodes and plasma is formed. Since plasma source provide the necessary energy for the reaction, high temperature is not necessary as in thermal CVD method. Hence, MWCNTs could be grown at much lower temperatures [57]. PECVD methods (especially DC PECVD) allow extremely dense vertically aligned CNTs, because a local electric field could be generated, perpendicular to the substrate, between the substrate holder and the plasma source [58] resulting in vertically aligned CNTs. The other common PECVD methods that could be used

for CNT growth are RF PECVD [59], [60], microwave PECVD [61], and inductively coupled PECVD [62].

In order to maintain the plasma discharge, it is important to keep the distance (d) between the two parallel electrodes and the chamber pressure (P) at a constant value. Another parameter that is important to keep stable is the substrate temperature due to the nucleation density increment at varying temperatures [63]. A separate heater could be beneficial to maintain the desired temperature for this reason. The pressure of the chamber is usually kept between 1 – 20 mTorr [64] and hydrocarbon gases (methane, ethylene, acetylene, ethane etc.) are introduced to the chamber from the parallel plate electrode next to the one that is holding the substrate.

In short, the low temperature production and vertical growth abilities make PECVD methods the desirable mechanisms for semiconductor and the other device applications at industrial level. Figure 2.8 shows an RF PECVD schematic diagram to growth CNTs [65].

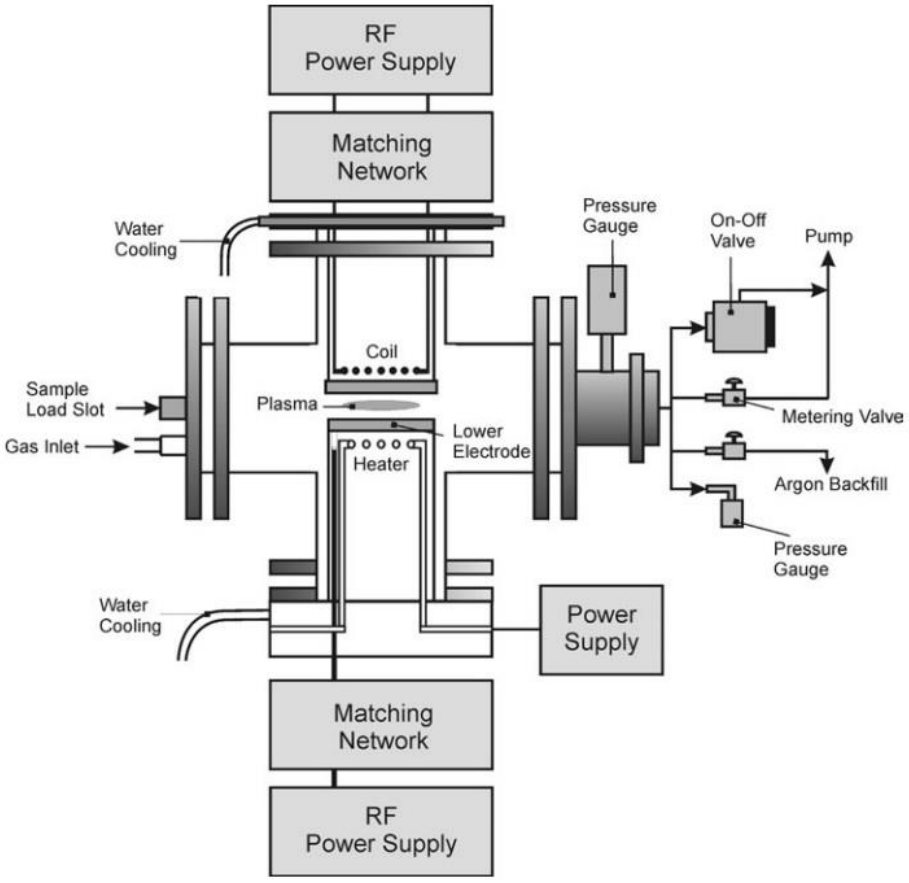

Fig. 2.8 RF PECVD schematic diagrams to growth CNTs [65]

2.4 CNT Growth Mechanism

CNT growth models and mechanisms have been a widely discussed topic since the discovery of CNTs in the literature. Although, multiple different and contradicting growth mechanisms are reported, the common agreement is settled on two namely tip-growth mechanism [66] and base-growth mechanism [66]. CNT growth depends on multiple parameters such as carbon source, catalyst type, catalyst deposition time and/or thin-film thickness, hydrocarbon gas flow rate, pressure, oven temperature, and others. The tip-growth occurs when the catalyst and the substrate interaction is weak. When the substrate material interacting weakly with the carbon

source, CNTs grow out from the substrate pushing the whole metal particle out and growth continues as long as the metal top can react with the carbon source and carbon decomposition happens. CNT growth stops once the metal particle is fully covered with carbon and the carbon decomposition with the metal particle no longer happens. This is called tip-growth mechanism and shown in Figure 2.9 (a) [66]. On the other hand, based-growth occurs when the catalyst and the substrate interaction is strong. In this case, carbon atoms cannot push the metal particle and reaches out as a smooth and continuous graphitic cylinder, forming CNTs. The carbon decomposition happens at the rooted metal particle dome as long as it's covered with carbon likewise to the tip-growth. This is called based-growth mechanism and shown in Figure 2.9 (b) [66].

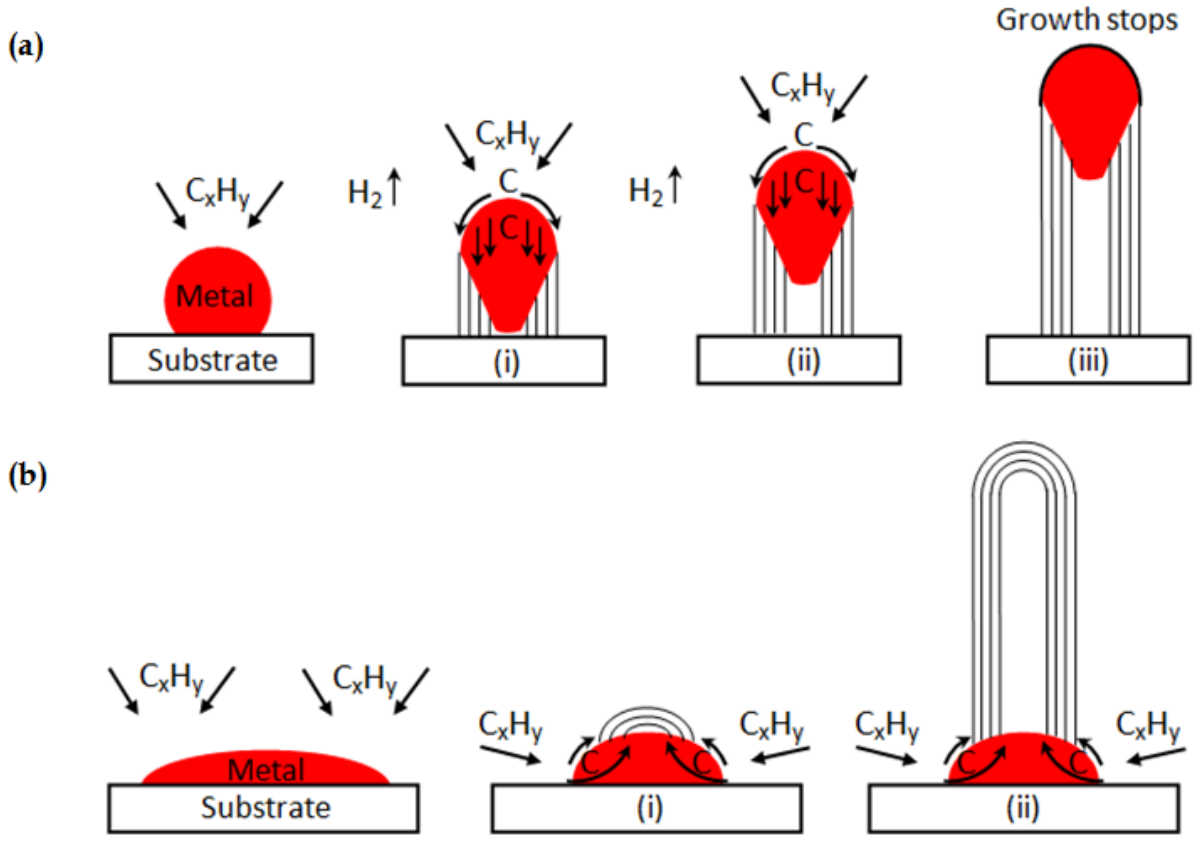

Fig. 2.9 CNT a) tip – growth and b) based – growth mechanisms [66]

2.5 CNT Control and Purification Methods

There are multiple control mechanisms over CNT structure, length, and electronic character. While it is possible to have a controlled growth of CNTs for desired properties, there are also multiple post synthesis separation methods that eliminates or filters out the “unwanted” tubes to have purified CNTs [67]. Table 2.5.1 shows a summary of these mechanisms that are used to control and separate CNTs by structure, length, and chirality [67].

Chromatographic Methods	*Structural Variable*	*Precision*	*Scalability*
Size Exclusion Chromatography	Length	Poor	Poor
High Performance Liquid Chromatography	Length	Poor	Poor
Gel Permeation Chromatography	Length	Poor	Poor
Ion Exchange Chromatography	Diameter	Poor	Poor
Electrophoretic Methods			
Capillary Electrophoresis	Metallicity Length	Good Poor	Average Poor
Alternating Current Dielectrophoresis	Metallicity	Good	Average
Gel Electrophoresis	Metallicity Length Diameter	Good Poor Poor	Poor Poor Poor
Dielectrophoresis Field Flow Fractionation	Metallicity Diameter	Good Poor	Average Average
Fluid-based Methods			
Flow Field Fractionation	Length	Poor	Average
Nematic Liquid Crystal Extraction	Length	Poor	Average
Dielectrophoresis Field Flow Fractionation	Metallicity Diameter	Good Poor	Average Average
Destructive Methods			
Current-induced Oxidation	Metallicity	Good	Poor
Fluorination and Annealing	Metallicity	Good	Good
Chemical Methods			
Amino Acid/Amine Adsorption	Metallicity	Good	Good
Photoelectrochemistry	Metallicity	Good	Average
Density-Gradient Ultracentrifugation	Metallicity Diameter	Good Average	Average Average
Other Methods			
Phase Transfer Catalysis	Length	Poor	Average
Synthesis Variables			
Catalyst Particle Size	Diameter	Good	Good
Carbon Feed Rate	Diameter	Average	Average
Seeded Growth	Chirality	Unknown	Unknown
Specific Processes	Metallicity Chirality	Average Average	Good Good

Table 2.5.1 CNT control and post synthesis purification methods [67]

REFERENCES

[1] H. O. Pierson, “Handbook of carbon, diamond, and fullerenes,” William Andrew Publishing, Norwich, 1993.

[2] A. A. El-Barbary, R. H. Telling, C.P. Ewels, M.I. Heggie, P.R. Briddon, “Structure and energetics of the vacancy in graphite,” Phys. Rev. B, vol. 68, no. 14 pp. 144107 – 144114, 2003. doi: 10.1103/PhysRevB.68.144107

[3] B. Simon, S. Flandrois, A. Fevrier – Bouvier, P. Biensan, “Hexagonal vs Rhombohedral Graphite: the Effect of Crystal Structure on Electrochemical Intercalation of Lithium Ions,” Molecular Crystals and Liquid Crystals, vol. 310, no. 1, pp. 333 – 340, 1998.

[4] R. F. Davis, G. Kelner, M. Shur, J. W. Palmour and J. A. Edmond, "Thin film deposition and microelectronic and optoelectronic device fabrication and characterization in monocrystalline alpha and beta silicon carbide," in *Proceedings of the IEEE*, vol. 79, no. 5, pp. 677-701, May 1991. doi: 10.1109/5.90132

[5] M.S. Dresselhaus, G. Dresselhaus, P.C. Eklund, “Science of fullerenes and carbon nanotubes,” Academic Press, 1996.

[6] K. Koziol, B.O. Boskovic, N. Yahya, “Synthesis of Carbon Nanostructures by CVD Method. In: Carbon and Oxide Nanostructures,” Advanced Structured Materials, vol 5. Springer, Berlin, Heidelberg, 2010. doi: 10.1007/8611_2010_12

[7] H.W. Kroto, J.R. Heath, S.C. O’Brien, R.F. Curl, R.E. Smalley, “C_{60}: Buckminsterfullerene,” Nature, vol. 318, pp. 162 – 163, 1985. doi: 10.1038/318162a0

[8] S. Iijima, "Helical microtubules of graphitic carbon,” Nature, vol. 354, pp. 56 – 58, Nov. 1991. doi:10.1038/354056a0

[9] Number of journal and total publications on nanotubes per year. Source: WOS (Web of Science) Results Analysis. In the search window, a term of “nanotube” was used.

[10] M.S. Dresselhaus, P. Avouris, “Introduction to Carbon Materials Research. In: Dresselhaus M.S., Dresselhaus G., Avouris P. (eds) Carbon Nanotubes,” Topics in Applied Physics, vol 80, Springer, Berlin, Heidelberg, 2001. doi: 10.1007/3-540-39947-X_1

[11] W.G. Jeroen Wildoer et al. "Electronic Structure of Atomically Resolved Carbon Nanotubes." *Nature* vol. 391.6662, pp. 59-62. 1998

[12] S. Banerjee, T. Hemraj-Benny, S.S. Wong, “Routes Towards Separating Metallic and Semiconducting Nanotubes,” Journal of Nanoscience and Nanotechnology, vol. 5, no. 6, pp. 841 – 855, June 2005.

[13] T. W. Ebbesen, H. Lezec, H. Hiura, J. W. Bennett, H. F. Ghaemi, and T. Thio, “Electrical conductivity of individual carbon nanotubes”, Nature, 382, 54, 1996.

[14] H. S. Nalwa, (ed.), “Handbook of nanostructured materials and nanotechnology”, Academic Press, vol. 5, 2000.

[15] M. Kosaka, T. W. Ebbesen, H. Hiura, K. Tanigaki, “Electron spin resonance of carbon nanotubes”, Chemical Physics Lett., vol. 225, no. 1–3, pp. 161-164, 1994. ISSN 0009-2614, https://doi.org/10.1016/0009-2614(94)00641-5.

[16] H. Yusa, T. Watanuki, "X-ray diffraction of multiwalled carbon nanotube under high pressure: Structural durability on static compression", Carbon, vol. 43, no. 3, pp. 519-523, 2005. ISSN 0008-6223, https://doi.org/10.1016/j.carbon.2004.10.011.

[17] M. Varga et al., "Diamond/carbon nanotube composites: Raman, FTIR and XPS spectroscopic studies," Carbon, vol. 111, pp. 54-61, 2017. ISSN 0008-6223, https://doi.org/10.1016/j.carbon.2016.09.064.

[18] K.Safarova, A. Dvorak, R. Kubinek, M. Vujtek, A. Rek, "Usage of AFM, SEM, and TEM for the research of carbon nanotubes," Modern Research and Educational Topics in Microscopy, FORMATEX 2007.

[19] L. P. Biro et al., "Scanning tunneling microscope investigation of carbon nanotubes produced by catalytic decomposition of acetylene", Physical Review B, vol. 56, no.19, 1997.

[20] R. Kuzuo, M. Terauchi, and M. Tanaka, "Electron Energy-Loss Spectra of Carbon Nanotubes," Japanese J. of Appl. Phys., vol. 31, no. 10B, 1992.

[21] M.S. Dresselhaus, G. Dressehaus, R. Saito, and A. Jorio. "Raman spectroscopy of carbon nanotubes", Physics Reports, vol. 409, no. 2, pp. 47 – 100, 2004.

[22] A. Aqel, K. M. M. A. El-Nour, R. A.A. Ammar, A. Al-Warthan, "Carbon nanotubes, science and technology part (I) structure, synthesis and characterisation," Arabian J. of Chemistry, vol.5, no. 1, pp. 1-23, 2012. ISSN 1878-5352, https://doi.org/10.1016/j.arabjc.2010.08.022.

[23] H. Hiura, T. W. Ebbesen, K. Tanigaki, "Opening and purification of carbon nanotubes in high yields," Adv. Materials, vol. 7, pp. 275, 1995.

[24] H. TA, and J. Hill, "Modeling the Loading and Unloading of Drugs into nanotubes", Small, vol. 5, pp. 300-08, 2009.

[25] N. W. S. Kam, M. O'Connell, J. A. Wisdom, H. Dai, "Carbon Nanotubes as multifunctional biological transporters and near-infrared agents for selective cancer cell destruction," PNAS, vol. 102, pp. 11600, 2005.

[26] H. Muguruma, Y. Matsui, Y. Shibayama, "Carbon nanotube plasma polymer-based amperometric biosensors: Enzyme friendly platform for ultrasensitive glucose detection," Japanese J. of Appl. Physics, vol. 46, no. 9A, pp. 6078, 2007.

[27] J. Clendenin, J. Kim, S. Tung, "An aligned carbon nanotube biosensor for DNA detection", Proc of 2007 2nd IEEE Conference on Nanotechnology, pp. 1028, 2007.

[28] S. N. Habisreutinger, T. Leijtens, G. E. Eperon, S. D. Stranks, R. J. Nicholas, and H. J. Snaith, "Carbon Nanotube/Polymer Composites as a Highly Stable Hole Collection Layer in Perovskite Solar Cells," Nano Lett., vol. 14, no. 10, pp. 5561 – 5568, 2014. doi: 10.1021/nl501982b

[29] M. Yu, O. Lourie, M.J. Dyer, T.F. Kelly, R.S. Ruoff "Strength and breaking mechanism of multiwalled carbon nanotubes under tensile load," Science, vol.287, pp. 637–640, 2000.

[30] J.P. Salvetat et al., "Elastic and shear moduli of single-walled carbon nanotube ropes," Phys. Rev. Lett., vol.82, no.5, pp. 944–947, 1999.

[31] J. A. Kim, D. G. Seong, T. J. Kang, J. R. Youn, “Effects of surface modification on rheological and mechanical properties of CNT/epoxy composites”, Carbon, vol. 44, no. 10, pp. 1898-1905, 2006. ISSN 0008-6223, doi:10.1016/j.carbon.2006.02.026.

[32] A. J. Cheng, “Cold Cathodes for Applications in Poor Vacuum and Low Pressure Gas Environments: Carbon Nanotubes vs. Zinc Oxide Nano needles”, Master Thesis, Auburn University, 2006.

[33] A.B. Dalton et al., “Super – tough carbon – nanotube fibres,” Nature, vol. 423, pp. 703, June 2003. doi: 10.1038/423703a

[34] A. Thess, R. Lee, P. Nikolaev, H. Dai, P. Petit, J. Robert, C. Xu, Y.H. Lee, S.G. Kim, A.G. Rinzler, D.T. Colbert, G.E. Scuseria, D. Tomanek, J.E. Fischer, and R.E. Smalley, “Crystalline Ropes of Metallic Carbon Nanotubes,” Science, vol. 273, pp. 483, 1996.

[35] S. Iijima, "Helical microtubules of graphitic carbon,” Nature, vol. 354, pp. 56 – 58, Nov. 1991. doi:10.1038/354056a0

[36] T.W. Ebbesen, “Carbon nanotubes,” Physics Today, vol. 49, no. 6, pp. 26, 1996. doi: 10.1063/1.881603

[37] M Terrones, “Science and technology of the twenty-first century: Synthesis, Properties and Applications of Carbon Nanotubes,” Annual Rev. Mater. Res., vol. 33, pp. 419–501, 2003.

[38] P. Redlich in M Terrones, “Science and technology of the twenty-first century: Synthesis, Properties and Applications of Carbon Nanotubes,” Annual Rev. Mater. Res., vol. 33, pp. 419–501, 2003.

[39] J. Prasek, J. Drbohlavova, J. Chomoucka, J. Hubalek, O. Jasek, V. Adam, R. Kizek, “Methods for carbon nanotubes synthesis-review,” J. of Materials Chemistry, vol. 21, no. 40, pp. 15872 – 84, 2011.

[40] T. Guo, P. Nikolaev, A. Thess, D. T. Colbert and R. E. Smalley, “Fullerene nanotubes in electric-fields”, Chem. Phys. Lett., vol. 243, pp. 49–54, 1995.

[41] R. Sen, Y. Ohtsuka, T. Ishigaki, D. Kasuya, S. Suzuki, H. Kataura, Y. Achiba, “Time period for the growth of single-wall carbon nanotubes in the laser ablation process: evidence from gas dynamic studies and time resolved imaging,” Chemical Physics Lett., vol. 332, no. 5–6, pp. 467-473, 200. ISSN 0009-2614, doi:10.1016/S0009-2614(00)01320-8.

[42] H Kataura, Y Kumazawa, Y Maniwa, Y Ohtsuka, R Sen, S Suzuki, Y Achiba, “Diameter control of single-walled carbon nanotubes,” Carbon, vol. 38, no. 11, pp. 1691 – 1697, 2000.

[43] Shunji Bandow, S. Asaka, Y. Saito, A. M. Rao, L. Grigorian, E. Richter, and P. C. Eklund, “Effect of the growth temperature on the diameter distribution and chirality of single-wall carbon nanotubes,” Physical Rev. Lett., vol. 80, pp. 3779 – 3782, 1998.

[44] A.C. Dillon, P. A. Parilla, J. L. Alleman, J. D. Perkins, M. J. Heben, “Controlling single-wall nanotube diameters with variation in laser pulse power,” Chemical Phys. Lett. Vol. 316, pp. 13–18, 2000.

[45] M. Daenen, R.D. de Fouw, B. Hamers, P.G.A. Janssen, K. Schouteden, M.A.J. Veld, “The Wondrous World of Carbon Nanotubes,” project, 2003.

[46] Michael J. Bronikowski, Peter A. Willis, Daniel T. Colbert, K. A. Smith, and Richard E. Smalley, "Gas-phase production of carbon single-walled nanotubes from carbon monoxide via the HiPco process: A parametric study," J. of Vacuum Sci. & Tech. A: Vacuum, Surfaces, and Films, vol. 19, pp. 1800 – 1805, 2001. doi: 10.1116/1.1380721

[47] R. Sen, A. Govindaraj, C.N.R. Rao, "Carbon nanotubes by the metallocene route," Chemical Physics Lett., vol. 267, no. 3–4, pp. 276-280, 1997. ISSN 0009-2614, doi:10.1016/S0009-2614(97)00080-8.

[48] K. Behler, S. Osswald, H. Ye, S. Dimovski, Y. Gogotsi, "Effect of Thermal Treatment on the Structure of Multi-walled Carbon Nanotubes," J. of Nanoparticle Research, vol. 8, no. 5, pp. 615 – 625, 2006.

[49] M. Yudasaka, R. Kikuchi, Y. Ohki, S. Yoshimura, "Nitrogen-containing carbon nanotube growth from Ni phthalocyanine by chemical vapor deposition", Carbon, vol. 35, no. 2, pp. 195-201, 1997. ISSN 0008-6223, doi:10.1016/S0008-6223(96)00142-X.

[50] P. Mauron, C. Emmenegger, A. Züttel, C. Nützenadel, P. Sudan, L. Schlapbach, "Synthesis of Oriented Nanotube Films by Chemical Vapor Deposition", Carbon, vol. 40, pp. 1339-1344, 2002.

[51] H.M. Cheng, F. Li, X. Sun, S.D.M. Brown, M.A. Pimenta, A. Marucci, G. Dresselhaus, M.S. Dresselhaus, "Bulk morphology and diameter distribution of single-walled carbon nanotubes synthesized by catalytic decomposition of hydrocarbons", Chemical Physics Lett., vol. 289, no. 5–6, pp. 602-610, 1998. ISSN 0009-2614, doi:10.1016/S0009-2614(98)00479-5.

[52] H. Lee, Y.S. Kang, P.S. Lee, and J. Y. Lee, "Hydrogen storage in Ni nanoparticle – dispersed multi-walled carbon nanotubes," J. of Alloys and Compounds, vol. 330, pp. 569-572, 2005.

[53] H. Zhao, "Design and construction of carbon nanotubes (CNTs) triggered pseudospark switch," Ph.D. dissertation, Dept. Elec. Eng., Auburn Univ., Auburn, AL, 2012.

[54] H. Ago, T. Komatsu, S. Ohshima, Y. Kuriki, M. Yumura, "Dispersion of metal nanoparticles for aligned carbon nanotube arrays," Appl. Physics Lett., vol. 77, no. 1, pp. 79 – 81, 2000.

[55] M.L. Terranova1, V. Sessal, and M. Rossi, "The world of carbon nanotubes: an overview of CVD growth methodologies", Chemical Vapor Deposition, vol. 12, pp. 315–325, 2006.

[56] M. Daenen et al., "The Wondrous World of Carbon Nanotubes: a review of current carbon nanotube technologies," Eindhoven University of Technology. February 2003.

[57] B. O. Boskovic, V. Stolojan, R. U. Khan, S. Haq, S. R. Silva, "Large area synthesis of carbon nanofibres at room temperature," Nat. Mater., vol. 1, no. 3, pp. 165-168, 2002.

[58] V. I. Merkulov, D. H. Lowndes, Y. Y. Wei, and G. Eres, "Patterned growth of individual and multiple vertically aligned carbon nanofibers," Appl. Phys. Lett., vol. 76, pp. 3555, 2000. doi: 10.1063/1.126705

[59] M. Meyyappan, (ed), "Carbon nanotubes science and applications", CRC Press, 2004

[60] Y. H. Wang, J. Lin, C. H. A. Huan, G. S. Chen, "Synthesis of large area aligned carbon nanotube arrays from C_2H_2-H_2 mixture by rf plasma-enhanced chemical vapor deposition," Appl. Physics Lett., vol. 79, no. 5, pp. 680, 2001.

[61] L. C. Qin, D. Zhou, A. R. Krauss, D. M. Gruen, “Growing carbon nanotubes by microwave plasma-enhanced chemical vapor deposition,” Appl. Physics Lett., vol. 72, no. 26, pp. 3437 – 3439, 1998.

[62] J. Li, R. Stevens, L. Delzeit, H. T. Ng, A. Cassell, J. Han, and M. Meyyappan, “Electronic properties of multiwalled carbon nanotubes in an embedded vertical array,” Appl. Physics Lett., vol. 81, pp. 910, 2002. doi: 10.1063/1.1496494

[63] M. Li, D. Liu, D. Wei, X. Song, D. Wei, A. T. S. Wee, “Controllable Synthesis of Graphene by Plasma-Enhanced Chemical Vapor Deposition and Its Related Applications,” Advanced Sci., vol. 3, no. 11, pp. 1600003, November 2016. doi: 10.1002/advs.201600003

[64] J. Xu, T. S. Fisher, “Enhancement of thermal interface materials with carbon nanotube arrays,” Int. J. of Heat and Mass Transfer, vol. 49, no. 9–10, pp. 1658-1666, 2006. ISSN 0017-9310, doi:10.1016/j.ijheatmasstransfer.2005.09.039.

[65] M Meyyappan, Lance Delzeit, Alan Cassell1 and David Hash, “Carbon nanotube growth by PECVD: a review,” Plasma Sources Sci. and Tech., vol. 12, no. 2, pp. 205 – 216, 2003.

[66] M. Kumar, “Carbon Nanotube Synthesis and Growth Mechanism in Carbon Nanotubes - Synthesis, Characterization, Applications," InTech, 2011. ISBN 978-953-307-497-9, doi: 10.5772/19331

[67] M. D. Taczak, “Controlling the structure and properties of carbon nanotubes,” MITRE Corp., the MITRE Nanosystems Group, www.mitre.org/tech/nanotech, 2007.

Chapter 3

Carbon Nanotube Fabrication and Characterization

3.1 Overview

Randomly aligned multi-wall CNTs are synthesized by using thermal CVD technique in this work. Silicon (Si) and pure ceramic (Al_2O_3) are the substrates used for the CNT growth. Standard Clean-1 (RCA-1), HF (Hydrofluoric acid) dip, and/or piranha etch protocol are used to clean the Si substrates. A radio frequency / direct current (RF/DC) sputtering system is used to deposit metal catalyst onto the desired substrate. The sputtering chamber is capable of reaching $5x10^{-6}$ Torr pressure. Although both RF and DC sputtering are feasible for our chamber, only the DC sputtering is utilized due to the choice of the metal target materials. We used <100> orientation n – type Si substrate. In some cases, the substrate has SiO_2 pre-coating on it and/or been treated with heat or by other means. We classified our samples in this work as "untreated", if no treatment is applied to the sample. Tungsten (W), Iron (Fe), and Graphite (C) thin films are deposited as underlayer(s) or catalysts onto the substrates. As it is discussed later in this chapter, we optimized our chamber pressure and sputtering distance (d) accordingly. The distance is defined as the space between the sputtering gun and the sample. It is kept constant at 20 cm for all the experiments. After the sputtering chamber is initially pumped down to 5×10^{-6} T, Ar is introduced to the chamber as the buffer gas to initiate and form the plasma and the chamber pressure is kept constant at 7 mTorr during the metal deposition. The sputtering time is varied depending on the desired thin film thickness of the catalyst material. The substrate with the catalyst layer is transferred to the

thermal CVD chamber after the DC sputtering deposition. Our thermal CVD chamber is made of a 2-inch diameter quartz tube and is capable of reaching 1200^{O}C when heated through the heating elements wrapped around it. We optimized the thermal CVD temperature to 700^{O}C and all the samples in this work are grown at this temperature. The chamber pressure is maintained at 70 Torr after introducing the feed gases to the furnace. Acetylene (C_2H_2) is used as the hydrocarbon gas in our studies. Initially, base pressure of the chamber is established at 10^{-3} Torr using a mechanical pump and feed gases of Ar and C_2H_2 are introduced to the chamber. The flow rates of Ar and C_2H_2 feed gases are controlled by mass flow controllers and 75 sccm / 20 sccm flow rate is maintained for both gasses. After successful synthesis of MWCNTs on the chosen substrates, the samples are moved to the field emission test chambers to investigate their electrical characteristics at the room temperature and/or at the elevated temperatures up to 300^{O}C. The samples are also examined with scanning electron microscopy (SEM), atomic force microscopy (AFM), and Raman Spectroscopy. Field emission test setup and experimental details are further explained in this chapter. Wafer cleaning procedure, patterning and masking of our selectively grown CNT samples, catalyst deposition, CVD growth, field emission, and optimizations are the next sections that are discussed in this chapter, respectively. The high temperatures field emission test results are given in the following chapter.

3.2 Wafer Cleaning and Patterning

The wafers are cleaned with standard procedures Radio Corporation of America (RCA), hydrofluoric acid (HF) dip, or piranha etching. Most of the times, they are dipped to a BOE (buffer oxide etching) solution for couple of minutes to get rid of the impurities and native oxide. A deionized (DI) water rinse followed this step before wafers are sent to a dehydration bake at 120^{O}C

for 20 minutes. In some cases, piranha etch or 5:1:1 protocol is applied before the dehydration bake step. Deionized water, ammonium hydroxide (NH_4OH), and hydrogen peroxide (H_2O_2) mixed in 5:1:1 ratio and the wafers dipped in the solution that is raised to $70^{O}C$ with a hot plate. After 10 minutes a minute of HF dip is applied.

For the patterned CNT growth, wafer is processed as follows. After rinsing and dehydration bake steps as mentioned above, hexamethyldisilazane (HMDS), a surface adhesion promoter, used for 5 minutes as a pre-resist to improve the photoresist stickiness onto the wafer surface. Then, the samples are coated with positive-tone (AZ 5214) photoresist (PR) at 3000 rpm spin speed for 30 seconds and then put on a hot plate for the soft/pre-bake step for 1 minute at $105^{O}C$. The samples are exposed to the UV (ultraviolet) light for 10 seconds under the selected mask to remove the PR from the selected areas and actualize the patterns. The development concentration 2:1 (DI water: AZ400K developer, respectively) is used for 18 seconds. Figure 3.1 shows an in-house 0.5 cm^2 by 0.5 cm^2 square patterned Si wafer sample under yellow lights where the patterns become visible after the development stage. Lastly, 14 seconds plasma exposure applied to the samples to clean the sample surfaces. The samples are ready then for the DC magnetron sputtering system. Figure 3.2 shows the process flow for the patterned samples.

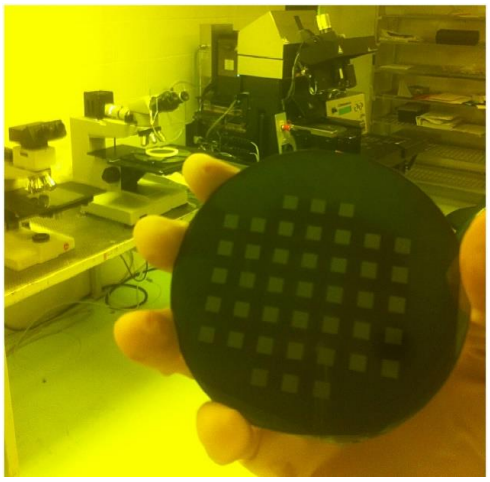

Fig. 3.1 Picture of the in-house patterned Si substrate just after the development step

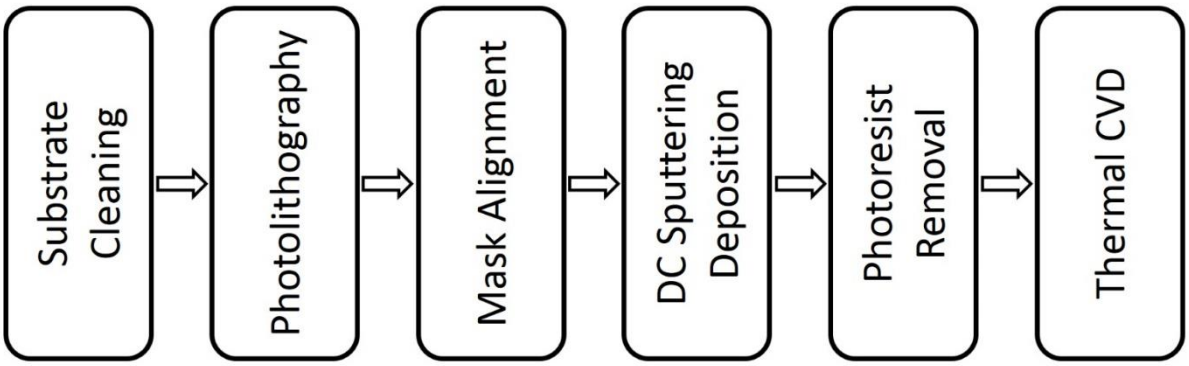

Fig. 3.2 Flow chart of patterned CNT synthesis on ceramic substrate

3.3 Catalyst Deposition and Chemical Vapor Deposition (CVD)

The DC sputtering system is a 2 inch diameter magnetron sputtering with the substrate holder mounted over the plasma (ion) gun that is an ion source without a filament and works with the microwave plasma discharge principle. Figure 3.3 shows a picture and schematic of the sputtering chamber during the W deposition, plasma gun, and substrate holder.

We used Fe, W, and graphite targets to have the desired thin films onto the surface of the substrates. The target and substrate distance is optimized and kept constant at 20 cm. The sputtering chamber is pumped down with a turbo mechanical pump to 5×10^{-6} initially and Ar, as a buffer gas, is introduced. The chamber pressure is optimized and maintained at 7 mTorr during the sputtering process. The catalyst deposition is varied from 1 minute to 10 minutes at a power of 100W in order to obtain the desired thin-film thickness. The Fe catalysis film is obtained around 7 nm with 5 minutes deposition time and W catalysis film thickness is discussed in Chapter 4. Figure 3.4 shows an SEM image of 5 minutes Fe sputtered onto Si substrate surface [13].

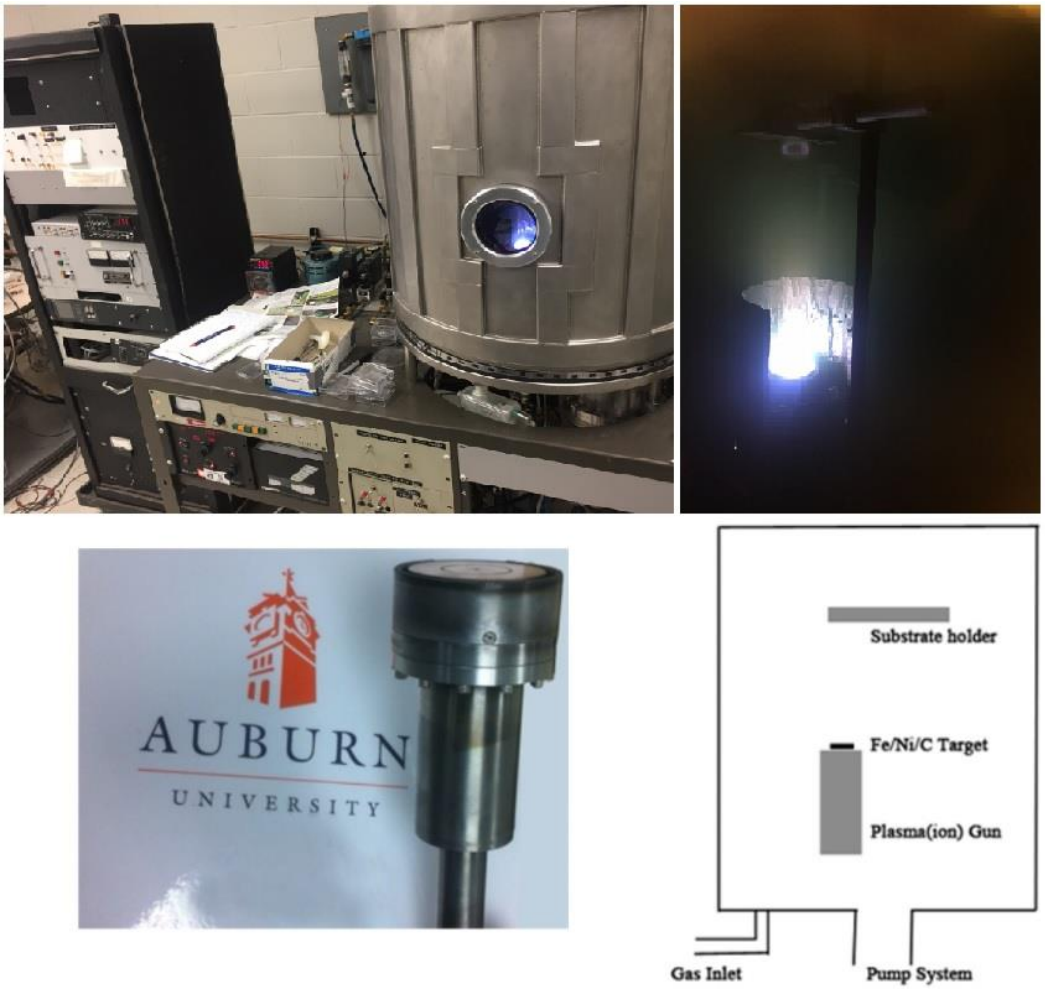

Fig. 3.3 Picture and schematic of the sputtering chamber and plasma gun during tungsten deposition at 100 W power

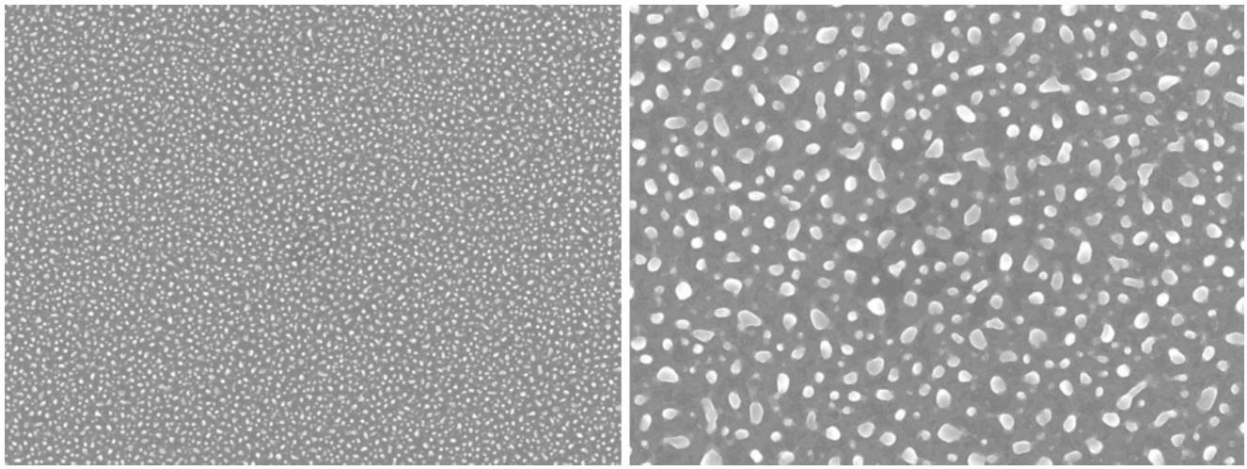

Fig. 3.4 SEM images of iron islands. (After 5 minutes Fe sputtered on Si substrate surface, under x2000 and x7000 magnification, respectively) [13]

The samples are loaded to the CVD chamber after the catalysis deposition process to fabricate CNTs. The resistive heaters are turned on and the temperature of the furnace is raised up to 700^{O}C, which is the optimized temperature of the work here. Acetylene (C_2H_2) and Ar gases are introduced to the chamber as the hydrocarbon and buffer gases, respectively. The flow rates of the gases are measured by flow meters connected to the system from the feeding gas cylinders. The temperature inside the chamber is measured by a thermocouple. The mixed gas blend pressure is kept constant at 70 Torr during the thermal CVD process after the first introduction of C_2H_2 and Ar with a flow rate of 20 sccm and 75 sccm, respectively. The chamber pressure is measured by an MKS Baratron pressure transducer during the initial 10^{-3} Torr pump down and through the experiment. A picture of our thermal CVD system is shown in Figure 3.5.

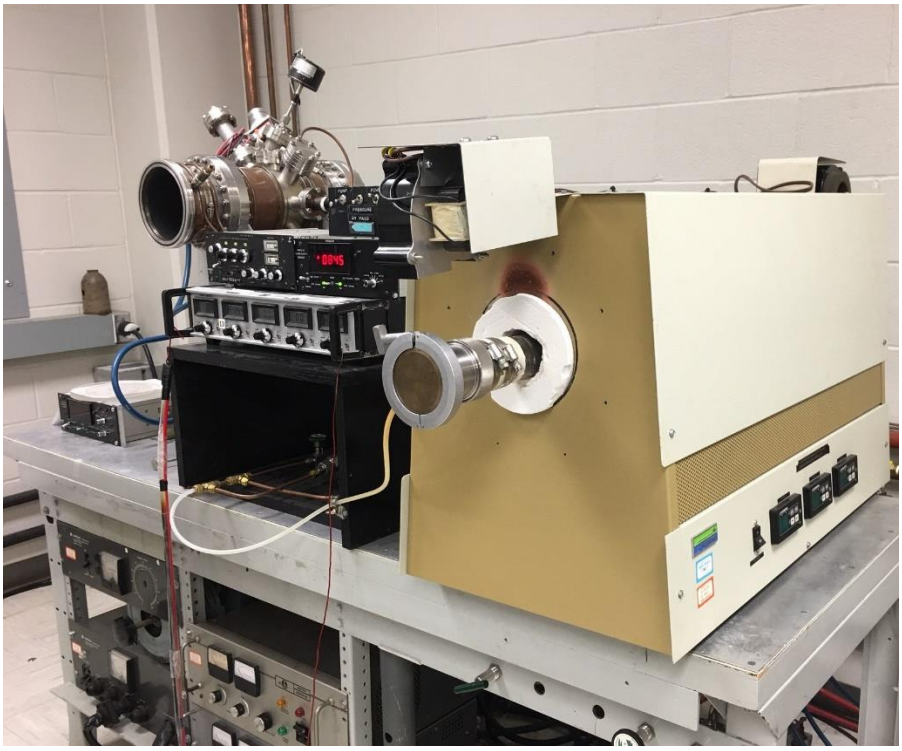

Fig. 3.5 Picture of the thermal CVD system to synthesize CNTs

After 20 minutes in the CVD, the synthesized CNT samples then ready to be transferred to the field emission test chambers, SEM, and AFM for further characterization. Figure 3.6 shows an AFM result of selectively grown CNT sample on ceramic substrate with W underlayer. The randomly oriented MWCNT height variation is measured from 3 different 10 µm long cross–sections of the sample and found around ~1µm. It also can be seen from the data that the CNT height changes throughout the sample since it is randomly oriented. The details of these processes are given in Chapter 4.

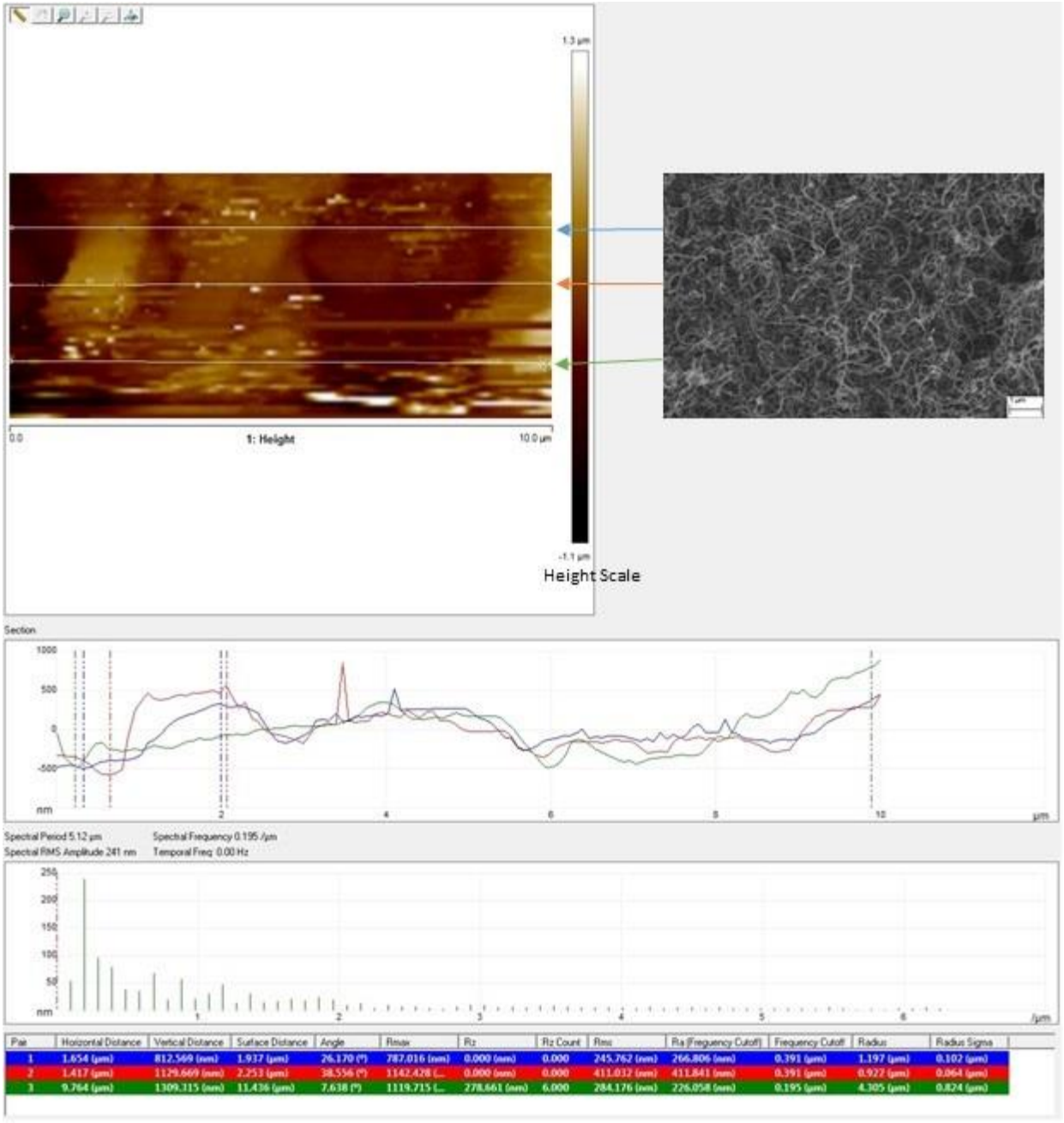

Fig. 3.6 AFM picture and data of randomly oriented 0.35 x 0.35 cm^2 MWCNT sample grown on ceramic substrate with a 0.5 x 0.5 cm^2 W underlayer

3.4 System Optimization for CNT Fabrication on Ceramic Substrates

Similar to Si substrate optimization, the experimental parameters such as thin film catalysis thickness, sputtering distance, sputtering pressure, CVD temperature, and flow rates have affected the CNT growth process on the ceramic samples. For this case, Fe thin film is used also, as the catalysis for the CNT growth and homogenous fabrication is achieved for 5nm-15 nm catalyst thickness regions. Sputtering pressure is optimized, because it was observed that higher deposition pressure resulted with thicker catalysis film and lower deposition pressure is resulted with thinner catalysis film. The catalysis thin film thicknesses are measured for multiple pressure points as it is shown in Table 3.4.1 by keeping the deposition time constant at 5 minutes for Fe catalyst.

Pressure	**10 mT**	**7 mT**	**5 mT**	**3 mT**
Fe Thickness	45 nm	12 nm	7 nm	5 nm

Table 3.4.1 Thin – film thicknesses of Fe catalyst depending on the deposition pressure at constant sputtering time of 5 minutes.

As it is stated in the previous chapter, the CVD temperature has a great effect on CNT synthesis and it is speculated that the hydrocarbon source decomposition is not efficient at low temperatures. Although, MWCNT fabrication can be achieved at temperatures as low as 300-350^{O}C with different synthesis techniques, our thermal CVD process did not yield good CNTs at temperatures lower than 700^{O}C. We obtained our experimental results at 700^{O}C with 20 minutes growth time for approximately 20 µm thick randomly oriented MWCNTs. Higher growth times than 20 minutes did not result in higher CNT height and that follows the CNT growth mechanism that is explained in Chapter 2. Some of the selectively grown samples that were not successful,

and some of the other selected samples with inhomogeneous CNT growth on them are shown in Figure 3.7 to demonstrate the patterning design of underlayer and CNT islands.

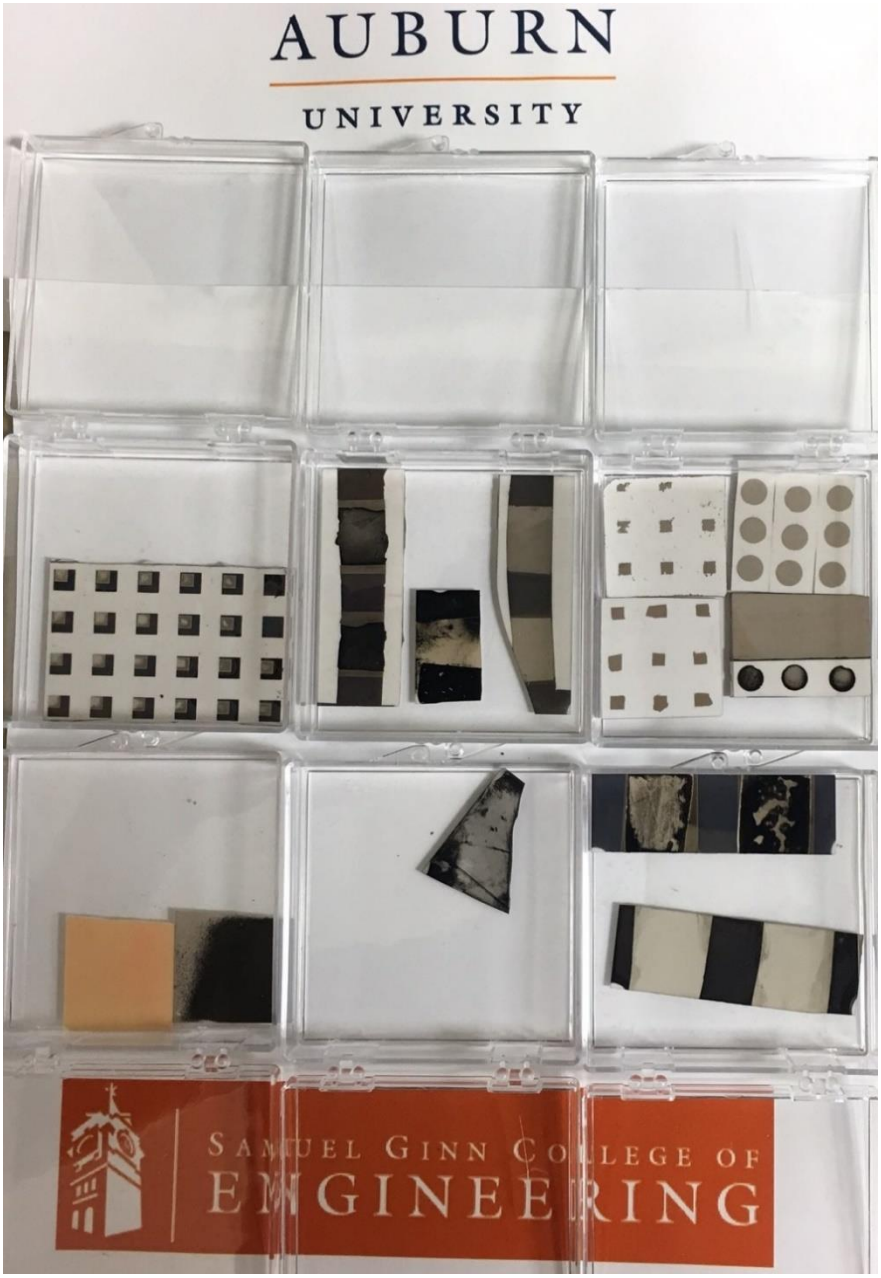

Fig. 3.7 Selected ceramic substrates with inhomogeneous or no CNT growth

3.5 Raman Spectroscopy of CNTs

This section discusses the Raman spectroscopy characterization results of the samples. The experiments were run using 442 nm excitation wavelengths with 8000 ms exposure time at 1500 being center of CCD (charge coupled device). For each sample we had total of 6 different plots (Raman shift vs Intensity). These plots are obtained from 3 different spots on the samples with running 2 different experiments on each of the spots.

All of our Raman characterization results show the intensity ratio Id/Ig is less than 1. It means the intensity of the D peak (disorder carbon line) is way lower than the intensity of the G peak (graphite carbon line). That indicates a higher graphitization, which also means low defects on CNT structure. Furthermore, all of our samples show sharp and narrow D and G bands. Sharp and narrow bands indicate less different types of defects in the CNT structure (i.e. wider the bands/lines, higher the defect types).

Figure 3.8 shows the 6 runs of Sample A. The average intensity ratio of Sample A is 0.66 and the lowest Id/Ig ratio is 0.63. Figure 3.9 shows the 6 runs of Sample B. The average intensity ratio of Sample B is 0.54 and the lowest Id/Ig ratio is 0.52. Figure 3.10 shows the 6 runs of Sample C. The average intensity ratio of Sample C is 0.44 and the lowest Id/Ig ratio is 0.40. Figure 3.11 shows the 6 runs of Sample D. The average intensity ratio of Sample D is 0.39 and the lowest Id/Ig ratio is 0.35.

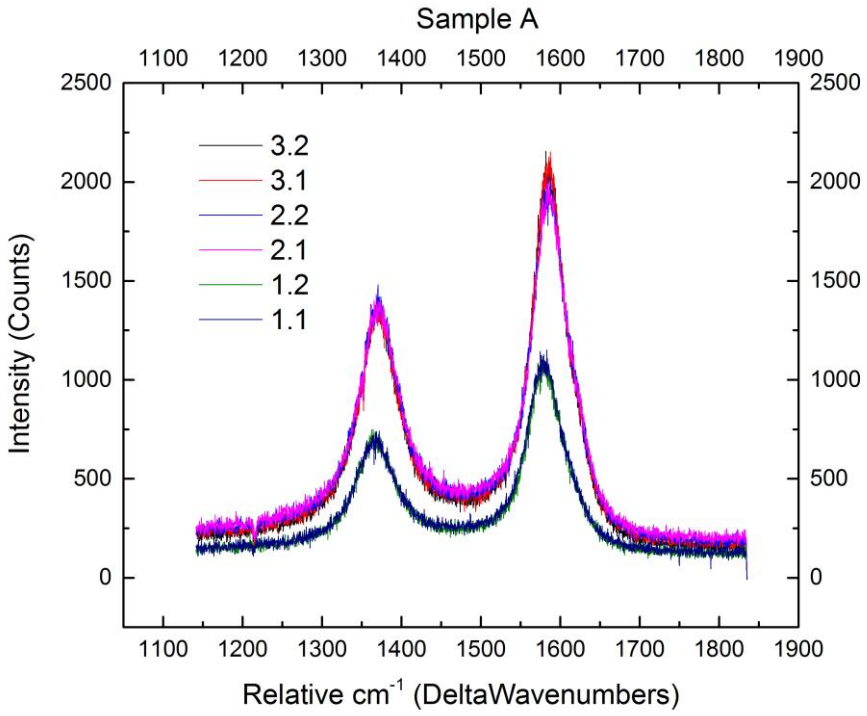

Fig. 3.8 Raman Spectroscopy results of Sample A

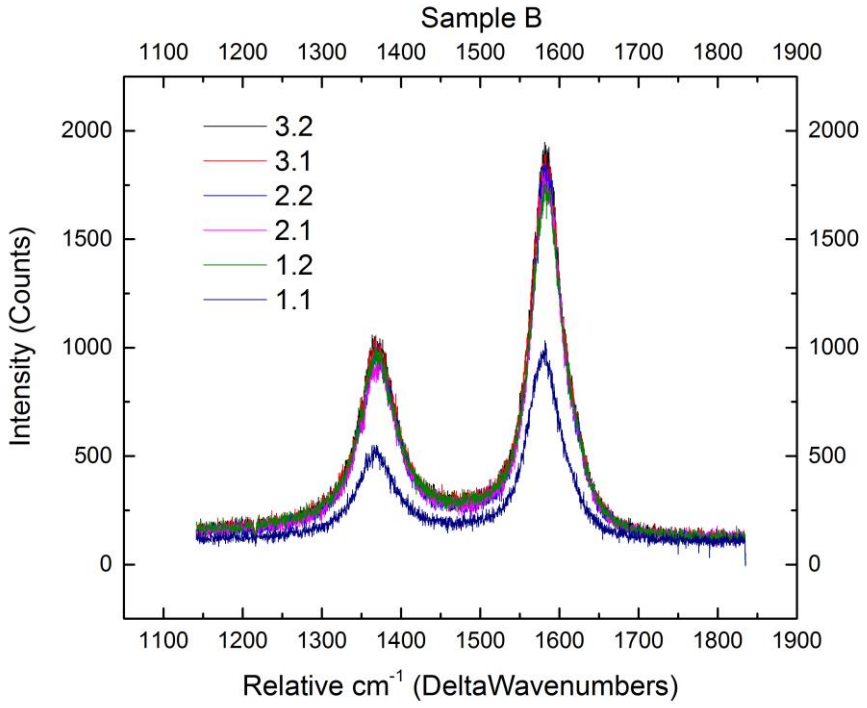

Fig. 3.9 Raman Spectroscopy results of Sample B

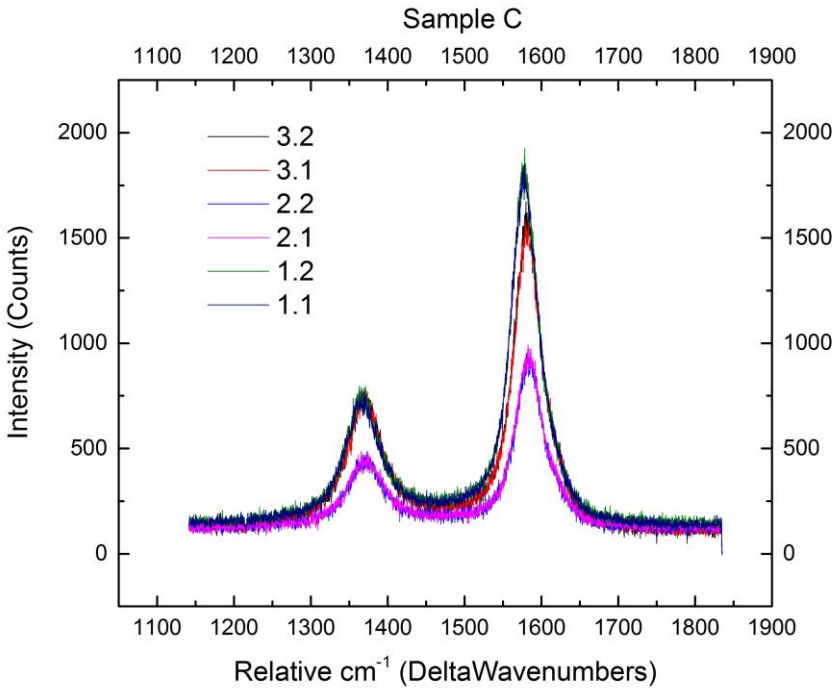

Fig. 3.10 Raman Spectroscopy results of Sample C

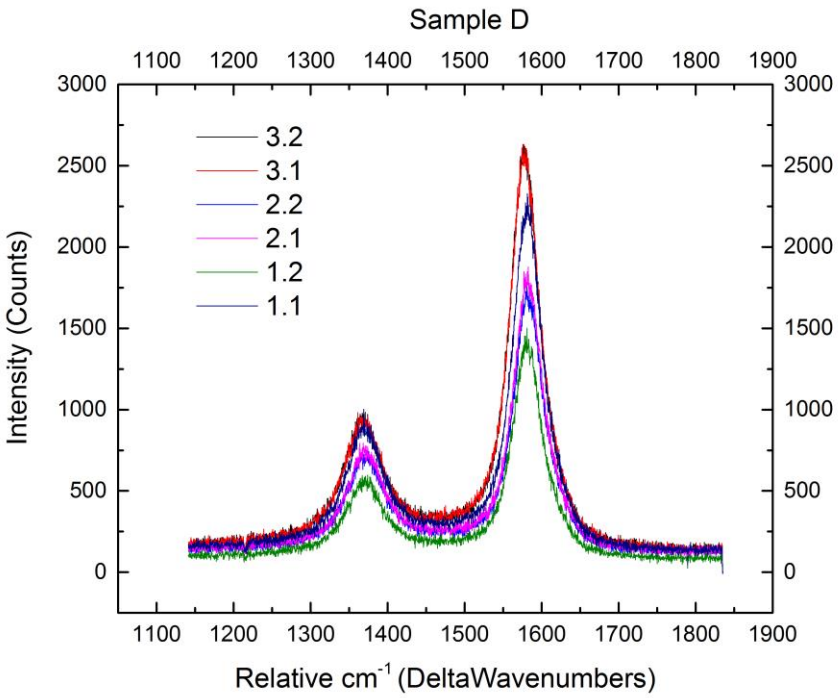

Fig. 3.11 Raman Spectroscopy results of Sample D

Chapter 4

Field Emission Characteristics of Selectively Grown MWCNT Samples on Ceramic

In this chapter, we will compare some of the selectively and non-selectively grown randomly oriented multi-walled carbon nanotubes (MWCNTs) that are synthesized on the polished side of ceramic (aluminum oxide) substrate by using thermal Chemical Vapor Deposition (CVD) technique. Tungsten (W) and Iron (Fe) metal layers are deposited as underlayer and catalysts, respectively on the substrate using a DC plasma sputtering system first, and then CNTs are grown as described before. Different pattern sizes are formed for each CNT sample and field emission characteristics are measured and the Fowler–Nordheim curves are plotted.

Carbon Nanotubes (CNTs) having high length to radius ratio [1] makes them excellent candidates for cold cathode applications among others [2]. CNTs are about micrometers in length and have relatively small diameter in the order of nanometer size. Hence, CNTs are capable of having large electric field enhancement when biased at low applied fields to generate high density of electron emission. They are considered in numerous applications of vacuum microelectronics as well [3]. In this work, we tested selectively and non-selectively grown CNTs field emission characteristics. From F-N curves, the effective emission areas for four different samples are determined. These samples are listed in Table 4.1.1. The images of the shapes and sizes of samples are shown in Figure 4.1.

Sample Name	Size	Shape	Properties
A	0.35 cm x 0.35 cm	Square	Fe catalyst and W underlayer for contact pad
B	0.75 cm x 0.5 cm	Rectangular	Fe catalyst only w/ CNT feedlines
C	3.5 cm x 1 cm	Rectangular	Fe catalyst and W underlayer for contact pad
D	2.5 cm x 2.5 cm	Square	Fe catalyst only

Table 4.1.1 Comparison of four in-house fabricated MWCNT samples

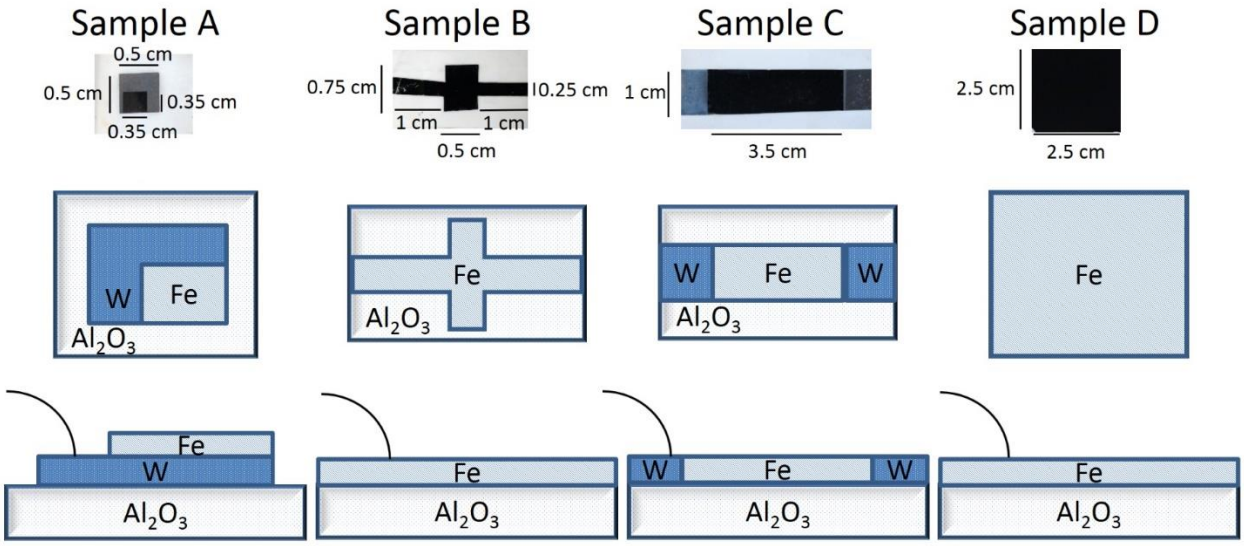

Fig. 4.1 Sample images, top-view and cross-sectional view illustrations

4.1 Sample Preparation

Four different samples of selectively growing randomly oriented CNTs with different pattern and size are synthesized on ceramic substrates by using thermal CVD technique. Then, the field emission characteristics are measured and compared. The growth conditions, catalyst thicknesses, CVD times and pressures are kept the same for all samples. Three of the substrates are patterned, while one is not to keep it as the control sample. Tungsten is deposited as an underlayer and is used as the electrical contact for field emission measurements. Approximately 7nm thin film of metal thickness is formed. Sample A is square shaped with 0.35 cm x 0.35 cm dimensions and fabricated onto 0.5 cm x 0.5 cm tungsten contact layer, with an off-set to the corner. Sample B is 0.75 cm x 0.5 cm, rectangular shaped and fabricated with 1 cm x 0.25 cm CNT feedlines which are also CNTs, on both short sides. Sample C has a rectangular shape with 3.5 cm x 1 cm dimensions and short sides are followed by tungsten contact layers. Lastly, Sample D is square shaped with 2.5 cm x 2.5 cm dimensions with no specific patterning. We used a 99.4% pure ceramic (aluminum oxide) as the substrate to grow CNTs on its polished surface. The samples once CNTs are formed are taken out of the furnace after 20 minutes and visually examined before the SEM images are taken. Then, field emission characteristics of the MWCNTs are measured in vacuum at the room temperature. The substrate containing the CNTs assembled in a diode configuration [8] to measure field emission. CNTs act as cathodes in such a setup and the distance between the CNT sample and the anode is set as 140 μm, which is provided by a glass spacer. A 2 mm diameter rod is used as the anode. Our group also investigated field characteristics with shorter distances that is achieved with packaging techniques. The results of this work is shown elsewhere [9]. The experimental setup schematic is shown in Figure 4.3. The electrodes are biased with a variable high voltage supply and

the voltage value is gradually increased. Applied voltages and emission currents are recorded through a pico ammeter and GPIB port. More detailed processing steps are given elsewhere [10].

Samples are examined using Zeiss Evo 50 Scanning Electron Microscopy (SEM) at 20 kV and shown in Figure 4.4. The SEM images show that all the samples have dense and good quality CNTs grown randomly and that there are no carbon clusters or carbonaceous particles. The randomly synthesized MWCNT diameters are estimated to be between 10 to 30 nm in diameter and about 20-30 μm in lengths as shown in Figure 4.2.

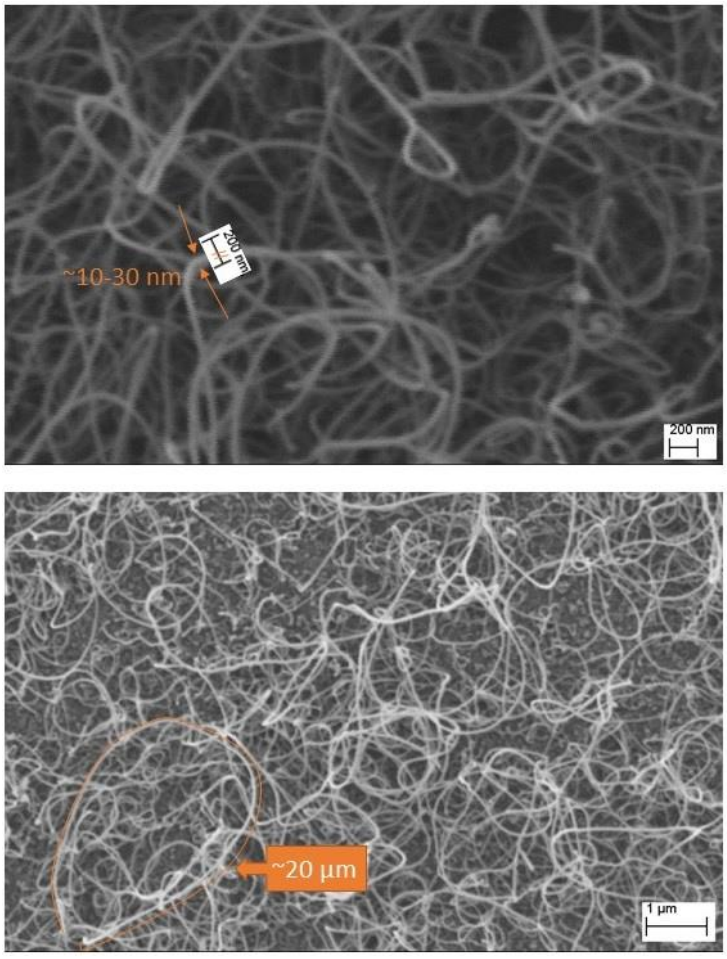

Fig. 4.2 MWCNT SEM Images with the length and diameter scales

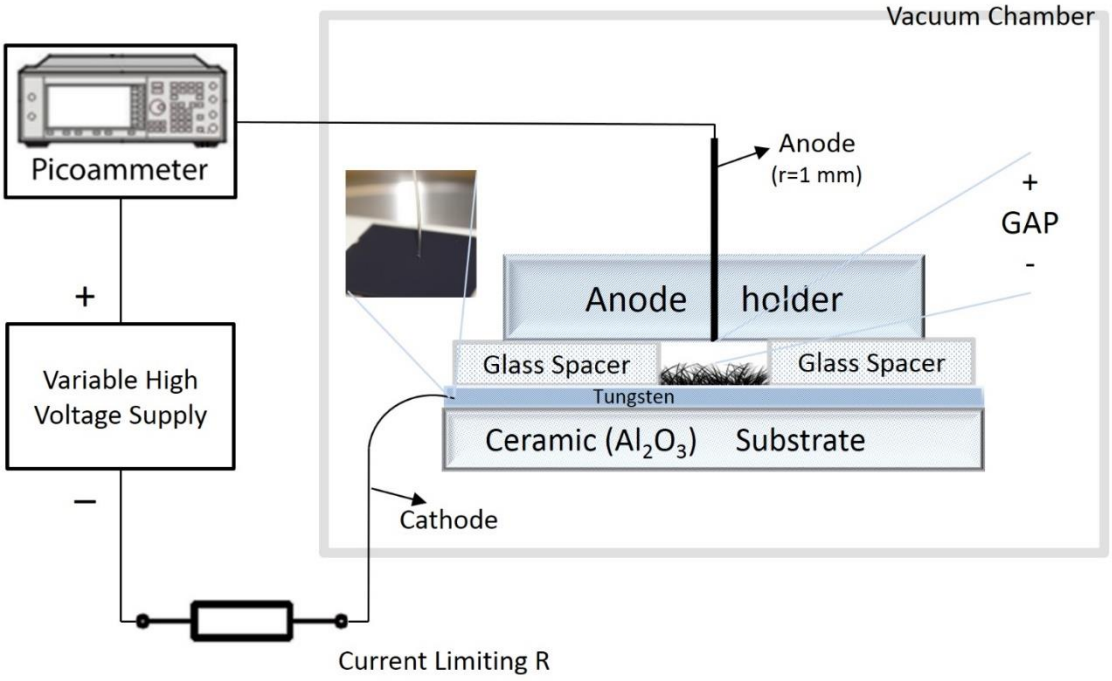

Fig. 4.3 Schematic of the field emission test chamber and the measurement setup

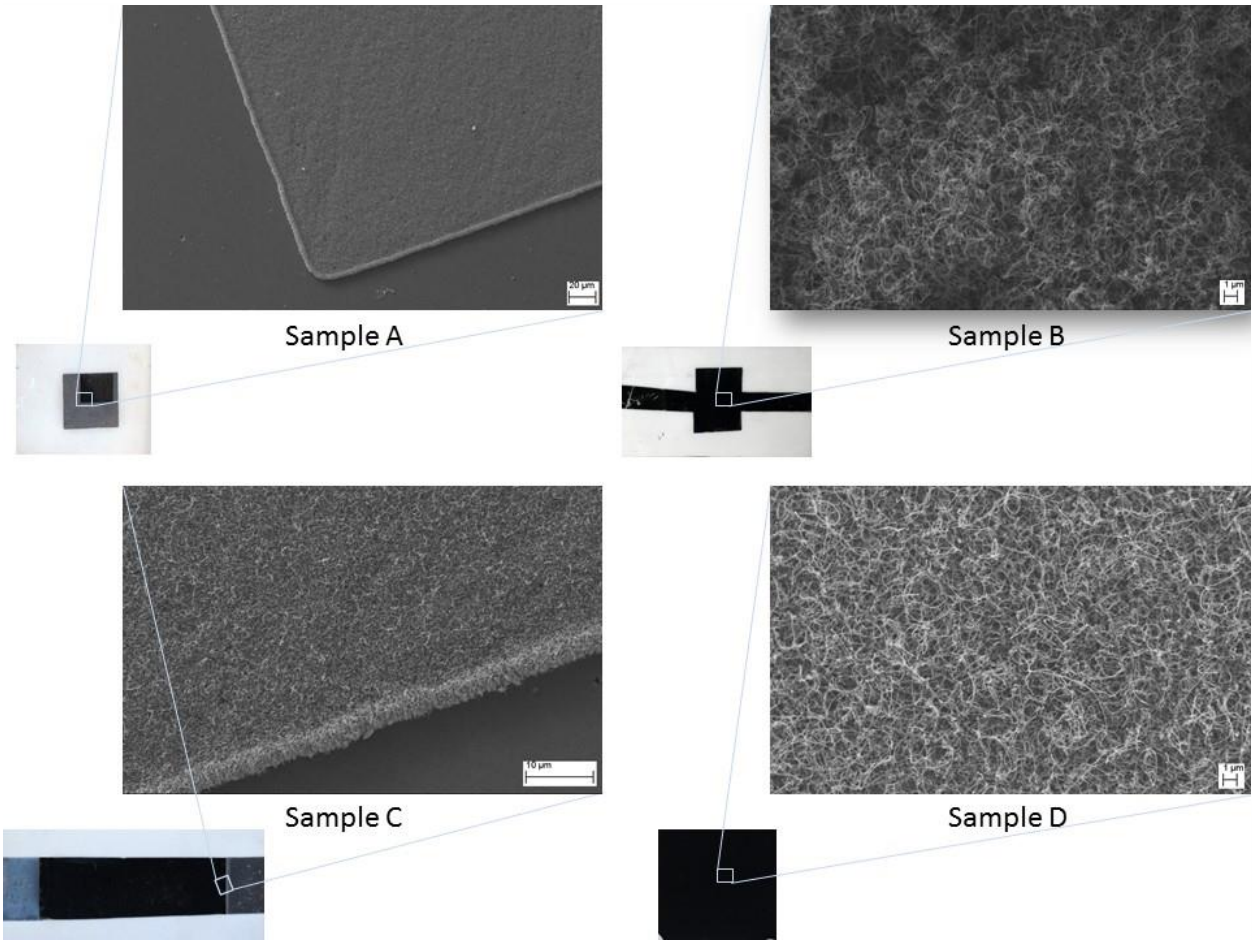

Fig. 4.4 (a) Cross – sectional image of sample A, Fe catalyst sputtered for 5 minutes on .35 cm^2 x .35cm^2 patterned ceramic substrate with .5 cm^2 x .5cm^2 W underlayer (resolution x1k), (b) SEM image of sample B, Fe catalyst sputtered for 5 minutes and CVD growth for 20 mins (resolution x10k), (c) Cross – sectional image of sample C, Fe catalyst sputtered for 5 minutes and CVD growth for 20 mins (resolution x5k), (d) SEM image of sample D, Fe catalyst sputtered for 5 minutes and CVD growth for 20 mins (resolution x10k)

4.2 Results

The following equations are used to calculate field strength and current density data from the raw voltage and current values that are collected as described earlier.

$$E = \frac{V_s - IR}{d} \quad \text{and} \quad J = \frac{I}{S}$$

where V_s is the applied voltage, I is the collected current data, R is 4.2 MΩ current limiting resistor, d is 140 µm gap distance that is the glass spacer, and S is 0.0316 cm^2 electron emission collection area that is the exposed area of the collector tungsten rod (anode). The data acquisition software is set in a way that six current data points with five seconds intervals are recorded and averaged to obtain a data point for every applied voltage value for the test accuracy. From these data, the field emission curves are obtained and turn on voltages are calculated. Field emission curves of all four samples with ceramic substrate at room temperature are shown in Figure 4.5. The turn on voltage values are given in Table 4.2.1.

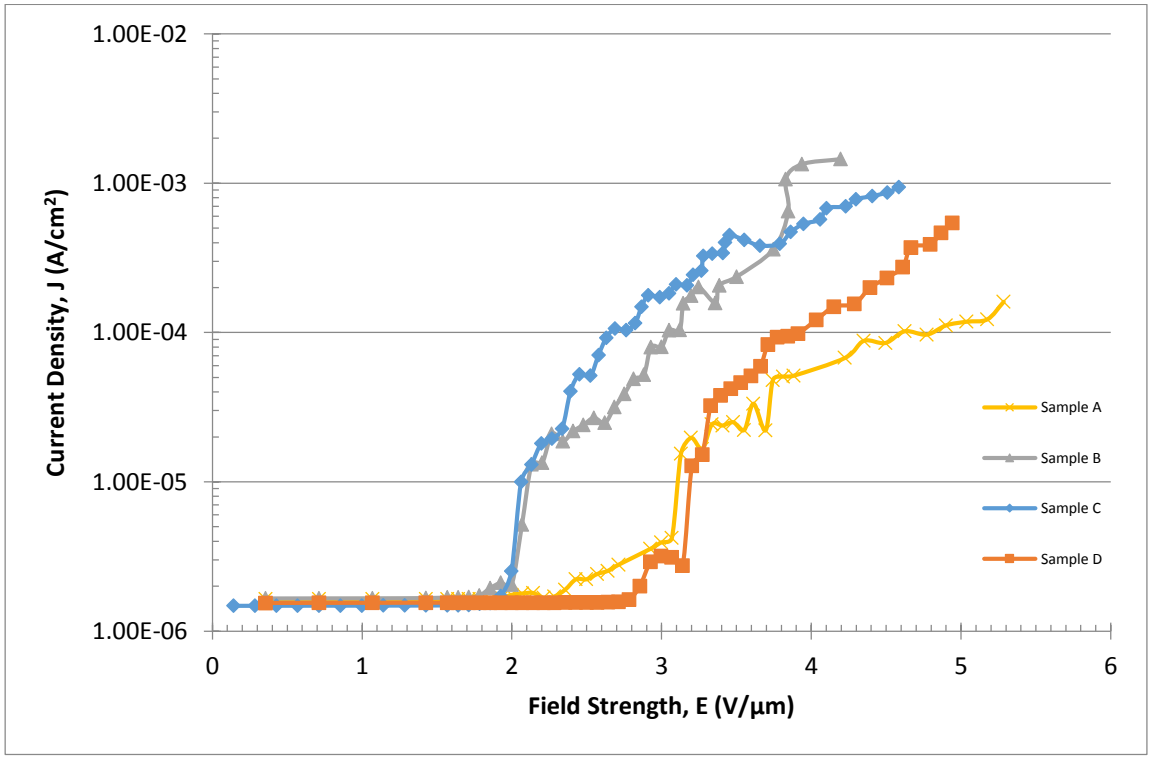

Fig. 4.5 Field emission characteristics of the CNT samples

Sample Name	Turn – on Field
A	2.35 V/μm
B	1.99 V/μm
C	1.92 V/μm
D	2.85 V/μm

Table 4.2.1 Turn-on voltages and emission currents of the samples

4.3 Discussion

Field emission characteristics of the samples have similar curves, but turn-on voltages don't have any specific tendency depending on the sample shapes and sizes. Both samples C and B have rectangular shapes, 3.5 cm x 1cm and 0.75 cm x 0.5 cm sizes, respectively, and have the lowest turn-on voltages of 1.92 V/μm and 1.99 V/μm. Samples A and D, which have the smallest pattern and the biggest pattern area, respectively, have the higher turn-on voltage values. Sample D has the highest turn-on voltage, 2.85 V/μm, although it has the biggest fabricated CNT area.

Field emission process relies on field enhancement factor (β) of the emitting surface area. Furthermore, the emission current density has an exponential relationship with β [11], [12]. The tips of the nanotubes are the emitting area in the field emission mechanism of CNTs. So, the emission current values should be expected to be similar. Also, MWCNTs have different lengths and not all the randomly oriented MWCNTs are actively involved in the field emission process, because longer or sharper nanotubes can dominate the field emission in the adjacent area [13]. Hence, turn-on voltage might be affected by the MWCNTs that are available and act as emitters at

the sample's surface area. These results are similar to the field emission characteristics of MWCNTs fabricated on silicon (Si) substrates in terms of sample pattern sizes and shapes have none or small dependence on the turn-on fields and emission currents [14], [15].

In a field emission process, the injected electrons are emitted into the vacuum from the cathode to the anode, passing through the nanotube surfaces. Meanwhile, the local electric field is enhanced since CNTs have sharp needlelike morphology when compared to the flat emitting structures. The local electric field is defined as $F = \beta E$ where β is the field enhancement factor and E is the applied electric field between the anode and the cathode. The exponential relation between the local electric field (the field enhancement factor) with the emission current density and the work function is defined by Fowler–Nordheim (F–N) theory [16] and given as

$$J = \frac{a b^2 E^2}{f} \exp\left(- \frac{b f^{3/2}}{bE} \right)$$

This is called F–N equation and the emission current is $I = J \times S$ (A) Then the equation becomes:

$$I = \frac{a b^2 E^2 S}{f} \exp\left(- \frac{b f^{3/2}}{bE} \right)$$

where *a* is a constant and defined as $a = \left(e^3 / 8\pi h\right) = 1.54 \times 10^{-6}$ $(\mathrm{A.eV/V^2})$, *b* is another constant and defined by $b = \left(-8\pi\sqrt{2me}/3h\right) = 6.83 \times 10^9$ $(\mathrm{eV^{-(3/2)}.Vm^{-1}})$, and ϕ is work function, which is given between 4.5 eV to 5.0 eV for CNTs in the literature [17], [18], [19], [20]. In this work, ϕ =5.0 eV is used. This equation can be re-written in terms of $\ln(J/E^2)$ and $(1/E)$ as $\ln(J/E^2) = A - B(1/E)$. This equation represents a straight line with and intercept *A* and slope – *B*. Therefore, the slope of such a curve for F-N plots yield the field enhancement factor β of the

material in question and the intercept yields the information about the effective emission area of the emitters. Figure 4.6 shows the F-N plots of four CNT samples studied in this work. This data usually forms a straight line, and slopes and intercept points can be calculated from the plot. Then, field enhancement factor β can be calculated from the slope of the curve using the following equation:

$$\beta = -\frac{b\phi^{3/2}}{B}.$$

Slope and intercept values are found from Figure 4.6 and field enhancement factors are calculated. Results are shown in Table 4.3.1. Sample A with 0.35 cm^2 CNT area has the biggest field enhancement factor. Sample B and sample C follow the sample A and have the second and third biggest field enhancement factors, respectively. Lastly, sample D with 2.5 cm^2 area, which has the biggest CNT area, has the smallest field enhancement factor. Although these results show that field enhancement factor decreases with the increasing pattern size, these results are not sufficient to make any firm conclusions. Most important results is that, the order of the magnitude of the field enhancement factor of all four samples are the same. Similarly, the intercept values of the samples have about the same order of magnitude as expected.

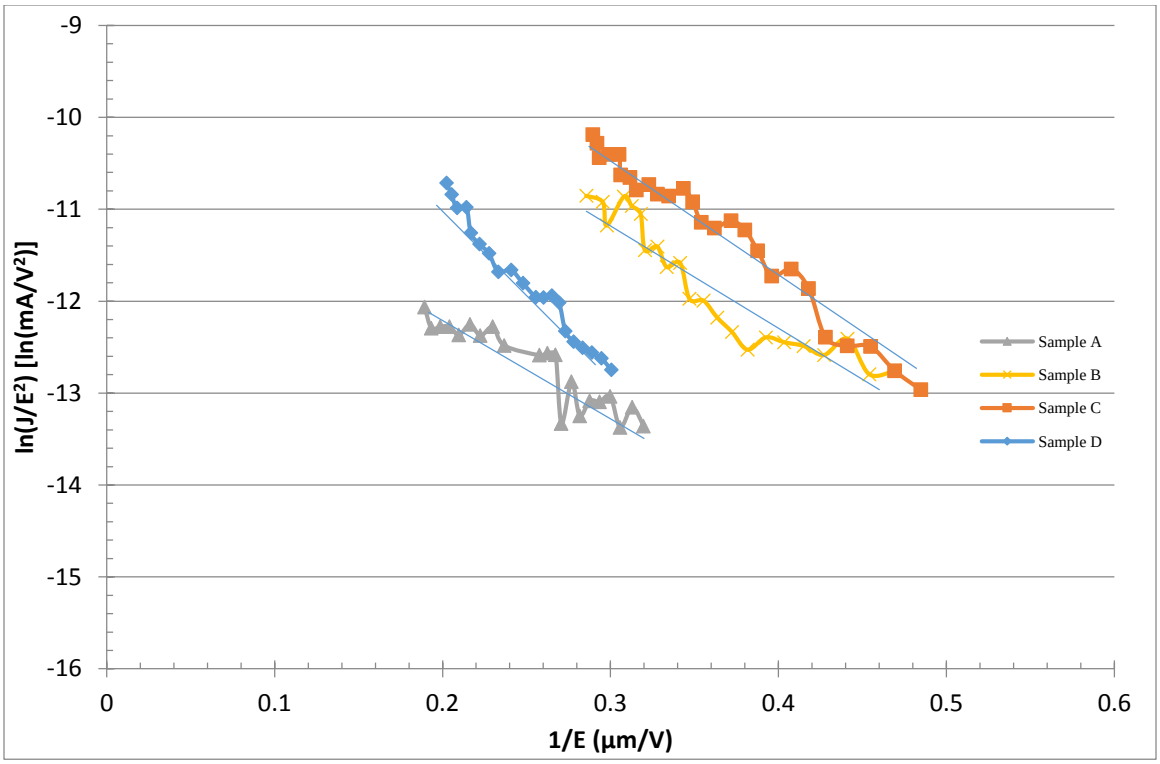

Fig. 4.6 Fowler – Nordheim Curves of the CNT samples

Sample Name	Slope	Intercept	β – Field Enhancement Factor
A	-9.553	-10.285	7993
B	-11.592	-7.657	6587
C	-13.548	-6.324	5636
D	-19.484	-6.933	3919

Table 4.3.1 Slope, intercept, and field enhancement factor values of the CNT samples

From these results, it is difficult to conclude if patterning may have an effect on the effective emission area, but there are also other factors that should be considered such as voltage dependence, space charge effect, and CNT tip shape.

In the literature, F-N plots of CNTs show nonlinear characteristics and forms a knee, which distinguishes the data into two regions [21]. These regions are simply called high electric field and low electric field. Although, it is still a phenomena and has not completely been understood the reasons why the F-N curves show such characteristics, there has been some studies presented in the literature [22], [23]. According to the literature, there are two factors that affect the slope of F-N plot of CNTs. First, electron interaction between the substrate and CNT surfaces and the second, electron emission from the CNT surfaces to the vacuum. It is stated in the literature when the substrate that is used to fabricate CNTs on is conducting such as nickel (Ni), F-N curves show linearity and no knees [24], [25]. On the other hand, if the substrate is a semiconductor even if there is an insulating layer (oxide layer) that acts as a barrier, such as SiO_2, CuO, and CuO_2, the F-N curves show nonlinearity and knee appearance occurs [26]. Our results are in agreement with the literature data and nonlinearity and knee formations is not seen in Figure 4.6 for all four CNT samples that are formed on ceramic substrate.

4.4 Conclusion

There might be a small correlation between patterning size and shape, and turn-on voltage, but it can't be stated without further studies due to limited number of samples compared in this paper. On the other hand, the under-layer and the way under-layer is patterned may have effects

on the field emission characterizes of CNTs studied in this work. Emission currents of all four samples at 4 V/μm field strength are determined and it's noted that they don't show an order regarding pattern sizes and shapes. Field enhancement factors and slope values of the samples also don't show an obvious difference based on the pattern size and shape. Although, these results are very promising, further studies with more number of sample are needed to make firm conclusions. Moreover, these results can be compared with the MWCNTs that are synthesized on different substrates such as Si, Ni, Cu, and these substrates with oxide layers for further understandings of field emission mechanisms of CNTs. It would also be interesting to investigate and see how the different substrates effect turn-on fields and emission current densities and if there is any correlations or trend between those results. These might ease the application implementations of CNTs and put the promising properties of CNTs in use in multiple and broad range of applications in the near future.

REFERENCES

[1] S. Iijima, "Helical microtubules of graphitic carbon," Nature, vol. 56, pp.354, 1991.

[2] Y. Saito, S. Uemura, "Field emission from carbon nanotubes and its application to electron sources," Carbon, vol. 38, no. 2, pp. 169-182, 2000.

[3] Q. Zhang, Carbon Nanotubes and their Applications, vol. 1. Pan Stanford, 2012, pp.289–317.

[4] Zujin Shi, Yongfu Lian, Xihuang Zhou, Zhennan Gu, Yaogang Zhang, Sumio Iijima, Lixia Zhou, Kwok To Yue, Shulin Zhang, Mass-production of single-wall carbon nanotubes by arc discharge method1, Carbon, Volume 37, Issue 9, 1999, Pages 1449-1453

[5] W.K. Maser, E. Muñoz, A.M. Benito, M.T. Martínez, G.F. de la Fuente, Y. Maniette, E. Anglaret, J.-L. Sauvajol, Production of high-density single-walled nanotube material by a simple laser-ablation method, Chemical Physics Letters, Volume 292, Issues 4–6, 14 August 1998, Pages 587-593

[6] M. J. Yacaman, M. M. Yoshida, L. Rendon, J. G. Santiesteban, "Catalytic growth of carbon microtubules with fullerene structure," Appl. Physics Lett., vol. 62, no. 6, pp. 657-659, 1993.

[7] J. Prasek, J. Drbohlavova, J. Chomoucka, J. Hubalek, O. Jasek, V. Adam, "Methods for carbon nanotubes synthesis," J. Mater. Chem., vol. 21, pp. 15872-15884, 2011.

[8] B. Yakupoglu and H. Kirkici, "Fabrication and operating characteristics of carbon nanotube diode," *2014 IEEE Int. Power Modulator and High Voltage Conf. (IPMHVC),* Santa Fe, NM, 2014, pp. 337-339.

[9] M. Jung, T. Baginski and H. Kirkici, "Test-bed of pulsed radio frequency (RF) signal used with a diode made of carbon nanotubes (CNTs)," *2014 IEEE Int. Power Modulator and High Voltage Conf. (IPMHVC),* Santa Fe, NM, 2014, pp. 599-602.

[10] B. Yakupoglu, M. Moxley and H. Kirkici, "Characterization and fabrication of carbon nanotubes grown on ceramic substrates for high temperature RFID applications," *2016 IEEE Int. Power Modulator and High Voltage Conf. (IPMHVC),* San Francisco, CA, 2016, in press.

[11] O. Gröning, O. M. Küttel, Ch. Emmenegger, P. Gröning and L. Schlapbach, "Field emission properties of carbon nanotubes," J. of Vacuum Sci. & Technology B, vol. 18, pp. 665-678, 2000.

[12] E. J. Radauscher, "Design, Fabrication, and Characterization of Carbon Nanotube Field Emission Devices for Advanced Applications," Ph. D. dissertation, Dept. Elec. Eng., Duke Univ., Durham, NC, 2016.

[13] N. de Jonge and JM. Bonard, “Carbon nanotube electron sources and applications,” Philosoph. Trans. of The Roy. Soc. A Math. Physical and Eng. Sci., vol 362, no. 1823, pp. 2239 – 2266, Nov. 2004.

[14] Y. M. Wong, W. P. Kang, J. L. Davidson, B. K. Choi, W. Hofmeister, and J. H. Huang, “Array geometry, size and spacing effects on field emission characteristics of aligned carbon nanotube,” Diamond Relat. Mater., vol. 14, no. 11/12, pp. 2078–2083, Nov./Dec. 2005.

[15] K. B. K. Teo et al., “Field emission from dense, sparse, and patterned arrays of carbon nanofibers,” Appl. Physics Lett., vol. 80, no. 11, pp. 2011-2013, 2002.

[16] R. H. Fowler and L. W. Nordheim, “Electron emission in intense electric fields, ”Proc. R. Soc. Lond. A, Math. Phys. Sci., vol. 119, no. 781, pp. 173– 181, May 1928.

[17] R. G. Forbes, “Physics of generalized Fowler-Nordheim-type equations,” J. of Vacuum Sci. & Technology B: Microelectronics and Nanometer Structures, vol. 26, no. 2, pp. 788 – 793, 2008.

[18] X. Lu, Q. Yang, C. Xiao, and A. Hirose, “Nonlinear Fowler–Nordheim plots of the field electron emission from graphitic nanocones: Influence of non-uniform field enhancement factor,” J. of Physics D: Appl. Physics, vol. 39, no. 15, pp. 3375–3379, Aug. 2006.

[19] R. Gao, Z. Pan and Z. L. Wang, ” Work function at the tips of multiwalled carbon nanotubes,” Appl. Physics Lett., vol. 78, pp. 1757-1759, 2001.

[20] P. Y. Chen, T. C. Cheng, J. H. Tsai, and Y. L. Shao, “Space charge effects in field emission nanodevices.,” Nanotechnology, vol. 20, no. 40, p. 405202, Oct. 2009.

[21] R. Bai, “Nonlinear Field Enhancement factor of Carbon Nanotubes (CNTs) in Vacuum and Partial Pressure,” M.S. thesis, Dept. Elec. Eng., Auburn Univ., Auburn, AL, 2013.

[22] R. G. Forbes, “Low-macroscopic-field electron emission from carbon films and other electrically nanostructured heterogeneous materials: hypotheses about emission mechanism,” Solid-State Electron., vol. 45, no. 6, pp. 779-808, June 2001.

[23] J. Zhang, C. Yang, W. Yang, T. Feng, X. Wang, and X. Liu, “Appearance of a knee on the Fowler–Nordheim plot of carbon nanotubes on a substrate,” Solid State Commun., vol. 138, no. 1, pp. 13–16, Apr. 2006.

[24] LF. Chen, ZG. Ji, YH. Mi, HL. Ni, and HF. Zhao, “Nonlinear characteristics of the Fowler–Nordheim plots of carbon nanotube field emission,” Physica Scripta, vol. 82, no. 3, p. 035602, Sep. 2010.

[25] M. Moxley, “Carbon Nanotube Based Vacuum Diode Characteristics at Elevated Temperatures,” M.S. thesis, Dept. Elec. Eng., Auburn Univ., Auburn, AL, 2016.

[26] J. Zhang et al., “Interaction between carbon nanotubes and substrate and its implication on field emission mechanism,” Carbon, vol. 44, no. 3, pp. 418-422, March 2006.

Chapter 5

High Temperature Data of CNTs on Ceramic and Tungsten Under-layer Thin Film Experiments on Silicon

5.1 Overview

Randomly aligned multi-wall CNTs are fabricated on ceramic substrates as it is explained in the previous chapter. One of the driving force behind this research is to look at the electrical properties of CNTs in order to operate under extreme conditions such as oil plants, nuclear plants, close to engine locations, in a car, and others, and see how they react in such aggressive environments. As known silicon's electrical properties changes at higher temperatures. Therefore, we have chosen ceramic (aluminum oxide-Al_2O_3) substrates due to its great thermal properties. Ceramic substrates known as their refractory properties and with stable chemical properties in high temperature conditions up to $1750^{O}C$ [1]. This research also brings diversity to studies and commercial applications where ambient/operating temperatures exceed $200^{O}C$-$250^{O}C$. Currently, mainly research in high temperature electronics is using SiC and its compounds.

The tungsten underlayer thin film and thickness effects on the field emission tests, turn-on voltages, Fowler-Nordheim curves, and β-field enhancement factor are investigated. The film thicknesses are formed for 1 minute, 3 minutes, 5 minutes, and 8 minutes DC plasma sputtering on silicon. The corresponded film thicknesses for the mentioned sputtering times are also measured with AFM and are reported at the end of this chapter.

5.2 High Temperature Data of Selectively Grown MWCNT Samples on Ceramic

The high thermal endurance against high temperatures makes CNTs a very promising alternative material where the temperature might be a concern. As it can be seen from the fabrication process in the last chapter, the CNTs are already fabricated around 700^{O}C. Although, the samples that grown on silicon substrates are limited to silicon's thermal properties, the samples that are fabricated on ceramic substrates are reliable for high temperature applications [1]. Considering majority of the electronic devices on the market are silicon based, our new approach of using ceramic as the substrate material and fabrication electronic devices using CNTs opens new potential application and implementation of CNTs into novel electronics devices.

5.2.1 Experimental Setup

In order to obtain and compare the high temperature data of MWCNTs, the growth conditions of CNTS are kept the same for these four samples. Only difference is the sizes and the shape of patterns of the under-layer and the CNTs in this work. The field emission characteristics at the elevated temperatures from room temperature to 300^{O}C by 50^{O}C increments are measured and results are discussed. The sample properties and experimental data are given in the results section of this chapter. Sputtering with iron (Fe) catalyst material is done for 5 minutes. A tungsten (W) under layer thin film is formed in two of the samples and used as contact pad points. The sputtering pressure is kept same at 7mTorr and the distance between the target and the substrate is kept at 20 cm. Following this, the CVD process for 20 minutes at 700^{O}C and 70 mTorr pressure is achieved. The flow rate of hydrocarbon, gas (Acetylene) is kept at 20 sccm and buffer gas (Argon) flow rate is kept at 75 sccm for all the samples. Once the CNTs are formed, the samples

are placed in a vacuum chamber for the high temperature field emission experiment. The specifications of the experimental setup for high temperature measurements are similar to the one that is described in the previous chapter with an addition of three tungsten filament heater lamps used as heating elements, a thermocouple to record the temperature in the chamber, and a controller the power supply providing the current to the lams and in return control the temperature in the chamber (a Kurt J. Lesker HTR Modular Adaptive Power Supply as it can be seen in Figure 5.1). Although this unit can be programmable with a ramp rate to control the temperature generated by the lamps, we manually controlled the output control to gradually increase the temperature inside the vacuum chamber.

Fig. 5.1 Kurt J. Lesker HTR Modular Adaptive Power Supply

The vacuum chamber is pumped down to $5x10^{-6}$ Torr pressure with a turbomolecular pump for the experiments. A Stanford Research Systems variable high voltage power supply and a Keithley pico ammeter is connected to the test bed as in the previous Chapter. The power supply for the lamps, the temperature controller, and thermocouple are added to the set-up additionally. We modified the MATLAB code that is originally written by our group, to acquire more data point [2]. This set up recorded six current data points with five seconds intervals are recorded. At given applied voltage these six data points averaged to obtain a data point for each applied voltage to obtain better test accuracy. The variable high voltage supply and the pico ammeter are connected to the computer via a GPIB port and the voltage values of the power supply are controlled by the code. The sample is placed on a black piece of ceramic baseplate where the 20' type K thermocouple wire is placed on it to measure the chamber temperature. CNTs act as the cathode in this setup and the anode is made of a 2 mm diameter tungsten rod that is tightly placed on the ceramic block. The distance between the anode and the cathode is provided by the 140 μm glass spacer. The three tungsten filament heater lamps are placed around the sample in a triangle shape with one lamp under the black ceramic baseplate and the other two are on top with 120 degrees apart from each other. All three tungsten filament heater lambs are connected in series in this experimental setup. Metal reflectors are used in the chamber in order to direct the radiation from the lamps only to the sample direction. The experimental setup schematic and the top and side pictures of the high temperature data collection test set-up is shown in Figure 5.2 and Figure 5.3.

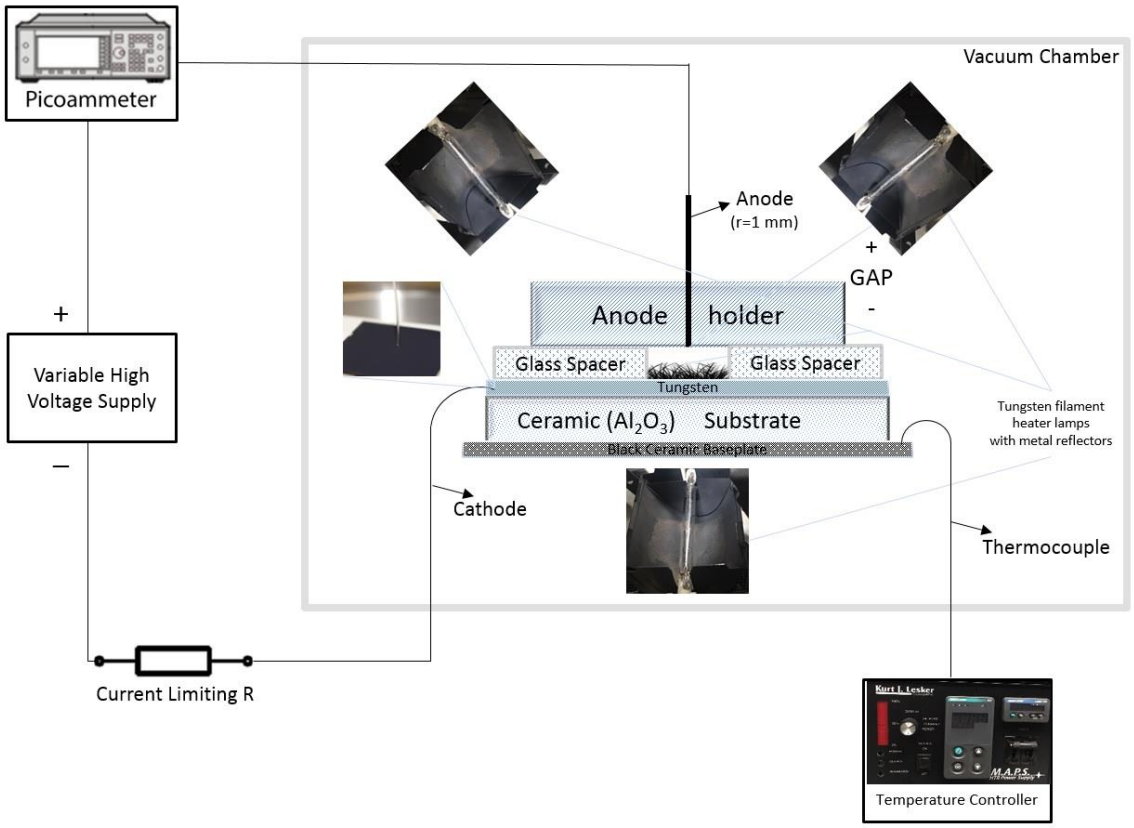

Fig. 5.2 Schematic of the high temperature field emission test chamber and the measurement setup

Fig. 5.3 Top and side pictures of the high temperature field emission test chamber and the measurement setup

5.2.2 Field Emission Test Results

Field strength and current density values are calculated after the current data is collected via data acquisition and MATLAB code as it is described above as described in the following equations. The field strength is calculated as:

$$E = \frac{V_S - IR}{d} \quad (\mathrm{V}/\mu\,\mathrm{m})$$

where V_S is the applied voltage, I is the collected current data, R current limiting resistor is equal to R=4.2 MΩ, and d is gap distance that is the glass spacer and equal to d=140 μm. The current density is calculated as:

$$\mathrm{J}=\frac{I}{S} \qquad \{A/cm^2\}$$

where S is emission area of the collector, that is the anode and is equal to S=0.0316 cm^2. Then the field emission characteristics are plotted for each sample. First sample is Sample A, which is square shaped with 0.35 cm x 0.35 cm MWCNTs fabricated onto 0.5 cm x 0.5 cm tungsten contact layer. Field emission curves of Sample A from room temperature to 300^{O}C are shown in Figure 5.4 and the turn-on voltage values are given in Table 5.2.1.

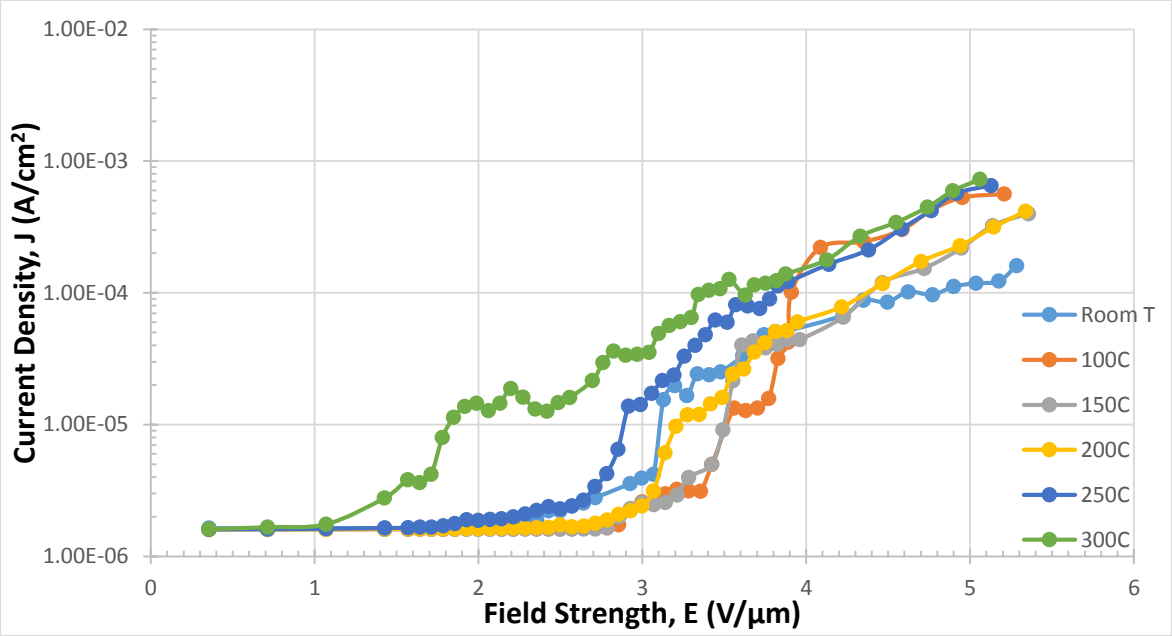

Fig. 5.4 Field emission characteristics of the Sample A for the elevated temperatures

Turn-on voltages of the Sample A

Temperature	Turn-on Field
Room T.	2.284 V/µm
100^{O}C	2.856 V/µm
150^{O}C	2.784 V/µm
200^{O}C	2.641 V/µm
250^{O}C	1.784 V/µm
300^{O}C	1.070 V/µm

Table 5.2.1 Turn-on voltages of the Sample A

Sample B is 0.75 cm x 0.5 cm, rectangular shaped and fabricated with 1 cm x 0.25 cm CNT feedlines used for electrical contact on both short sides. Field emission curves of Sample B from room temperature to 300^{O}C are shown in Figure 5.5 and the turn-on voltage values are given in Table 5.2.2.

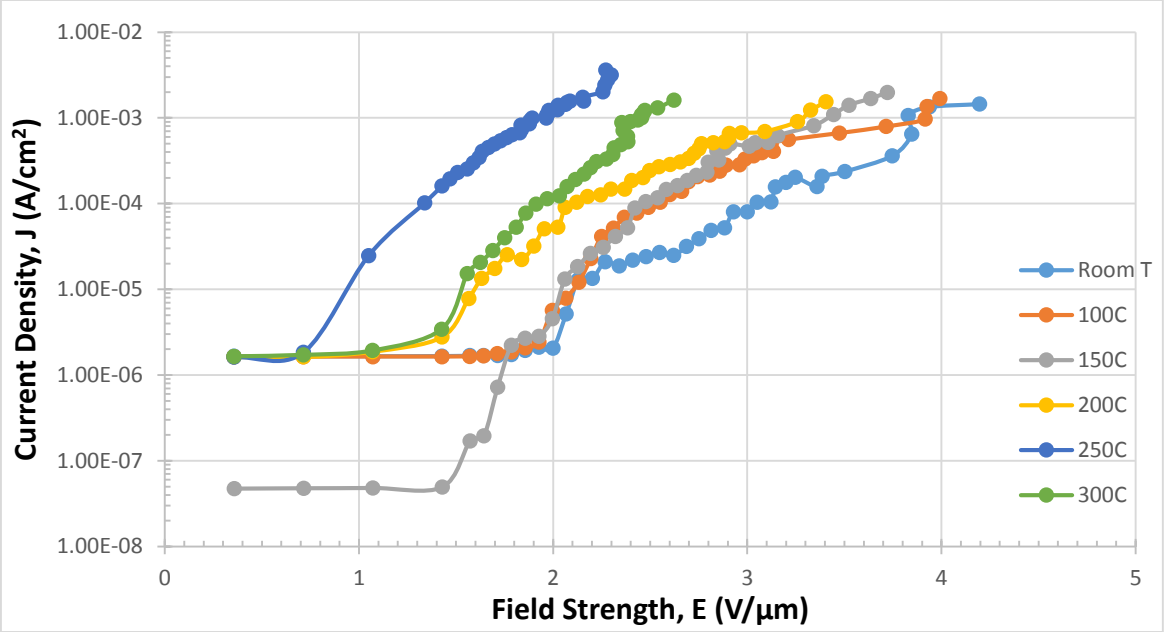

Fig. 5.5 Field emission characteristics of the Sample B for the elevated temperatures

Turn-on voltages of the Sample B

Temperature	Turn-on Field
Room T.	1.784 V/µm
100^{O}C	1.641 V/µm
150^{O}C	1.429 V/µm
200^{O}C	0.713 V/µm
250^{O}C	0.713 V/µm
300^{O}C	0.356 V/µm

Table 5.2.2 Turn-on voltages of the Sample B

Sample C has a rectangular shape with 3.5 cm x 1 cm dimensions and short sides are followed by tungsten contact layers. Field emission curves of Sample C from room temperature to 300^{O}C are shown in Figure 5.6 and the turn-on voltage values are given in Table 5.2.3.

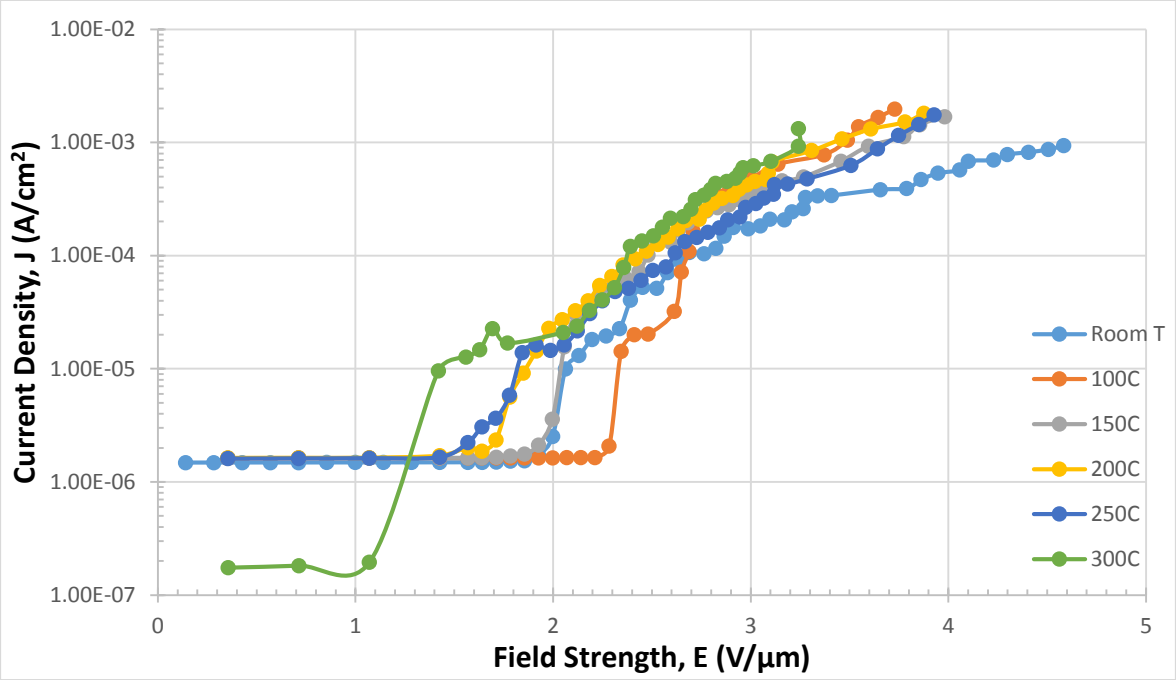

Fig. 5.6 Field emission characteristics of the Sample C for the elevated temperatures

Turn-on voltages of the Sample C

Temperature	Turn-on Field
Room T.	1.856 V/µm
100^{O}C	2.213 V/µm
150^{O}C	1.856 V/µm
200^{O}C	1.641 V/µm
250^{O}C	1.427 V/µm
300^{O}C	1.071 V/µm

Table 5.2.3 Turn-on voltages of the Sample C

Sample D is square shaped with 2.5 cm x 2.5 cm dimensions. Field emission curves of Sample D from room temperature to 300^{O}C are shown in Figure 5.7 and the turn-on voltage values are given in Table 5.2.4.

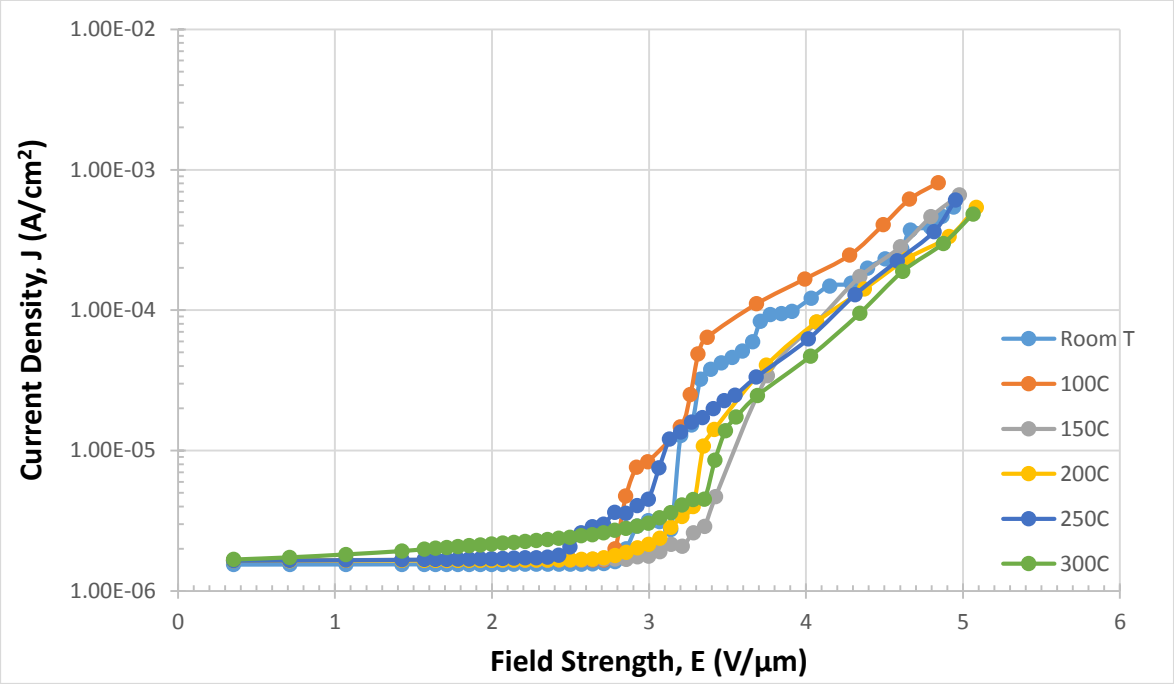

Fig. 5.7 Field emission characteristics of the Sample D for the elevated temperatures

Turn-on voltages of the Sample D

Temperature	Turn-on Field
Room T.	2.784 V/µm
100^{O}C	2.713 V/µm
150^{O}C	2.856 V/µm
200^{O}C	2.641 V/µm
250^{O}C	2.427 V/µm
300^{O}C	1.427 V/µm

Table 5.2.4 Turn-on voltages of the Sample D

The comparison charts of the field emission data of Sample A, B, C, and D for room temperature, 100^{O}C, 150^{O}C, 200^{O}C, 250^{O}C, and 300^{O}C are shown in Figure 5.8, Figure 5.9, Figure 5.10, Figure 5.11, Figure 5.12, and Figure 5.13, respectively.

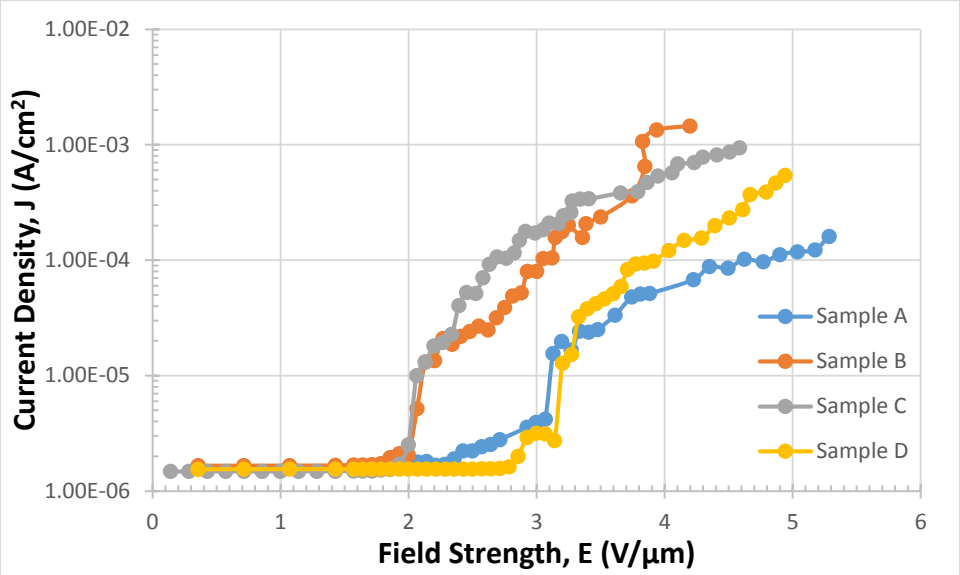

Fig. 5.8 Field emission characteristics of the CNT samples at room temperature

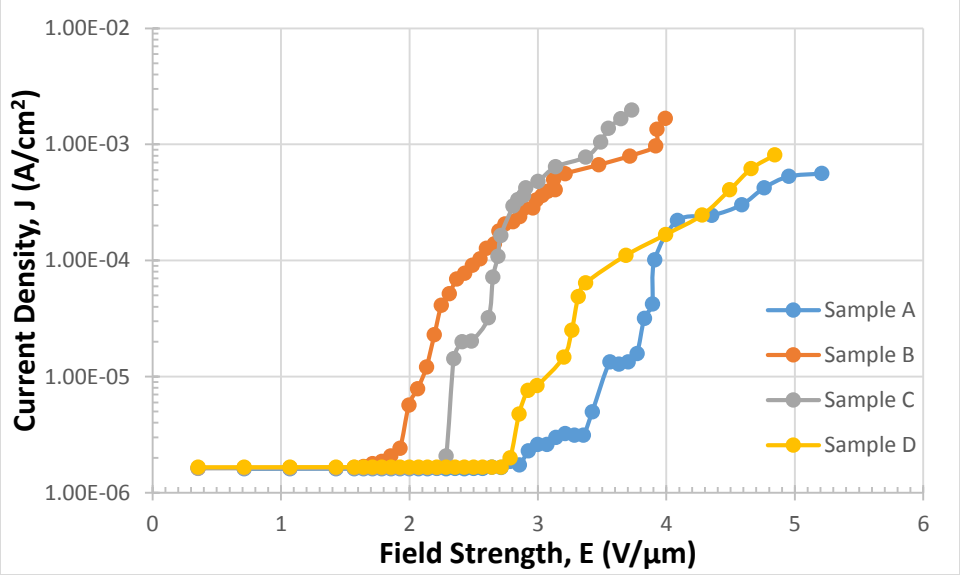

Fig. 5.9 Field emission characteristics of the CNT samples at 100^{O}C

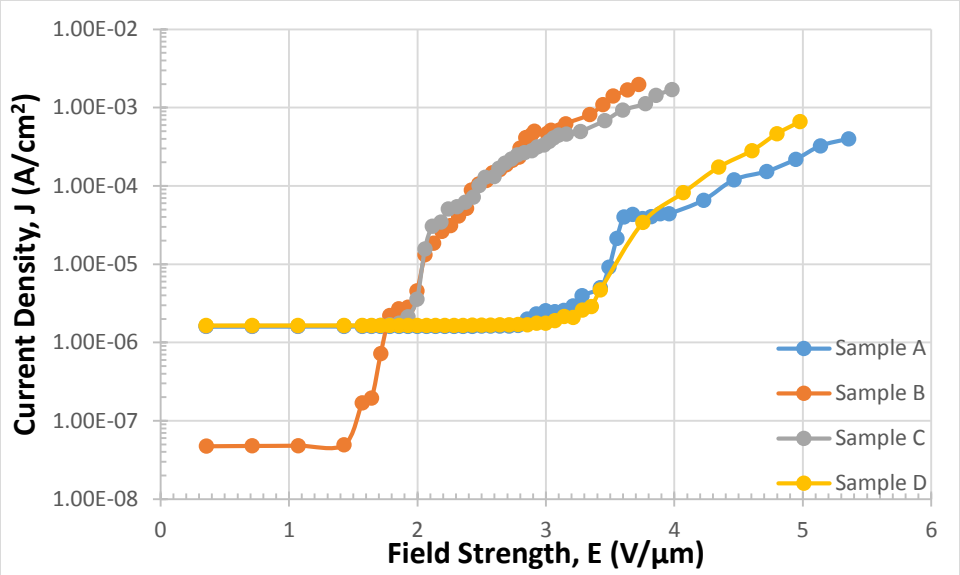

Fig. 5.10 Field emission characteristics of the CNT samples at 150^{O}C

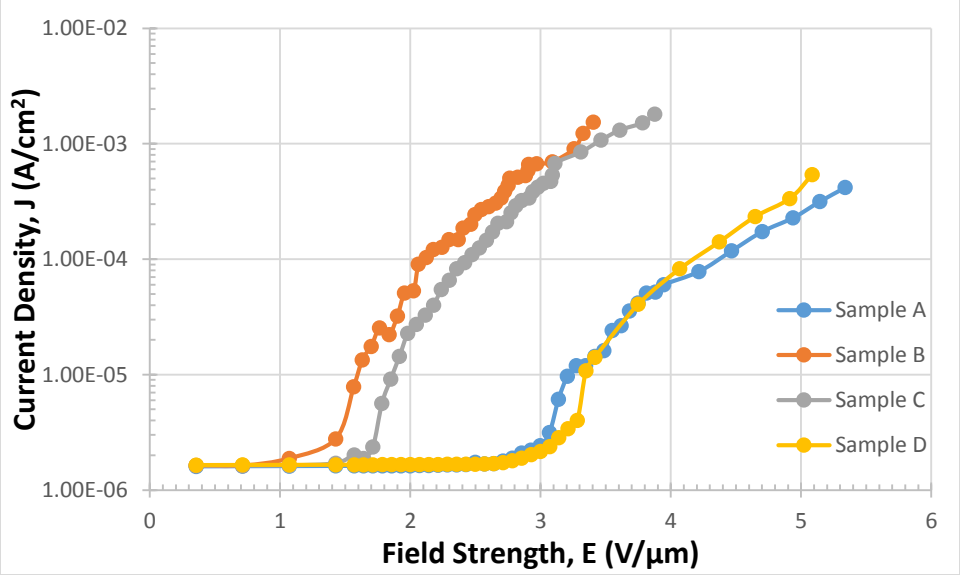

Fig. 5.11 Field emission characteristics of the CNT samples at 200^{O}C

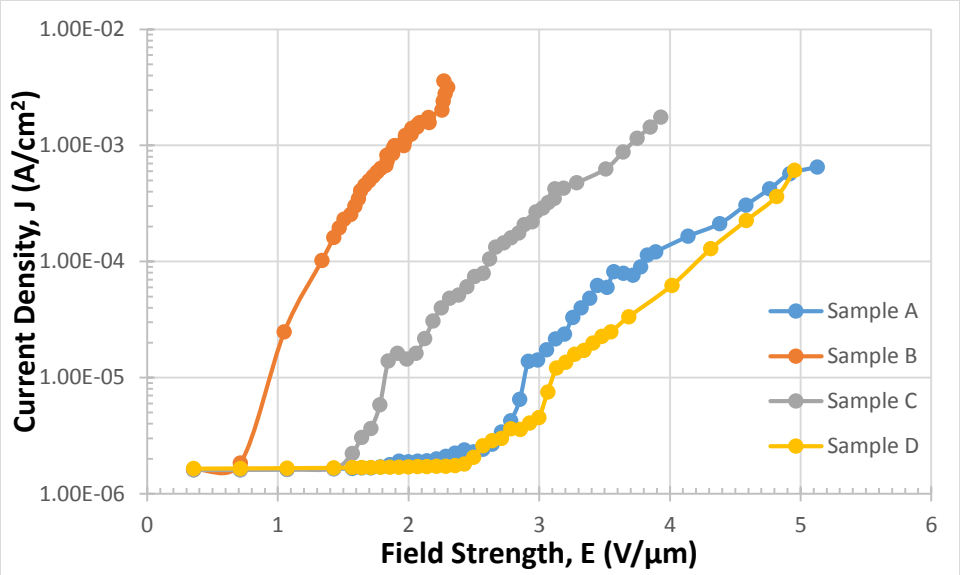

Fig. 5.12 Field emission characteristics of the CNT samples at 250^{O}C

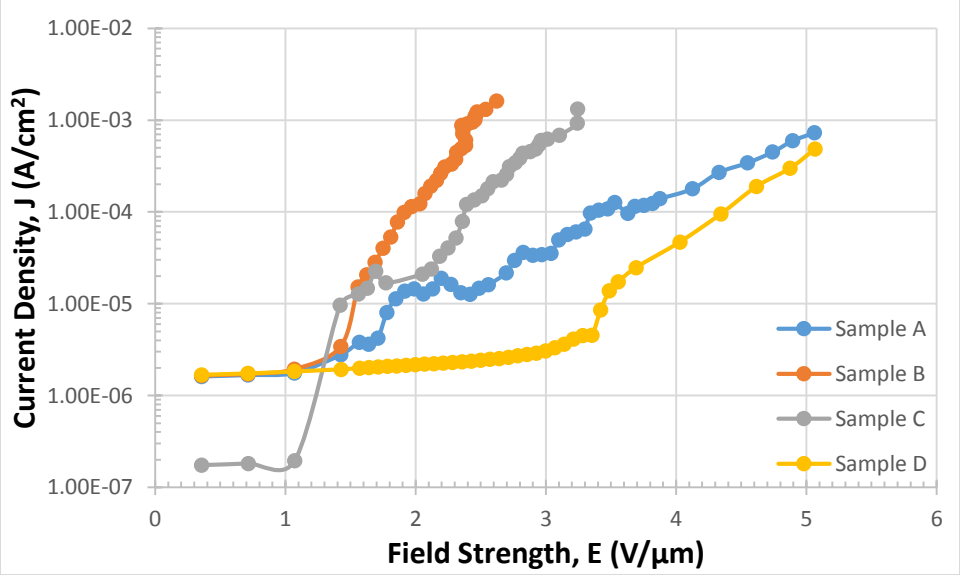

Fig. 5.13 Field emission characteristics of the CNT samples at 300^{O}C

The comparison of the turn-on voltage values from room temperature to 300^{O}C of the CNT samples are given in Table 5.2.5.

Temperature	Turn – on Field			
	Sample A	**Sample B**	**Sample C**	**Sample D**
Room T.	2.284 V/μm	1.784 V/μm	1.856 V/μm	2.784 V/μm
100^{O}C	2.856 V/μm	1.641 V/μm	2.213 V/μm	2.713 V/μm
150^{O}C	2.784 V/μm	1.429 V/μm	1.856 V/μm	2.856 V/μm
200^{O}C	2.641 V/μm	0.713 V/μm	1.641 V/μm	2.641 V/μm
250^{O}C	1.784 V/μm	0.713 V/μm	1.427 V/μm	2.427 V/μm
300^{O}C	1.070 V/μm	0.356 V/μm	1.071 V/μm	1.427 V/μm

Table 5.2.5 Comparison of the turn-on voltages of the CNT samples at elevated temperatures

5.2.3 Discussion

For all samples that are examined in this dissertation, the turn-on voltage decreases with the increasing temperature. There is no specific tendency found on field emission characteristics of the samples depending on the sample shapes and sizes. Sample B -0.75 cm by 0.5 cm rectangular shape- has the lowest turn-on voltage for all temperature levels. The 300^{O}C temperature level has the lowest turn-on voltage values for all samples. For all samples, the turn-on voltages decreased about half of their room temperature values at 300^{O}C. Sample D has the highest turn-on values for all temperature levels regardless of having the largest CNT area. This result confirms the literature data [3], [4], [5], [6]. Another consideration should also be given the fact that not all the fabricated MWCNTs have the same length and/or diameter. This might result with some of the longer and/or sharper nanotubes dominate the field emission in the close area and results with less CNTs available and act as emitters at the surface [7].

Fowler-Nordheim curves of Sample A from room temperature to 300^{O}C are shown in Figure 5.14. Slope and intercept values are found from this figure and field enhancement factors are calculated and results are shown in Table 5.2.6.

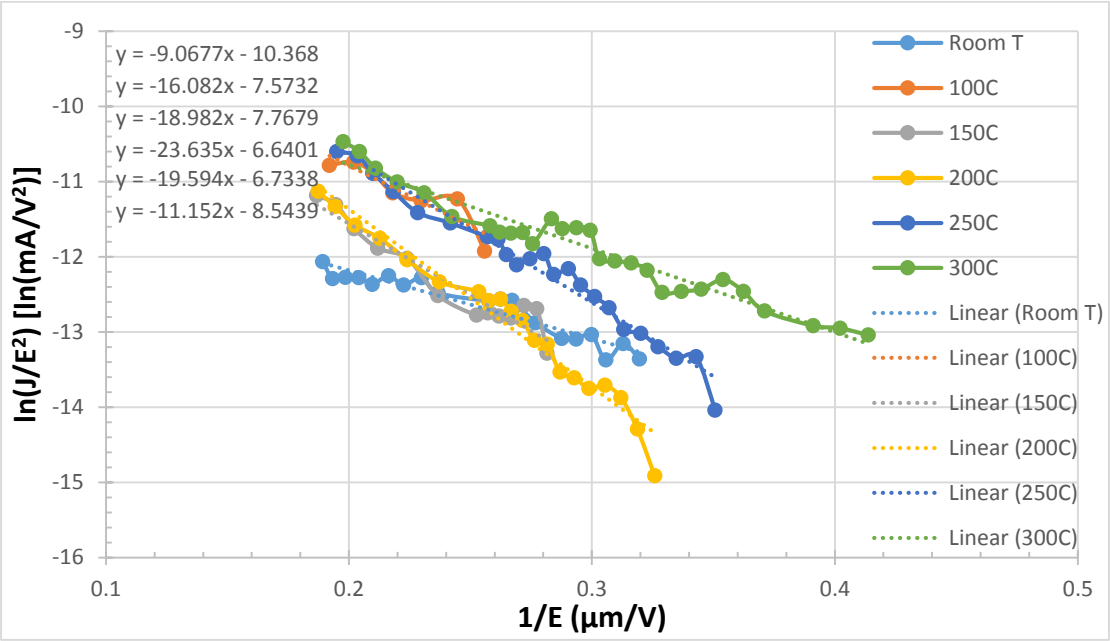

Fig. 5.14 Fowler-Nordheim curves of the Sample A for the elevated temperatures

Temperature	Slope	Intercept	β – Field Enhancement Factor
Room T.	- 9.0677	-10.37	8421
100^{O}C	- 16.082	-7.573	4748
150^{O}C	- 18.982	-7.768	4023
200^{O}C	- 23.635	-6.640	3231
250^{O}C	- 19.594	-6.734	3897
300^{O}C	- 11.152	-8.544	6847

Table 5.2.6 Slope, intercept, and field enhancement factor values of the Sample A for the elevated temperatures

Fowler-Nordheim curves of Sample B from room temperature to 300^{O}C are shown in Figure 5.15. Slope and intercept values are found from this figure and field enhancement factors are calculated and results are shown in Table 5.2.7.

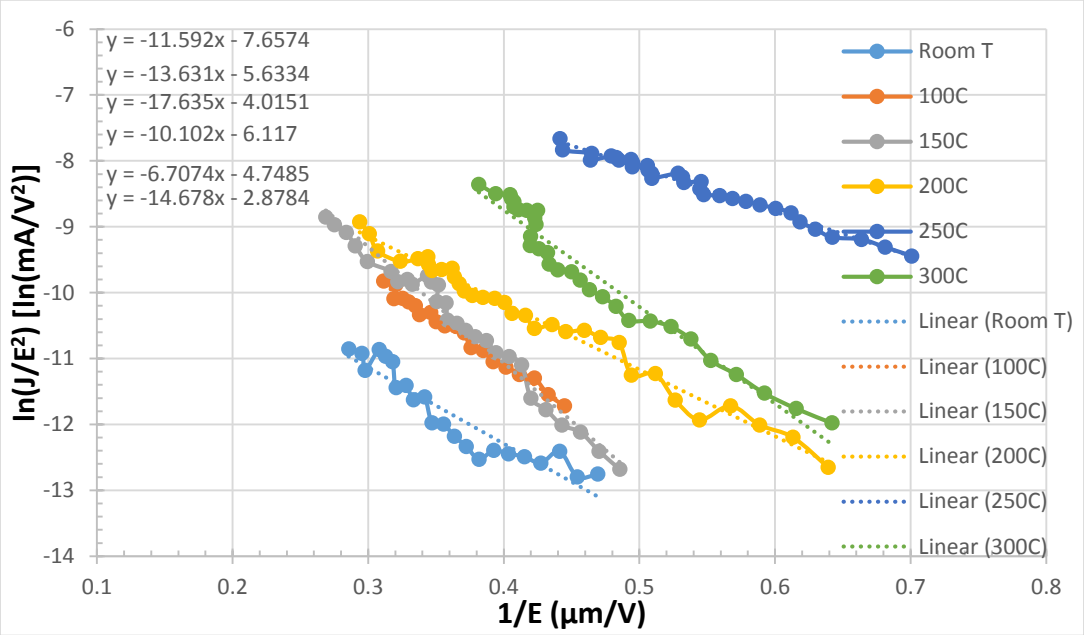

Fig. 5.15 Fowler-Nordheim curves of the Sample B for the elevated temperatures

Temperature	Slope	Intercept	β – Field Enhancement Factor
Room T.	- 11.592	-7.657	6587
100^{O}C	- 13.631	-5.633	5602
150^{O}C	- 17.635	-4.015	4330
200^{O}C	10.102	-6.117	7559
250^{O}C	- 6.707	-4.749	11385
300^{O}C	- 14.678	-2.878	5202

Table 5.2.7 Slope, intercept, and field enhancement factor values of the Sample B for the elevated temperatures

Fowler-Nordheim curves of Sample C from room temperature to 300^{O}C are shown in Figure 5.16. Slope and intercept values are found from this figure and field enhancement factors are calculated and results are shown in Table 5.2.8.

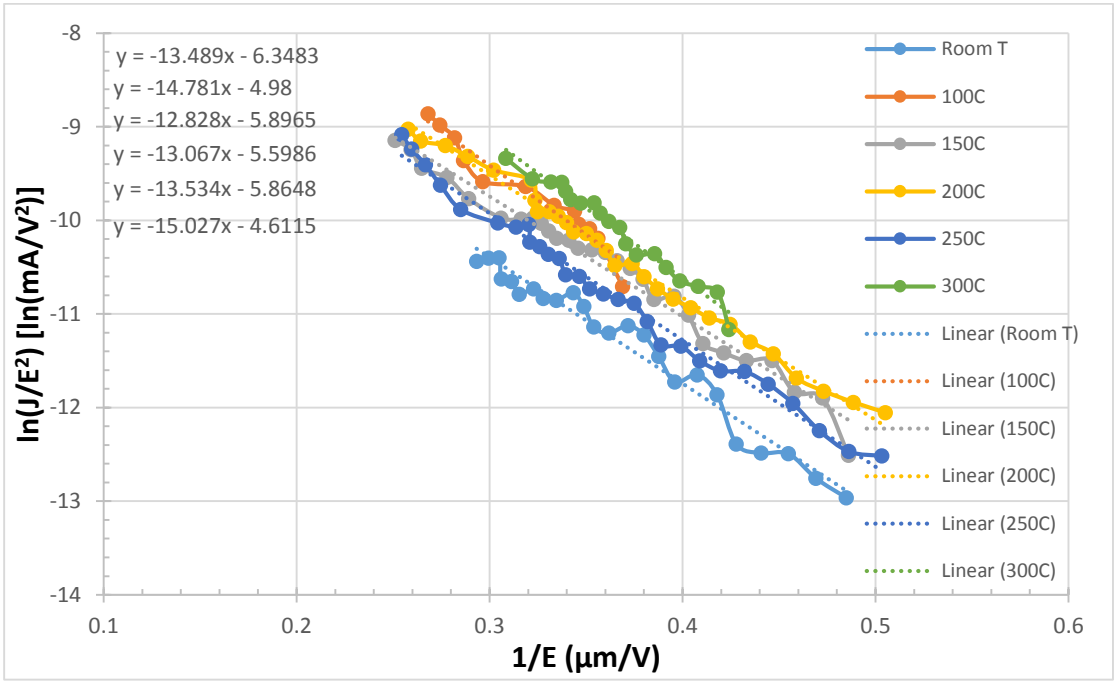

Fig. 5.16 Fowler-Nordheim curves of the Sample C for the elevated temperatures

Temperature	Slope	Intercept	β – Field Enhancement Factor
Room T.	-13.489	-6.348	5661
100^{O}C	-14.781	-4.980	5166
150^{O}C	-12.828	-5.897	5953
200^{O}C	-13.067	-5.599	5844
250^{O}C	-13.534	-5.865	5642
300^{O}C	-15.027	-4.611	5082

Table 5.2.8 Slope, intercept, and field enhancement factor values of the Sample C for the elevated temperatures

Fowler-Nordheim curves of Sample D from room temperature to 300^{O}C are shown in Figure 5.17. Slope and intercept values are found from this figure and field enhancement factors are calculated and results are shown in Table 5.2.9.

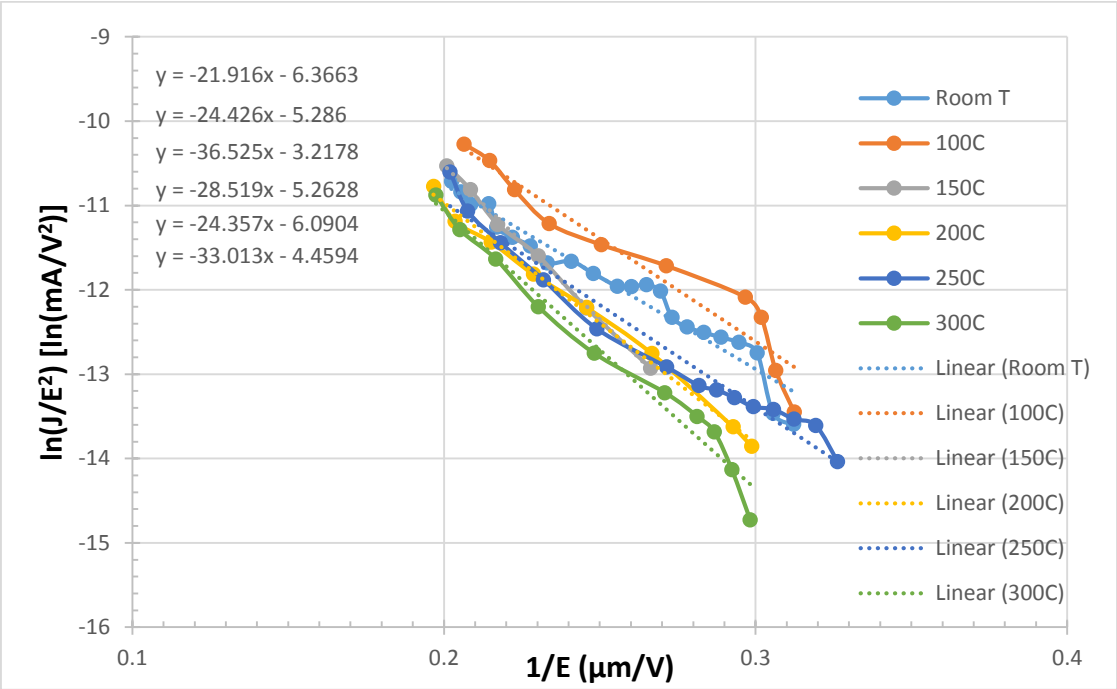

Fig. 5.17 Fowler-Nordheim curves of the Sample D for the elevated temperatures

Temperature	Slope	Intercept	β – Field Enhancement Factor
Room T.	-21.916	-6.366	3484
100^{O}C	-24.426	-5.286	3126
150^{O}C	-36.525	-3.218	2091
200^{O}C	-28.519	-5.263	2678
250^{O}C	-24.357	-6.090	3135
300^{O}C	-33.013	-4.459	2313

Table 5.2.9 Slope, intercept, and field enhancement factor values of the Sample D for the elevated temperatures

The comparison charts of the Fowler-Nordheim data of Sample A, B, C, and D for room temperature, 100^{O}C, 150^{O}C, 200^{O}C, 250^{O}C, and 300^{O}C are shown in Figure 5.18, Figure 5.19, Figure 5.20, Figure 5.21, Figure 5.22, and Figure 5.23, respectively.

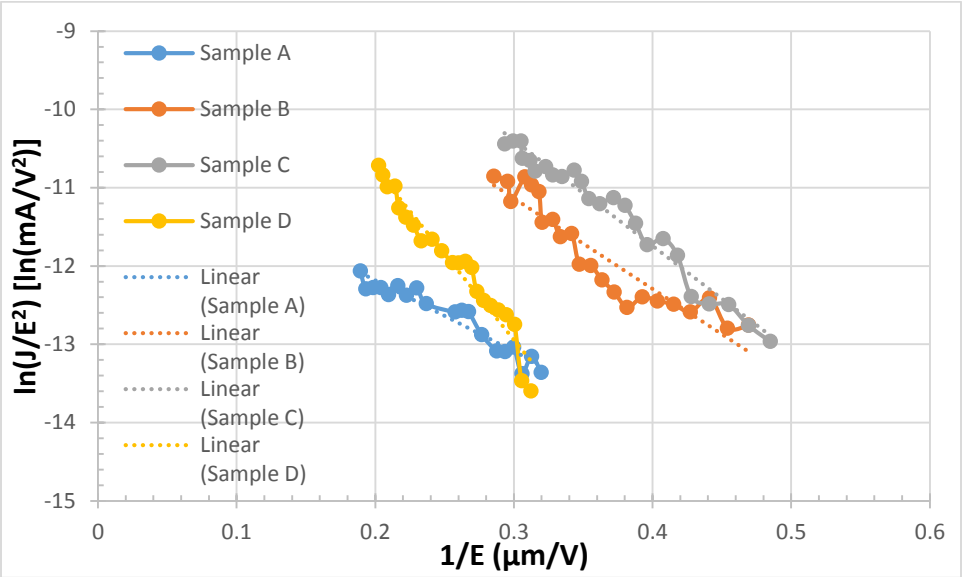

Fig. 5.18 Fowler-Nordheim characteristics of the CNT samples at room temperature

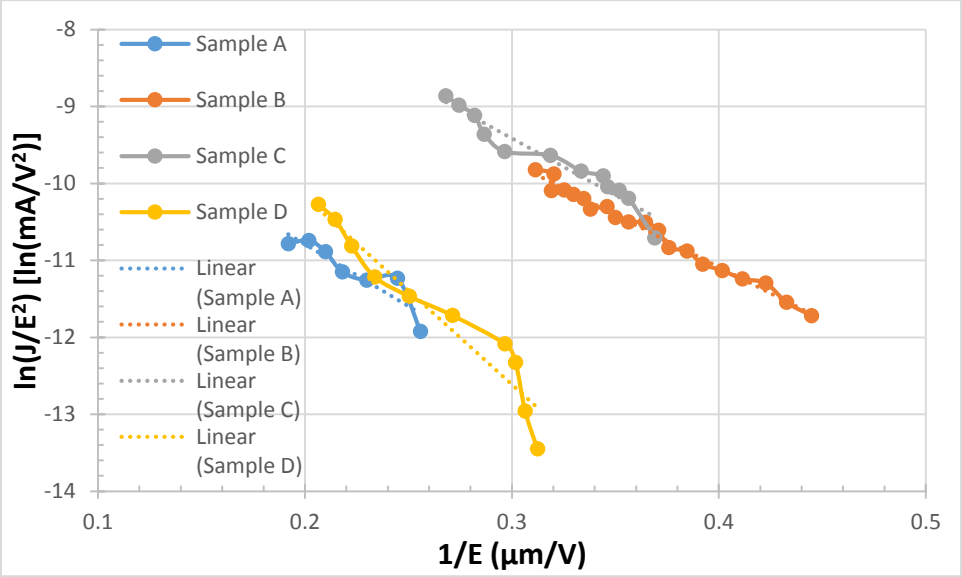

Fig. 5.19 Fowler-Nordheim characteristics of the CNT samples at 100^{O}C

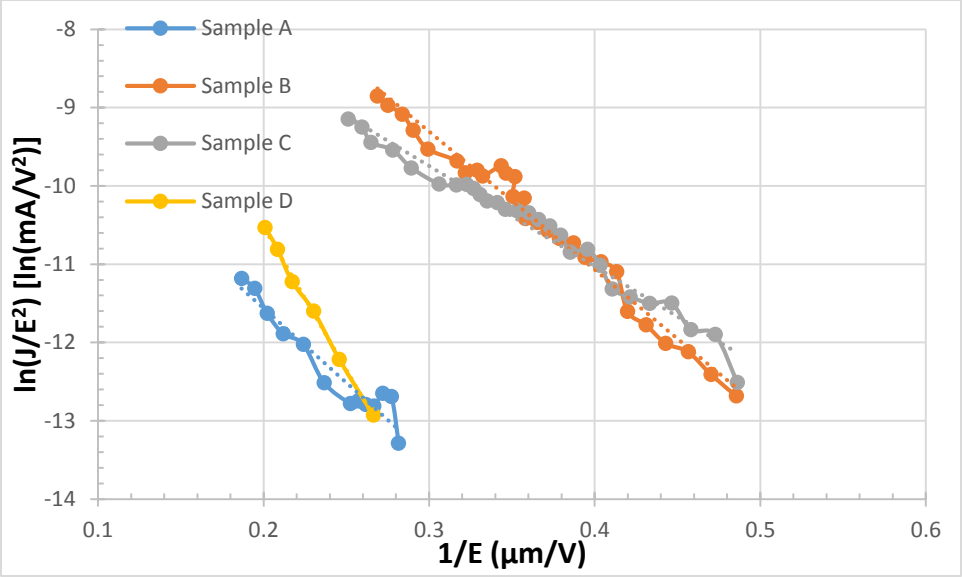

Fig. 5.20 Fowler-Nordheim characteristics of the CNT samples at 150^{O}C

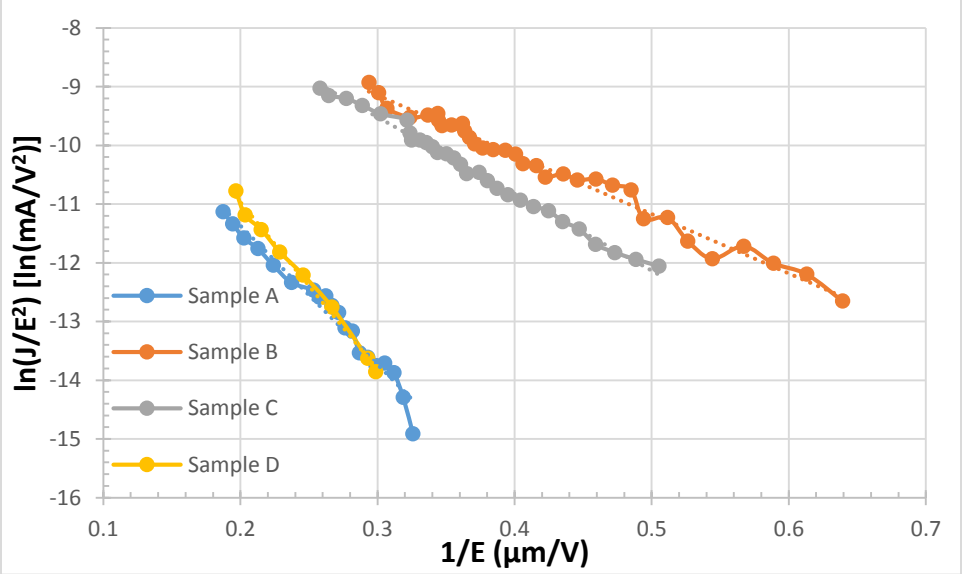

Fig. 5.21 Fowler-Nordheim characteristics of the CNT samples at 200^{O}C

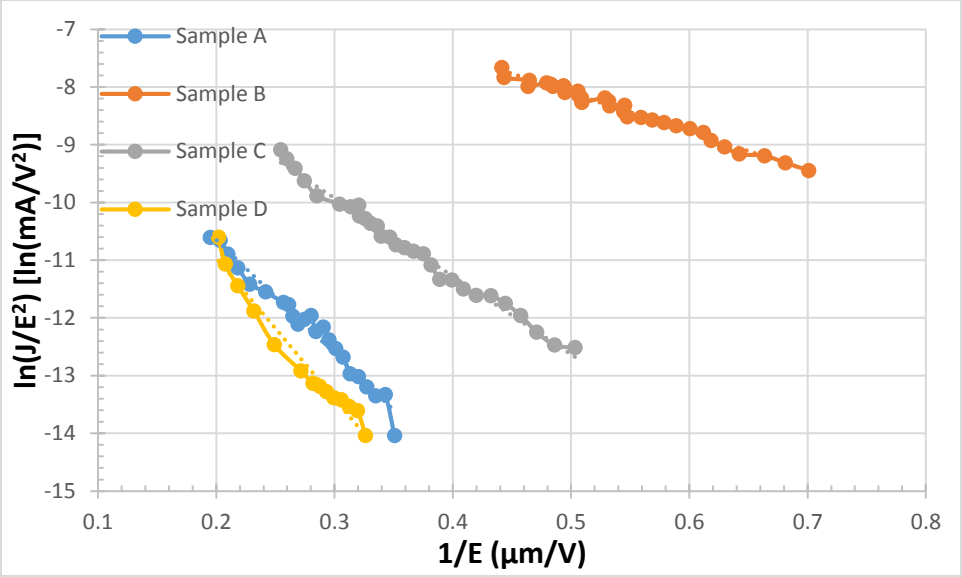

Fig. 5.22 Fowler-Nordheim characteristics of the CNT samples at 250^{O}C

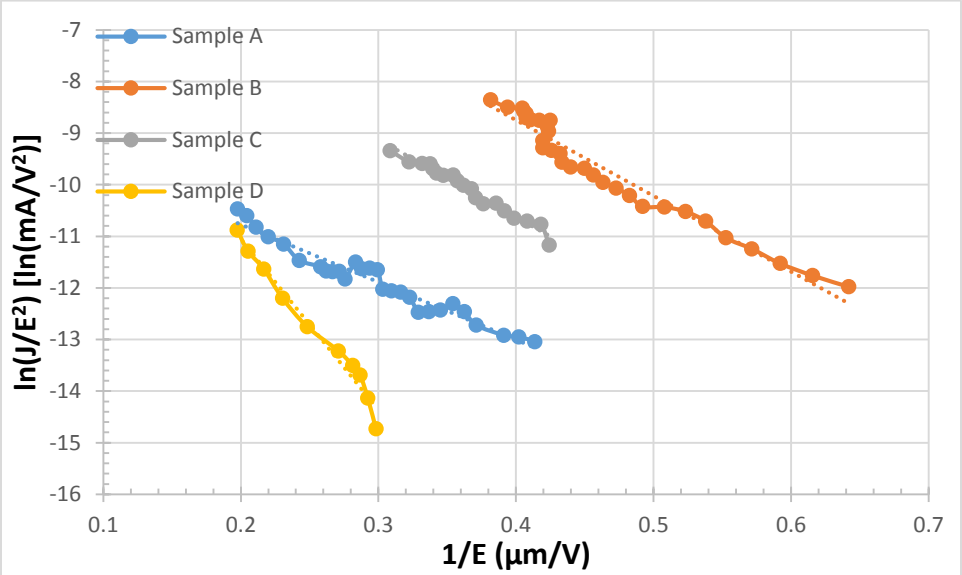

Fig. 5.23 Fowler-Nordheim characteristics of the CNT samples at 300^{O}C

The comparison of slope, intercept, and field enhancement factor values from room temperature to 300^{O}C of the CNT samples are given in Table 5.2.10.

Temp.	Slope				Intercept				β – Field Enhancement Factor			
	Sample A	Sample B	Sample C	Sample D	Sample A	Sample B	Sample C	Sample D	Sample A	Sample B	Sample C	Sample D
Room T	-9.0677	-11.592	-13.489	-21.916	-10.37	-7.657	-6.348	-6.366	8421	6587	5661	3484
100^{O}C	-16.082	-13.631	-14.781	-24.426	-7.573	-5.633	-4.980	-5.286	4748	5602	5166	3126
150 ^{O}C	-18.982	-17.635	-12.828	-36.525	-7.768	-4.015	-5.897	-3.218	4023	4330	5953	2091
200 ^{O}C	-23.635	-10.102	-13.067	-28.519	-6.640	-6.117	-5.599	-5.263	3231	7559	5844	2678
250 ^{O}C	-19.594	-6.707	-13.534	-24.357	-6.734	-4.749	-5.865	-6.090	3897	11385	5642	3135
300 ^{O}C	-11.152	-14.678	-15.027	-33.013	-8.544	-2.878	-4.611	-4.459	6847	5202	5082	2313

Table 5.2.10 Comparison of the slope, intercept, and field enhancement factor values of the CNT samples at elevated temperatures

Sample A with 0.35 cm^2 CNT area has the biggest field enhancement factor at room temperatures. Sample B and sample C follow sample A and have the second and third biggest field enhancement factors, respectively at room temperatures. Lastly, sample D with 2.5 cm^2 area, the largest fabricated CNT area, has the smallest field enhancement factor among them in comparison at room temperature. This comparison is also true for 300^OC test results. Although these results show that the field enhancement factor decreases with increasing pattern size at room temperature and 300^OC, when we look at the other elevated temperature results, the field enhancement factor does not show a consistent arrangement depending on the sample size and patterning. This confirms that even the patterning might affect the effective emission area of the samples, there are more parameters such as CNT tip shape, space charge effect, voltage dependence, and others, to consider while examining F-N results. Sample D, with the largest fabricated CNT area, has the biggest slope values at all temperatures from room temperature to 300^OC and Sample A, the smallest pattern size sample, has the smallest intercept values at all temperatures from room temperature to 300^OC as it can be seen at Table 5.2.10.

5.3 Tungsten under-layer Thickness measurements using AFM and SEM Images of CNTs

Tungsten (W) is a conducting material with extremely low vapor pressure and low contact to surface resistance even at high temperature, radiation, electric arc, humidity, and under vacuum conditions. These properties make it a great electrical contact material over the other conductive metals such as copper and silver [13]. We used W thin film under-layer as the contact pad in our experiments. This part of the dissertation compares the effect of the W thin film thickness over the field emission characteristics of MWCNTs. For this purpose, we fabricated four different samples on both silicon and ceramic substrates and each sample is tested for its field emissions using a) the fabricated CNT area as the cathode and b) the W contact pad area to the cathode. The other experimental parameters are kept the same. The first set of samples are with silicon samples and are named as Sample 1A, Sample 1B, Sample 2A, Sample 2B, Sample 3A, Sample 3B, Sample 4A and Sample 4B as it is shown in Table 5.3.1.

Comparison of CNT samples with different W under-layer thicknesses

Sample Name	W Sputtering Time	Cathode Contact	CNT Formation
1A	1 minute	CNT	Random
1B	1 minute	W pad	Random
2A	3 minutes	CNT	Random
2B	3 minutes	W pad	Random
3A	5 minutes	CNT	N/A
3B	5 minutes	W pad	N/A
4A	8 minutes	CNT	N/A
4B	8 minutes	W pad	N/A

Table 5.3.1 Comparison of CNT samples with different W under-layer thicknesses grown on Silicon Substrate

As it can be seen in the above table, the samples with 5 minutes and 8 minutes W sputtering onto the substrate didn't form any CNT structures. This is because W reacts with Si and forms tungsten silicide (WSi_2) [14], [15]. After a certain thickness is reached the Fe catalyst islands cannot form on WSi_2 and CNT growth doesn't occur. Figure 5.24 shows the 1 minute W sputtered thin film thickness AFM results that are taken from three different points and is approximately 5 nm.

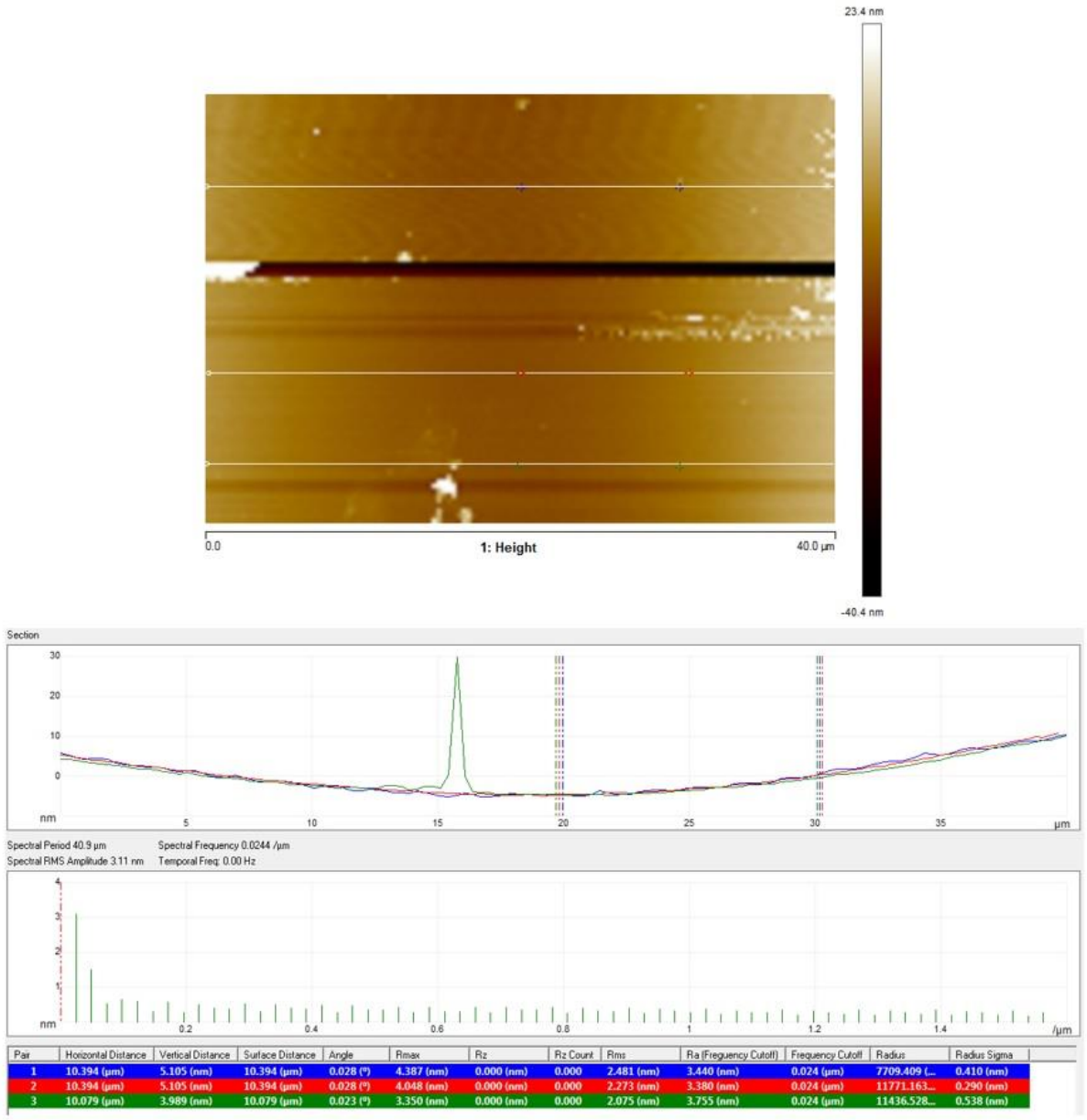

Pair	Horizontal Distance	Vertical Distance	Surface Distance	Angle	Rmax	Rz	Rz Count	Rms	Ra (Frequency Cutoff)	Frequency Cutoff	Radius	Radius Sigma
1	10.394 (µm)	5.105 (nm)	10.394 (µm)	0.028 (°)	4.387 (nm)	0.000 (nm)	0.000	2.481 (nm)	3.440 (nm)	0.024 (µm)	7709.409 (...	0.410 (nm)
2	10.394 (µm)	5.105 (nm)	10.394 (µm)	0.028 (°)	4.048 (nm)	0.000 (nm)	0.000	2.273 (nm)	3.380 (nm)	0.024 (µm)	11771.163...	0.290 (nm)
3	10.079 (µm)	3.989 (nm)	10.079 (µm)	0.023 (°)	3.350 (nm)	0.000 (nm)	0.000	2.075 (nm)	3.755 (nm)	0.024 (µm)	11436.528...	0.538 (nm)

Fig. 5.24 AFM results of 1 minute W sputtered sample

3 minutes W sputtered thin film thickness AFM results that also are taken from three different points and is approximately 12 nm as it is shown in Figure 5.25.

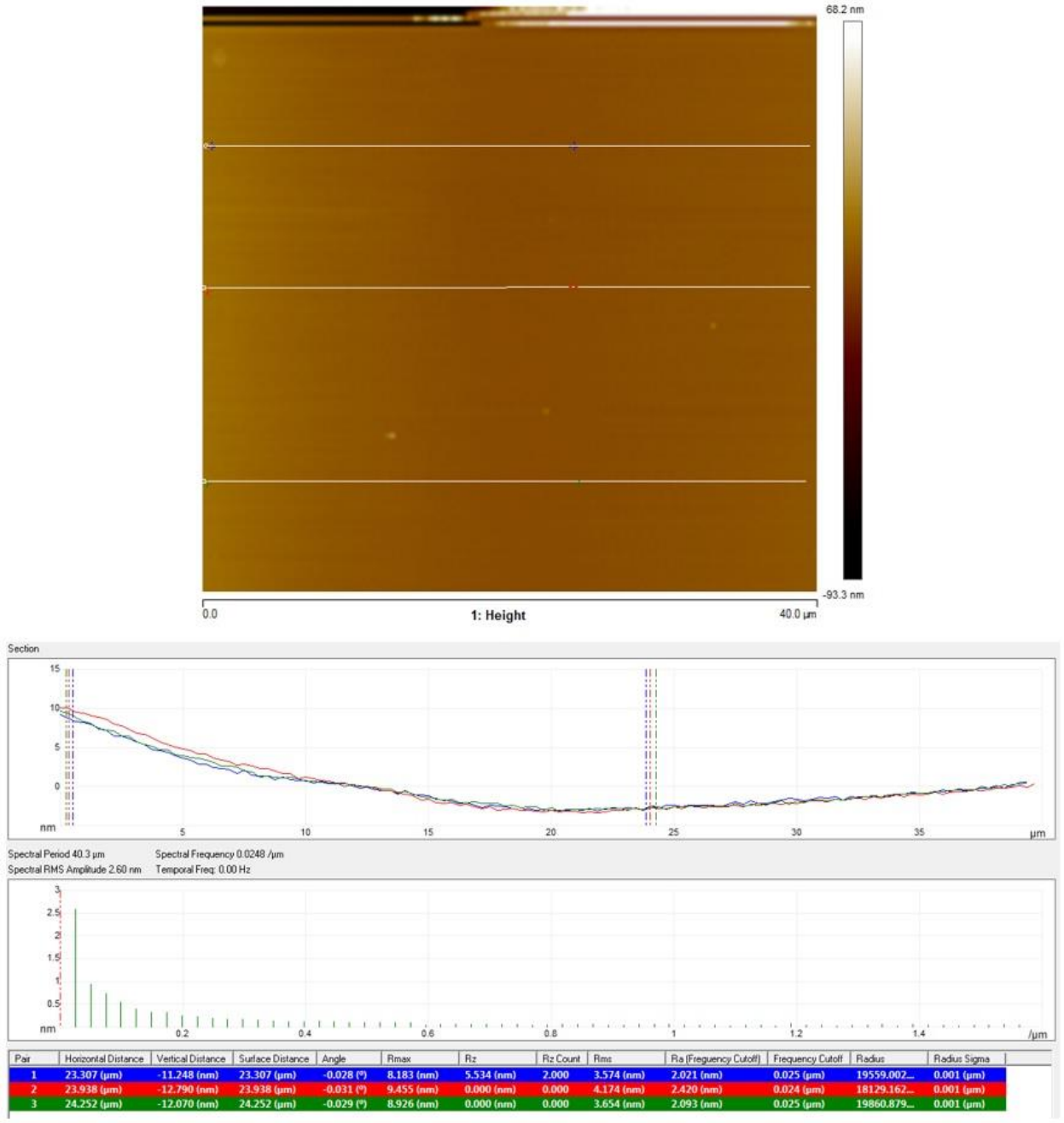

Pair	Horizontal Distance	Vertical Distance	Surface Distance	Angle	Rmax	Rz	Rz Count	Rms	Ra (Frequency Cutoff)	Frequency Cutoff	Radius	Radius Sigma
1	23.307 (µm)	-11.248 (nm)	23.307 (µm)	-0.028 (°)	8.183 (nm)	5.534 (nm)	2.000	3.574 (nm)	2.021 (nm)	0.025 (µm)	19559.002...	0.001 (µm)
2	23.938 (µm)	-12.790 (nm)	23.938 (µm)	-0.031 (°)	9.455 (nm)	0.000 (nm)	0.000	4.174 (nm)	2.420 (nm)	0.024 (µm)	18129.162...	0.001 (µm)
3	24.252 (µm)	-12.070 (nm)	24.252 (µm)	-0.029 (°)	8.926 (nm)	0.000 (nm)	0.000	3.654 (nm)	2.093 (nm)	0.025 (µm)	19860.879...	0.001 (µm)

Fig. 5.25 AFM results of 3 minutes W sputtered sample

5 minutes W sputtered thin film thickness AFM results that also are taken from three different points and is approximately 15 nm as it is shown in Figure 5.26.

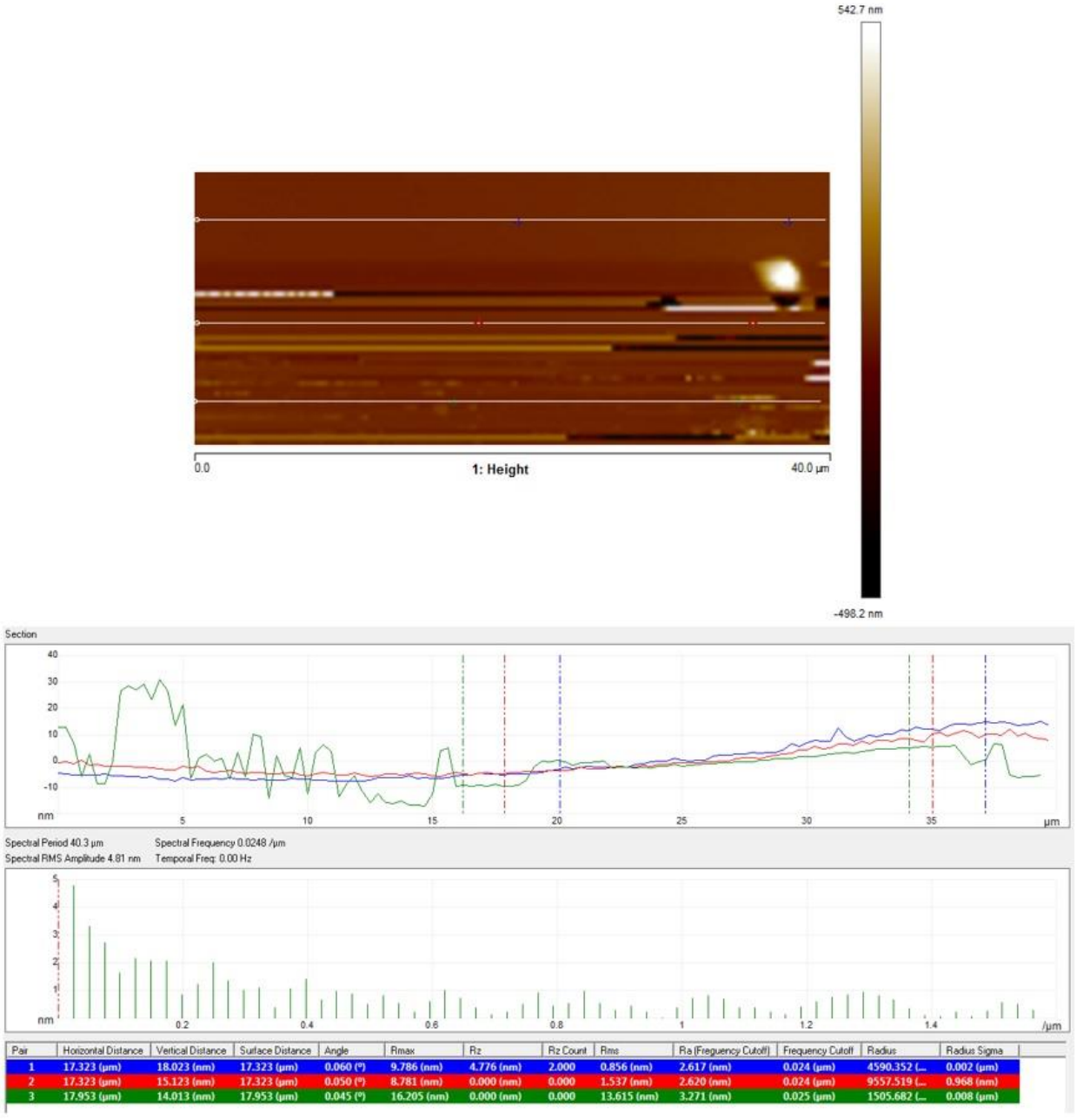

Pair	Horizontal Distance	Vertical Distance	Surface Distance	Angle	Rmax	Rz	Rz Count	Rms	Ra (Frequency Cutoff)	Frequency Cutoff	Radius	Radius Sigma
1	17.323 (µm)	18.023 (nm)	17.323 (µm)	0.060 (°)	9.786 (nm)	4.776 (nm)	2.000	0.856 (nm)	2.617 (nm)	0.024 (µm)	4590.352 (...	0.002 (µm)
2	17.323 (µm)	15.123 (nm)	17.323 (µm)	0.050 (°)	8.781 (nm)	0.000 (nm)	0.000	1.537 (nm)	2.620 (nm)	0.024 (µm)	9557.519 (...	0.968 (nm)
3	17.953 (µm)	14.013 (nm)	17.953 (µm)	0.045 (°)	16.205 (nm)	0.000 (nm)	0.000	13.615 (nm)	3.271 (nm)	0.025 (µm)	1505.682 (...	0.008 (µm)

Fig. 5.26 AFM results of 5 minutes W sputtered sample

8 minutes W sputtered thin film thickness AFM is approximately 25 nm and it is shown in Figure 5.27.

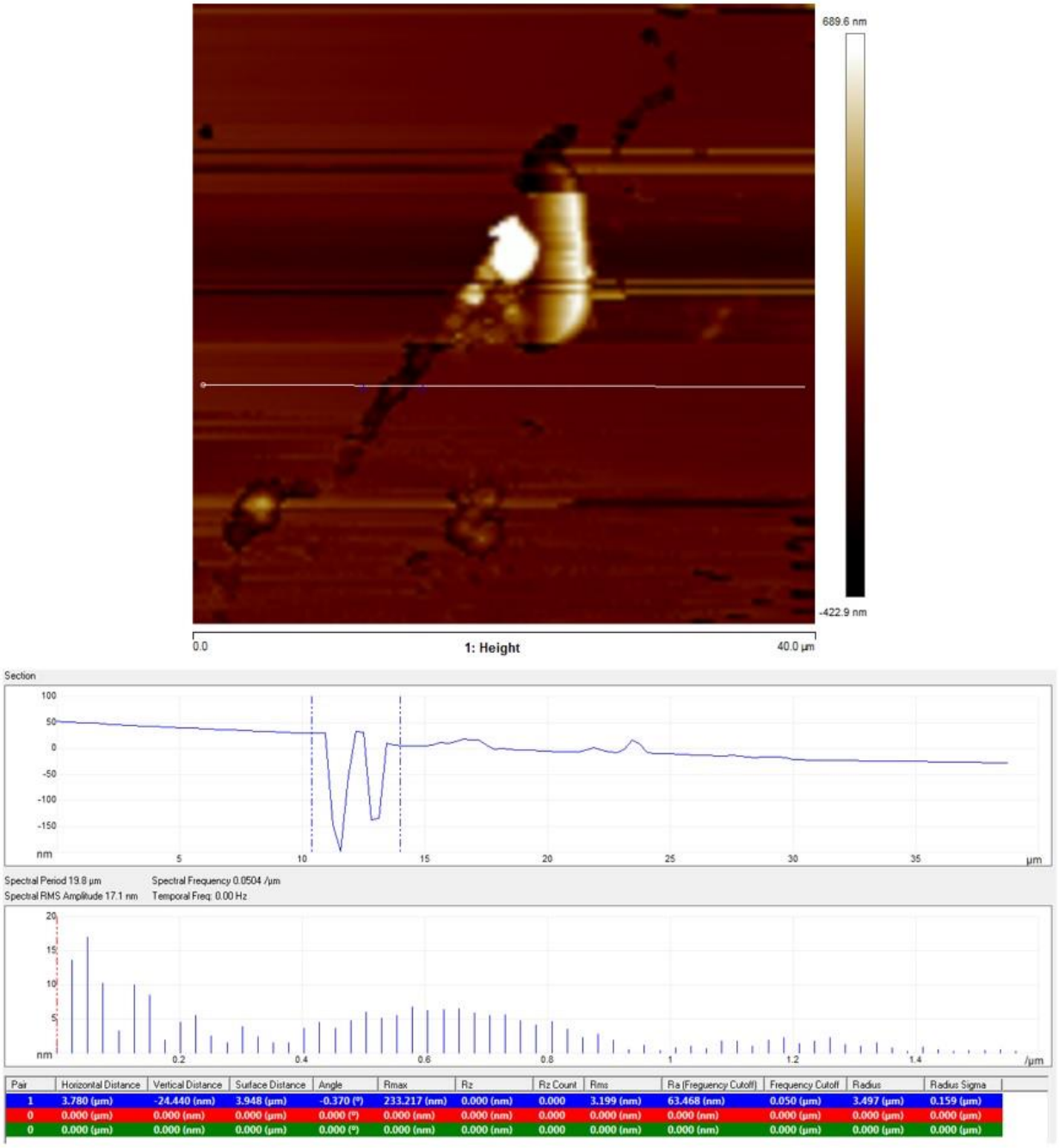

Pair	Horizontal Distance	Vertical Distance	Surface Distance	Angle	Rmax	Rz	Rz Count	Rms	Ra (Frequency Cutoff)	Frequency Cutoff	Radius	Radius Sigma
1	3.780 (µm)	-24.440 (nm)	3.948 (µm)	-0.370 (°)	233.217 (nm)	0.000 (nm)	0.000	3.199 (nm)	63.468 (nm)	0.050 (µm)	3.497 (µm)	0.159 (µm)
0	0.000 (µm)	0.000 (nm)	0.000 (µm)	0.000 (°)	0.000 (nm)	0.000 (nm)	0.000	0.000 (nm)	0.000 (nm)	0.000 (µm)	0.000 (µm)	0.000 (µm)
0	0.000 (µm)	0.000 (nm)	0.000 (µm)	0.000 (°)	0.000 (nm)	0.000 (nm)	0.000	0.000 (nm)	0.000 (nm)	0.000 (µm)	0.000 (µm)	0.000 (µm)

Fig. 5.27 AFM results of 8 minutes W sputtered sample

5.3.1 AFM Measurement of Tungsten under-layer on Ceramic

An 8 minutes W under layer sputtered and 0.5 cm by 0.5 cm patterned ceramic sample AFM thickness measurement is also done and the approximate thickness is found as 35 nm in Figure 5.28. 3D images of the same sample is also shown in Figure 5.29.

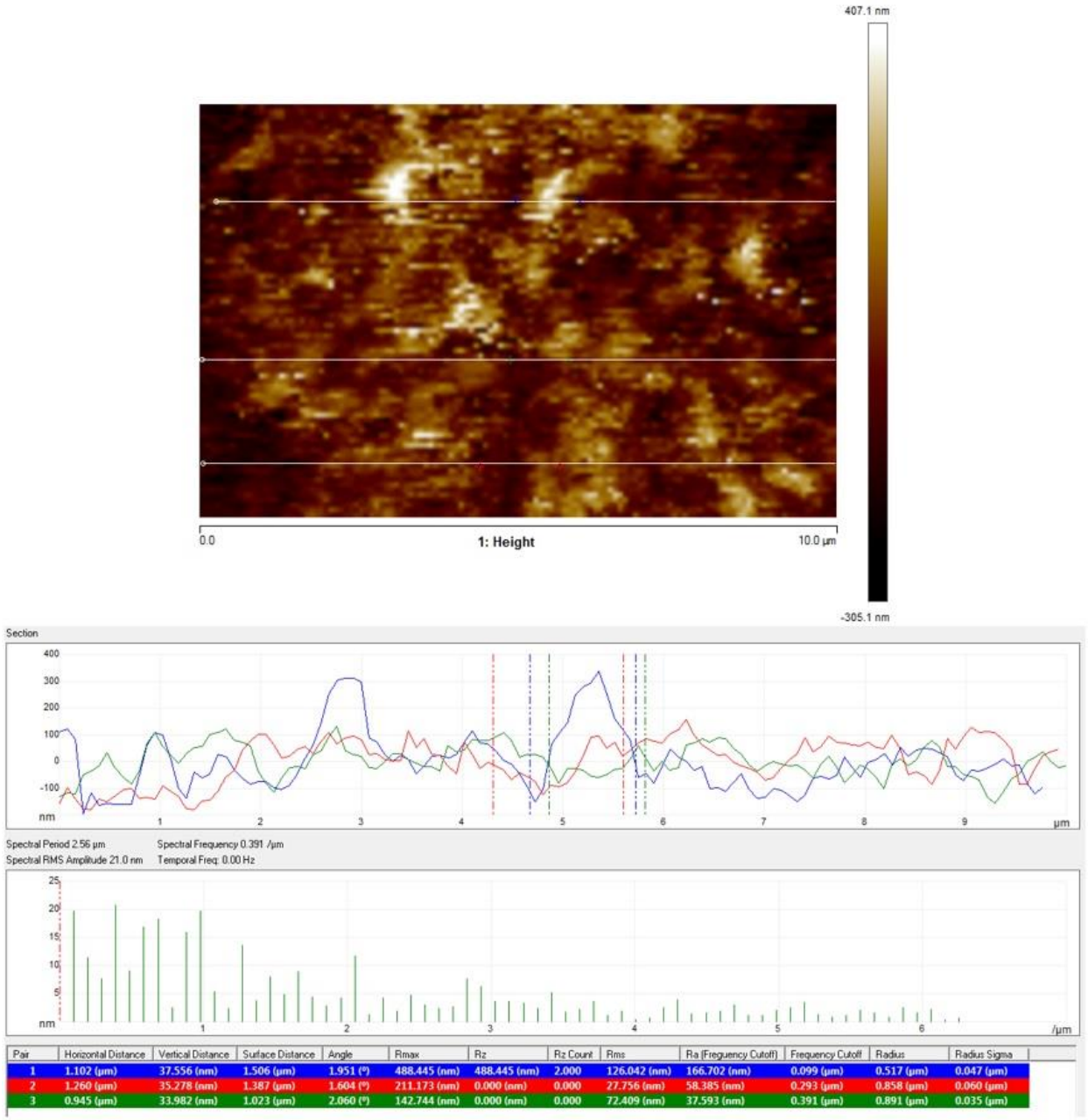

Pair	Horizontal Distance	Vertical Distance	Surface Distance	Angle	Rmax	Rz	Rz Count	Rms	Ra (Frequency Cutoff)	Frequency Cutoff	Radius	Radius Sigma
1	1.102 (µm)	37.556 (nm)	1.506 (µm)	1.951 (°)	488.445 (nm)	488.445 (nm)	2.000	126.042 (nm)	166.702 (nm)	0.099 (µm)	0.517 (µm)	0.047 (µm)
2	1.260 (µm)	35.278 (nm)	1.387 (µm)	1.604 (°)	211.173 (nm)	0.000 (nm)	0.000	27.756 (nm)	58.385 (nm)	0.293 (µm)	0.858 (µm)	0.060 (µm)
3	0.945 (µm)	33.982 (nm)	1.023 (µm)	2.060 (°)	142.744 (nm)	0.000 (nm)	0.000	72.409 (nm)	37.593 (nm)	0.391 (µm)	0.891 (µm)	0.035 (µm)

Fig. 5.28 AFM results of 8 minutes W sputtered ceramic sample

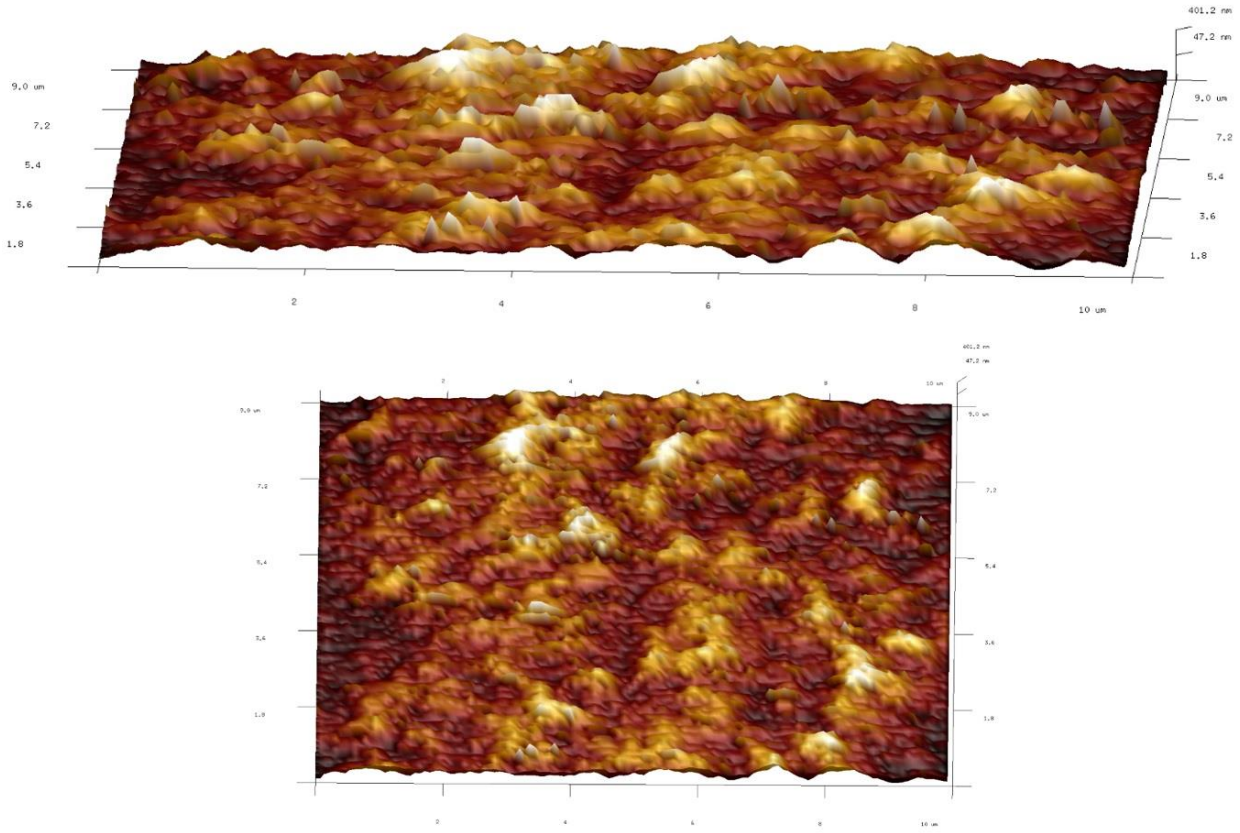

Fig. 5.29 3D AFM results of 8 minutes W sputtered ceramic sample

5.3.2 Field Emission Test Results and Discussion

As it can be concluded from the AFM results that MWCNT growth was not possible over the thickness of 15 nm W under layer thin films on Si substrates. Hence, we couldn't get any field emission results from Sample 3A, Sample 3B, Sample 4A, and Sample 4B. For Sample 1A, Sample 1B, Sample 2A, and Sample 2B, the field emission characteristics measured and Fowler - Nordheim plots are generated with the same methodology explained in Sections 4.1 and 5.3. The comparison of the field emission curves of the samples are shown in Figure 5.30 and the turn-on voltage values for all samples are given in Table 5.3.2.

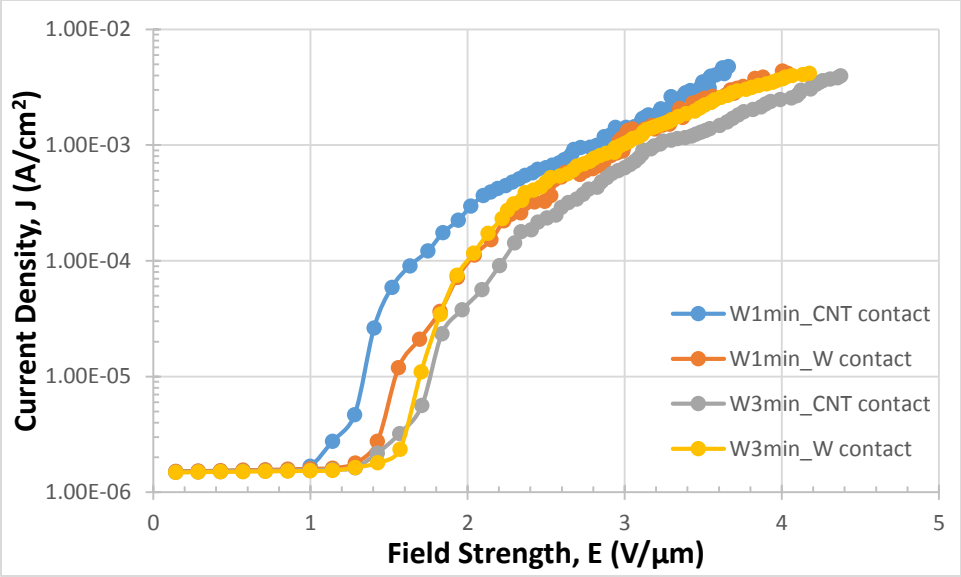

Fig. 5.30 Field emission characteristics of the CNT samples

Turn-on voltages of the CNT samples

Sample Name	Turn-on Field
Sample 1A	0.856 V/µm
Sample 1B	1.141 V/µm
Sample 2A	1.284 V/µm
Sample 2B	1.141 V/µm

Table 5.3.2 Turn-on voltages of the CNT samples

Sample 1A -one minute W sputtered under layer thin film with CNT cathode contact point- has the lowest turn on voltage of 0.856 V/µm. Sample 1B and Sample 2B, both with W pad cathode contact point and one minute and three minutes W sputtered under layer thin film, respectively, have the same turn-on voltage 1.141 V/µm. Lastly, Sample 2A -three minute W sputtered under

layer thin film with CNT cathode contact point has the highest turn-on voltage of 1.284 V/μm, although it is very close to the other samples.

The comparison of Fowler-Nordheim curves of the samples are shown in Figure 5.31. Slope and intercept values are found from this figure and field enhancement factors are calculated and results are shown in Table 5.3.3.

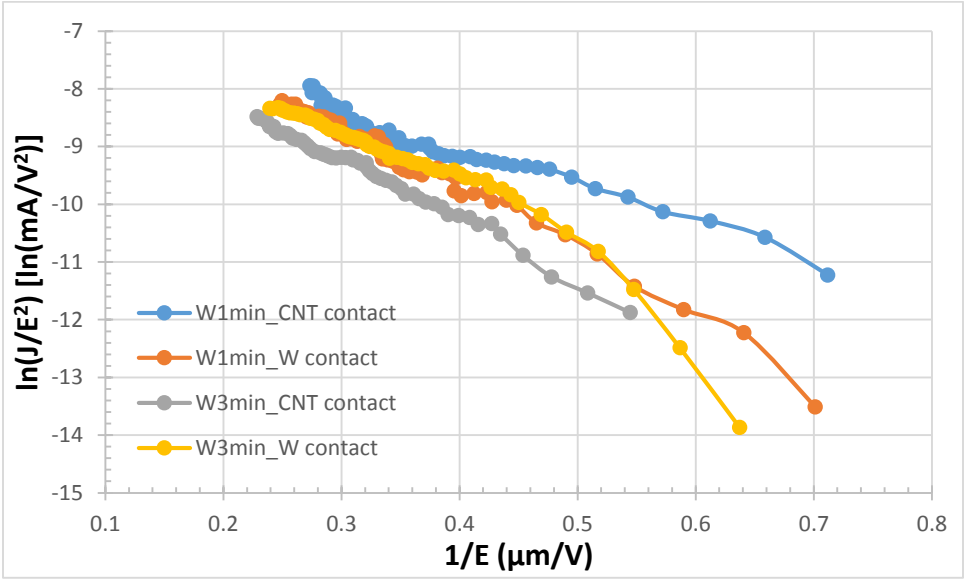

Fig. 5.31 Fowler-Nordheim Curves of the CNT samples

Sample Name	Slope	Intercept	β – Field Enhancement Factor
1A	-6.530	-6.461	11694
1B	-10.536	-5.544	7248
2A	-10.268	-6.146	7437
2B	-10.687	-5.511	7145

Table 5.3.3 Slope, intercept, and field enhancement factor values of the CNT samples

Sample 1A (one minute W sputtered under layer with CNT cathode contact point) has the biggest field enhancement factor. The other samples have a very close value of field enhancement factor to each other. The slope values are also very close for the Sample 1B, Sample 2A, and Sample 2B while the Sample 1A has a smaller slope than the others. Lastly, all samples have almost the same emitter areas as it can be seen from the intercept values of Table 5.3.3. Although more sample numbers are needed for more concrete conclusion, it could be reasonable to say from these results that W thin film under layer has a small to none effect on MWCNT field emission characteristics.

5.4 SEM Images of Samples

A collection of SEM images of CNT samples with different conditions, substrates, and thin film under layers are presented in this section.

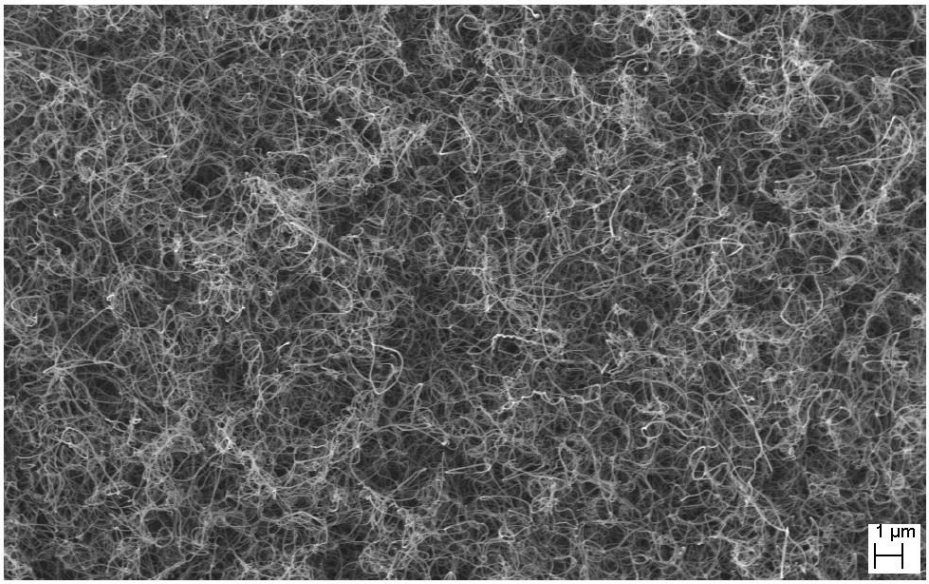

Fig. 5.32 MWCNTs grown of Fe catalyst sputtered for 5 minutes on Si substrate (x10k)

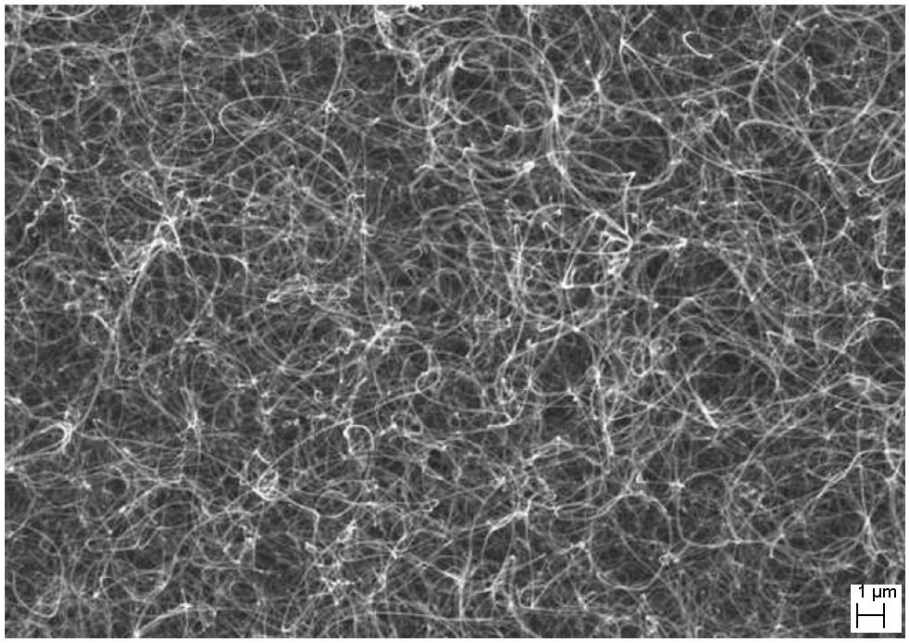

Fig. 5.33 MWCNTs grown of Fe catalyst sputtered for 1 minute on silicon substrate with SiO_2 coating (x10k)

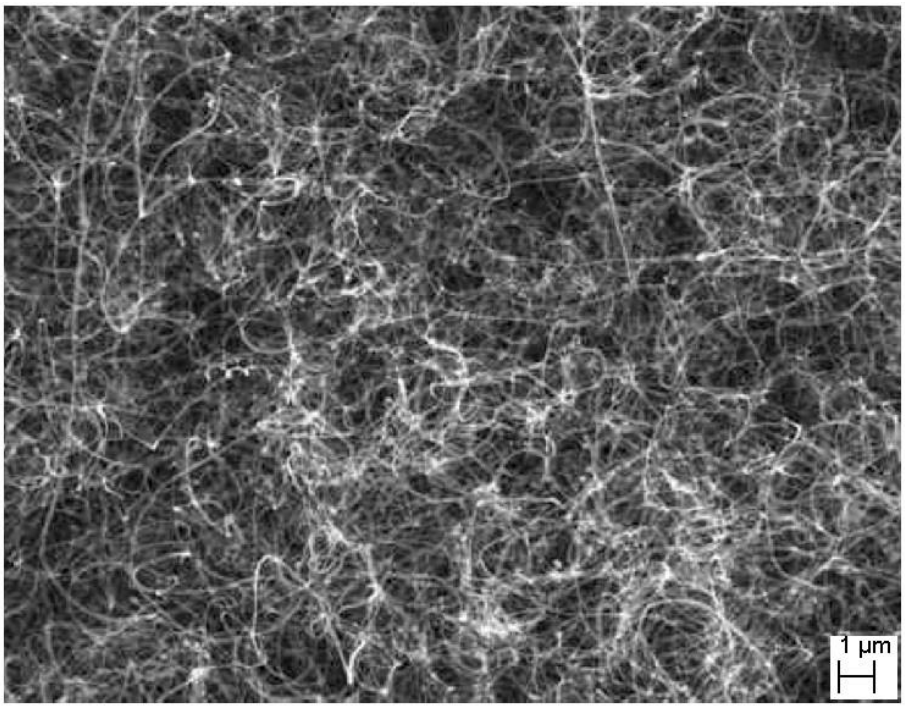

Fig. 5.34 MWCNTs grown of Fe catalyst sputtered for 5 minutes on silicon substrate with SiO_2 coating (x10k)

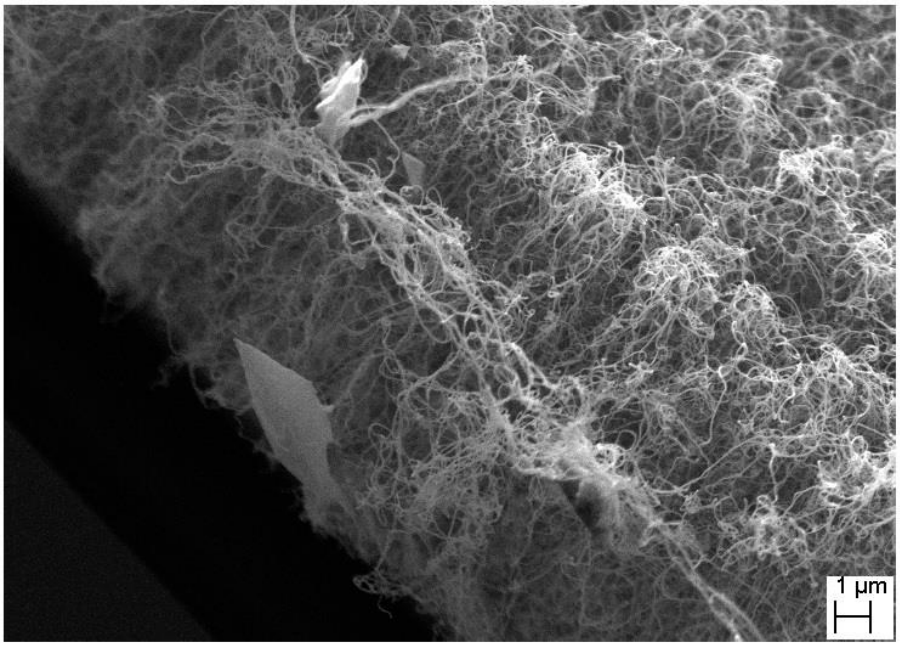

Fig. 5.35 Cross-sectional image of MWCNTs grown of C catalyst sputtered for 8 minutes on top of the Fe catalyst sputtered for 5 minutes Si substrate (x10k)

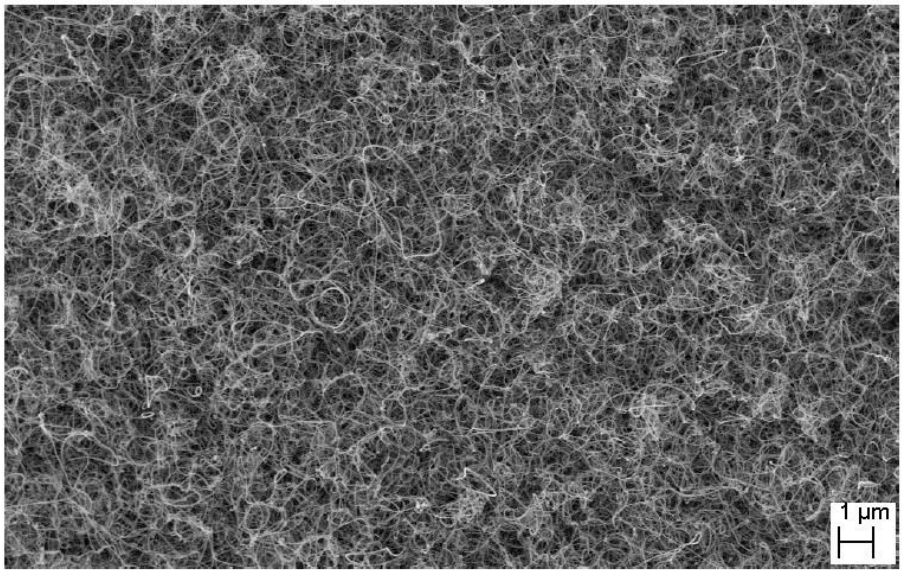

Fig. 5.36 MWCNTs grown of Ni catalyst sputtered for 5 minutes on top of the Fe catalyst sputtered for 5 minutes Si substrate w/ SiO_2 coating on it(x10k)

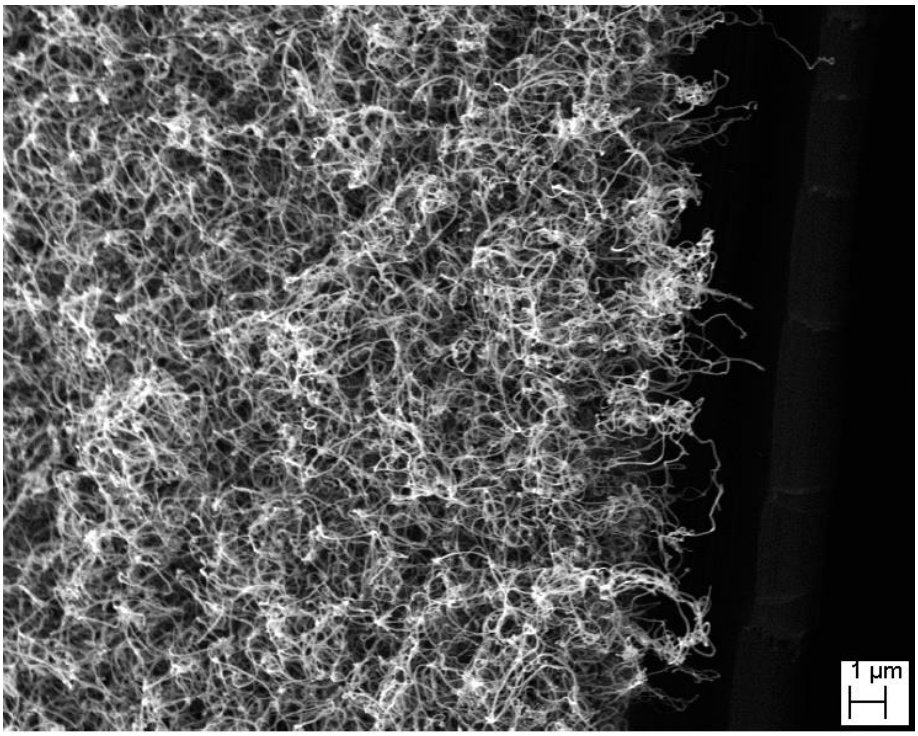

Fig. 5.37 Side image of MWCNTs grown of Fe catalyst sputtered for 5 minutes on 0.5 cm by 0. 5cm patterned Si substrate (x10k)

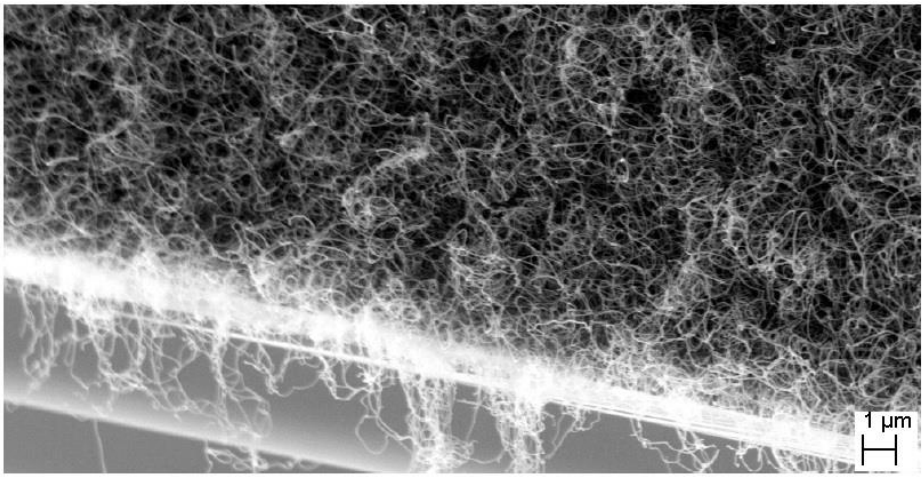

Fig. 5.38 Side image of MWCNTs grown of Fe catalyst sputtered for 5 minutes on 0.5 cm by 0. 5cm patterned Si substrate (x10k)

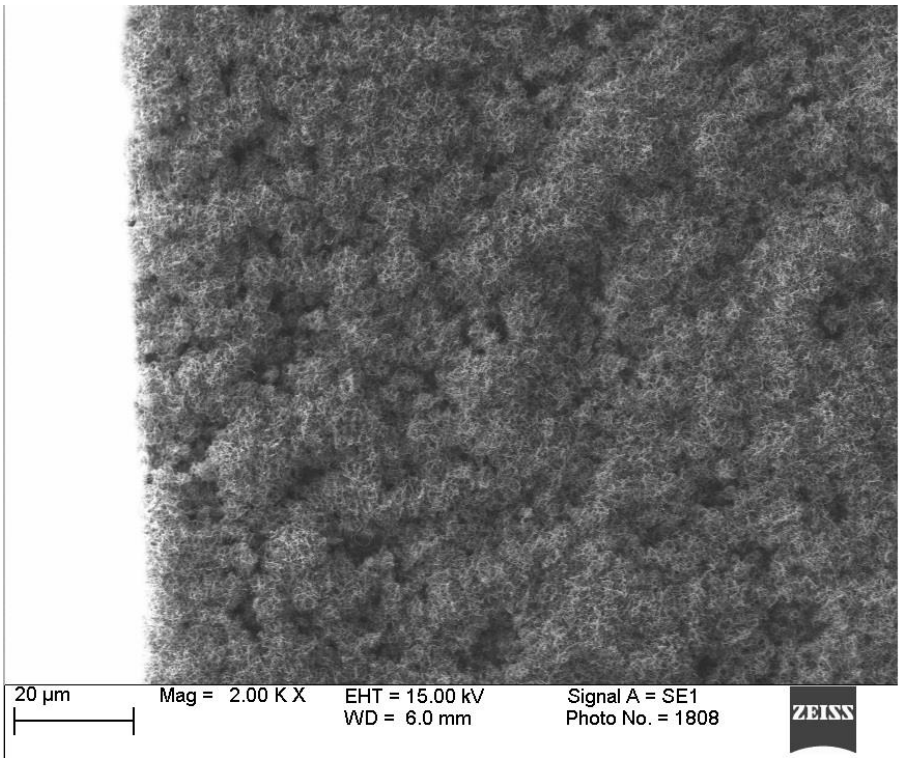

Fig. 5.39 Side image of MWCNTs grown of Fe catalyst sputtered for 5 minutes on 0.5 cm by 0. 5cm patterned ceramic substrate (x2k)

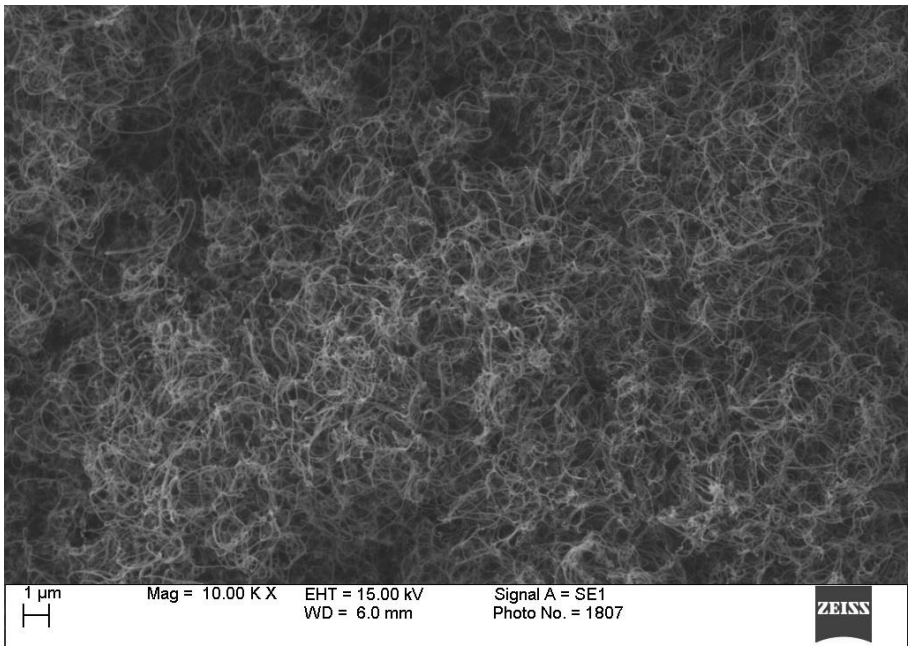

Fig. 5.40 MWCNTs grown of Fe catalyst sputtered for 5 minutes on ceramic substrate (x10k)

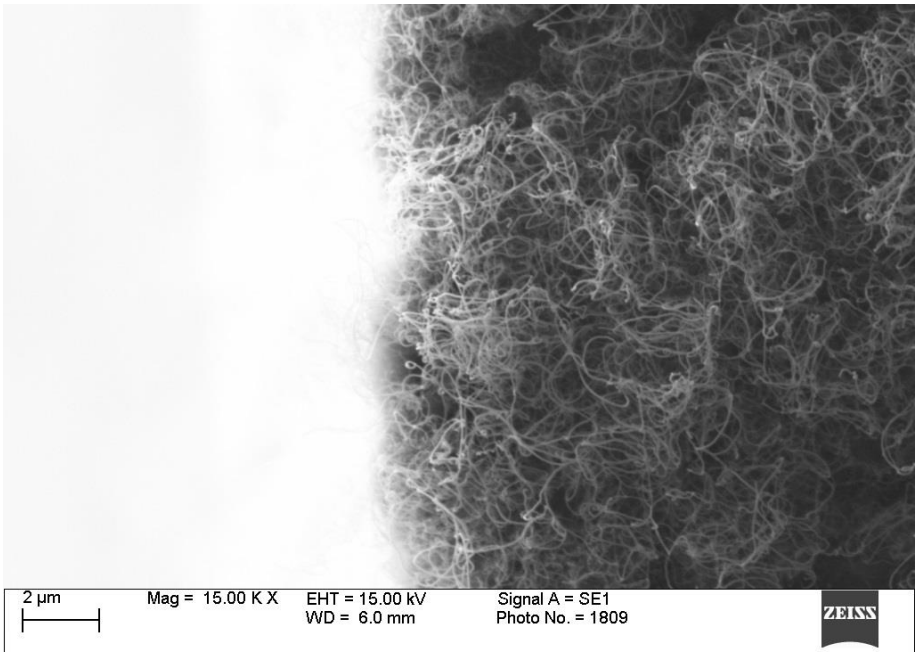

Fig. 5.41 Side image of MWCNTs grown of Fe catalyst sputtered for 5 minutes on 0.5 cm by 0. 5cm patterned ceramic substrate (x15k)

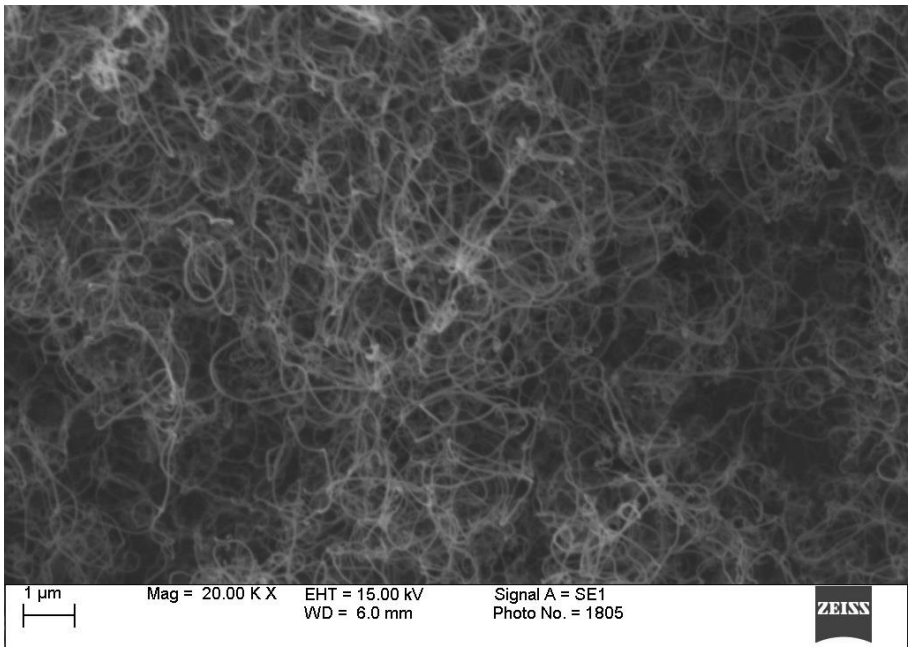

Fig. 5.42 MWCNTs grown of Fe catalyst sputtered for 5 minutes on ceramic substrate (x20k)

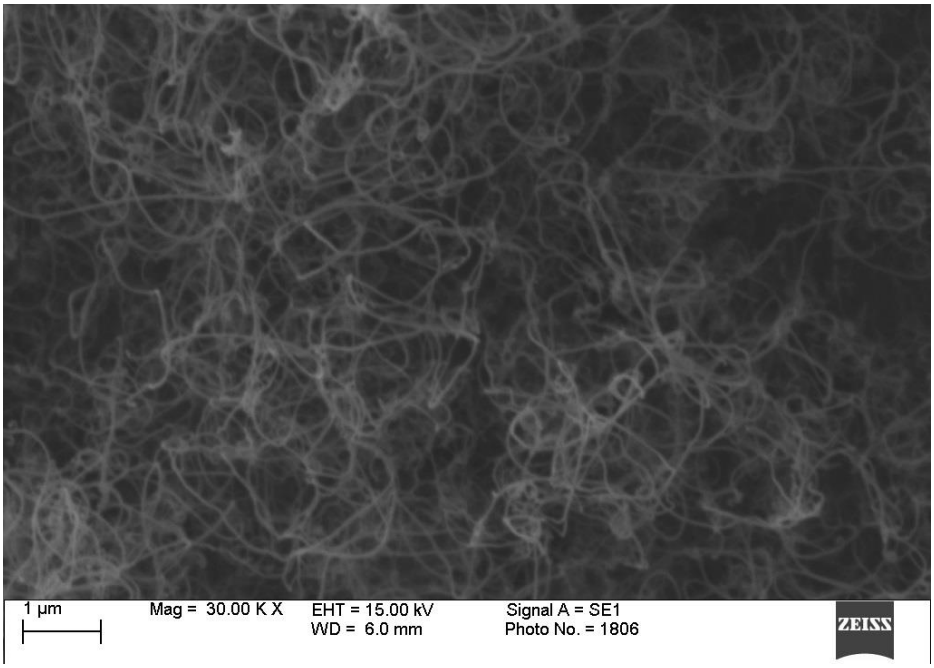

Fig. 5.43 MWCNTs grown of Fe catalyst sputtered for 5 minutes on ceramic substrate (x30k)

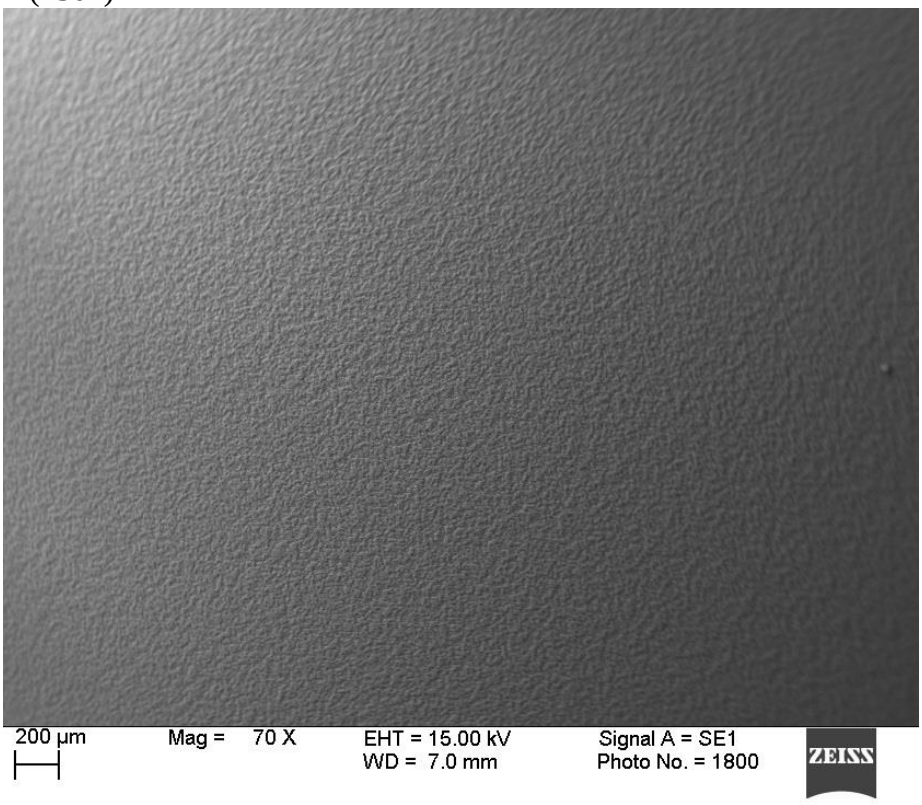

Fig. 5.44 MWCNTs grown of Fe catalyst sputtered for 5 minutes on ceramic substrate (x70)

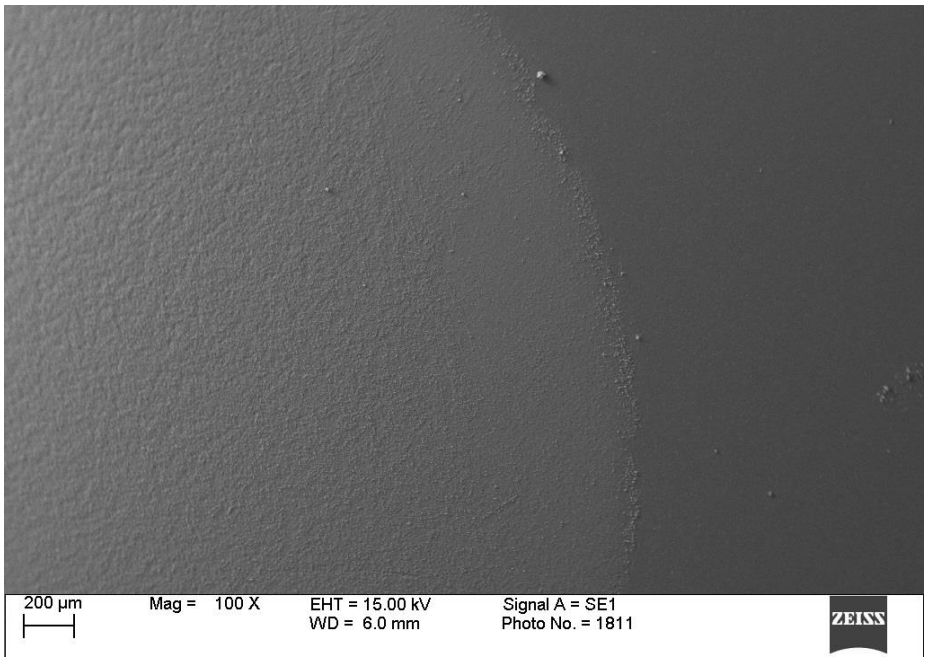

Fig. 5.45 Side image of MWCNTs grown of Fe catalyst sputtered for 5 minutes on circularly patterned ceramic substrate (x100)

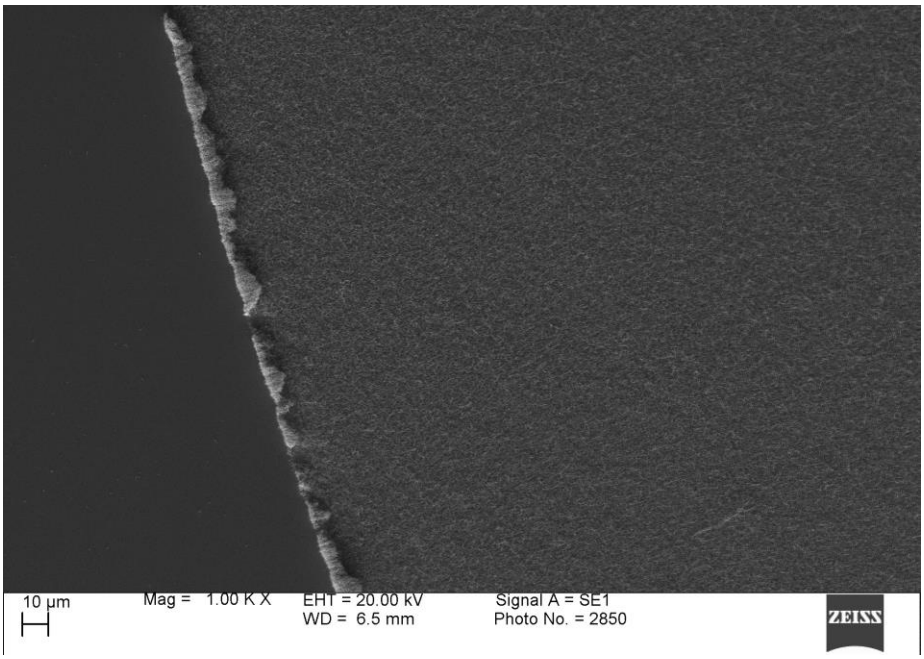

Fig. 5.46 Side image of MWCNTs grown of Fe catalyst sputtered for 5 minutes on 0.5 cm by 0. 5cm patterned on Si substrate after 900^{O}C bake (x1k)

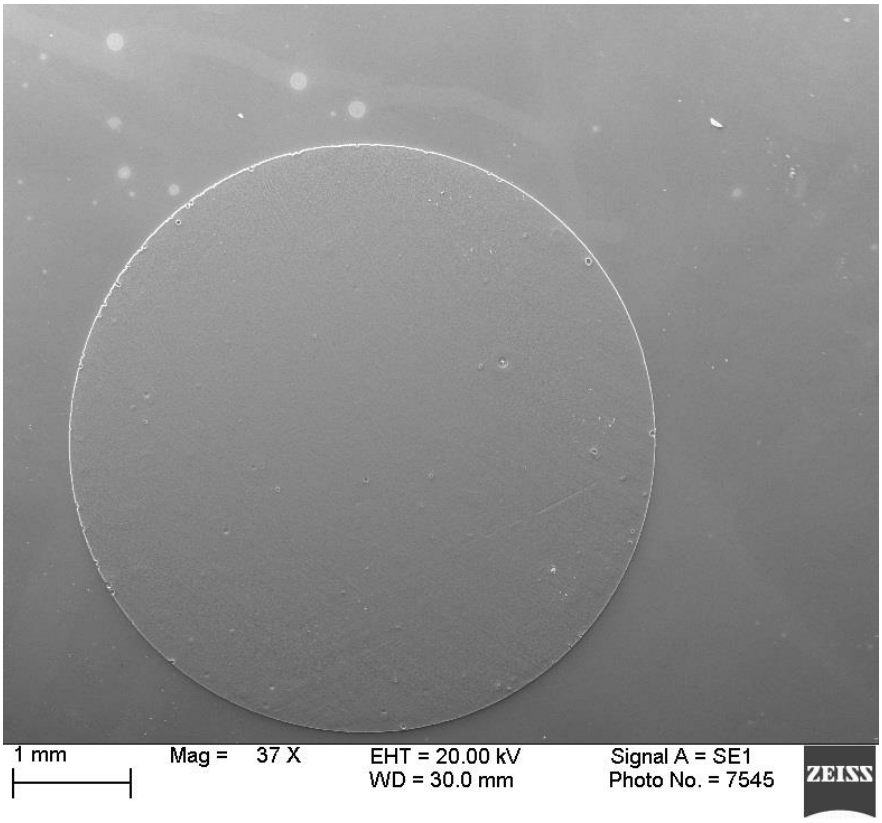

Fig. 5.47 Circularly patterned image of MWCNTs grown of Fe catalyst sputtered for 6 minutes on Si substrate after 8 hours annealing and 40 minutes CVD (x37)

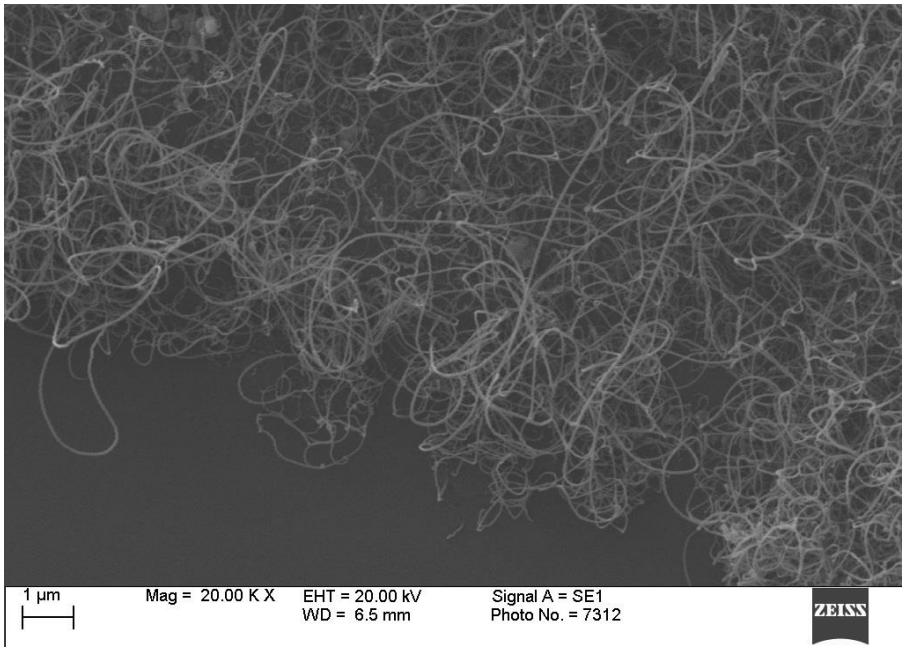

Fig. 5.48 Side image of MWCNTs grown of Fe catalyst sputtered for 5 minutes on Si substrate (x20k)

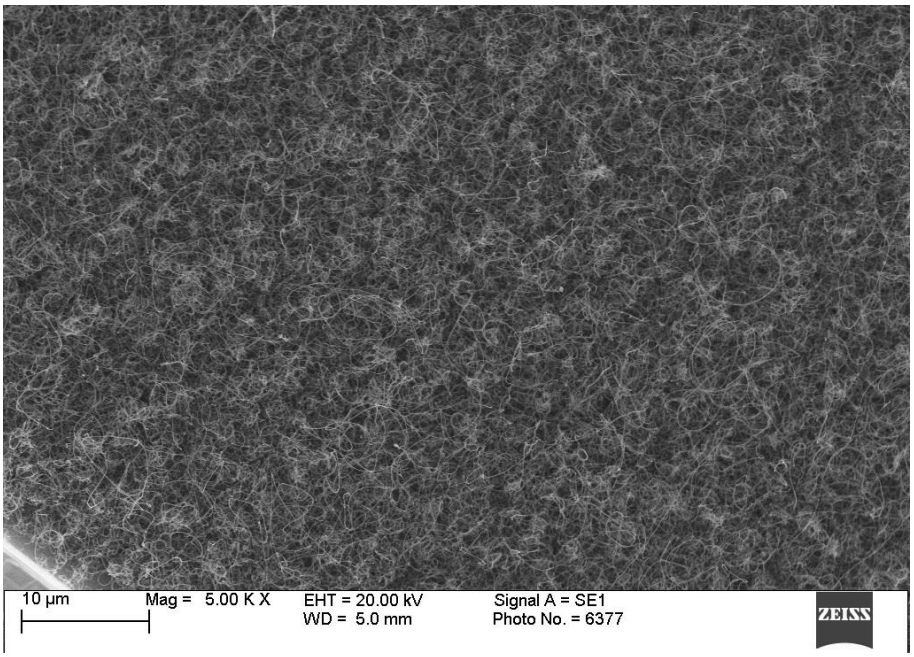

Fig. 5.49 MWCNTs grown of Fe catalyst sputtered for 8 minutes on Si substrate after 8 hours annealing (x5k)

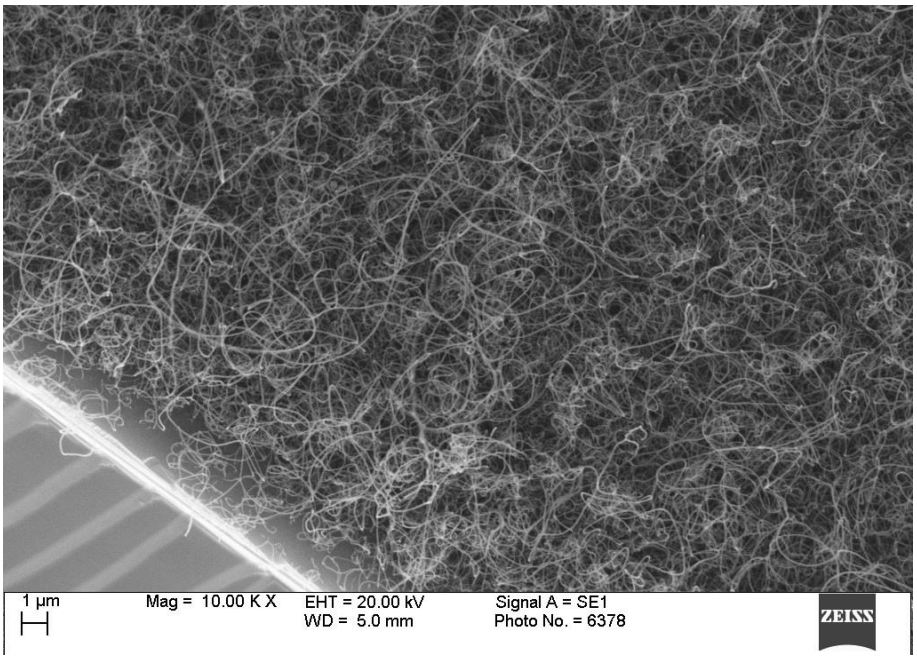

Fig. 5.50 MWCNTs grown of Fe catalyst sputtered for 8 minutes on Si substrate after 8 hours annealing (x10k)

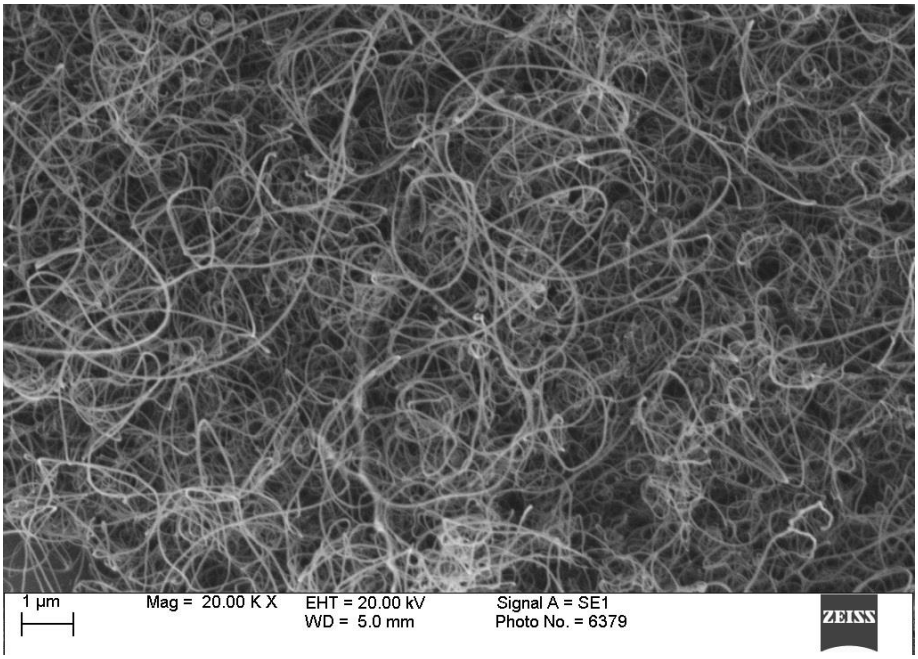

Fig. 5.51 MWCNTs grown of Fe catalyst sputtered for 8 minutes on Si substrate after 8 hours annealing (x20k)

REFERENCES

[1] Coorstek, "Advanced alumina semiconductor specific brochure", available at https://www.coorstek.com/media/2729/advanced-alumina-semiconductor-specific-brochure.pdf

[2] H. Zhao, "Design and construction of carbon nanotubes (CNTs) triggered pseudospark switch," Ph.D. dissertation, Dept. Elec. Eng., Auburn Univ., Auburn, AL, 2012.

[3] Y. M. Wong, W. P. Kang, J. L. Davidson, B. K. Choi, W. Hofmeister, and J. H. Huang, "Array geometry, size and spacing effects on field emission characteristics of aligned carbon nanotube," Diamond Relat. Mater., vol. 14, no. 11/12, pp. 2078–2083, Nov./Dec. 2005.

[4] K. B. K. Teo et al., "Field emission from dense, sparse, and patterned arrays of carbon nanofibers," Appl. Physics Lett., vol. 80, no. 11, pp. 2011-2013, 2002.

[5] O. Gröning, O. M. Küttel, Ch. Emmenegger, P. Gröning and L. Schlapbach, "Field emission properties of carbon nanotubes," J. of Vacuum Sci. & Technology B, vol. 18, pp. 665-678, 2000.

[6] E. J. Radauscher, "Design, Fabrication, and Characterization of Carbon Nanotube Field Emission Devices for Advanced Applications," Ph. D. dissertation, Dept. Elec. Eng., Duke Univ., Durham, NC, 2016.

[7] N. de Jonge and JM. Bonard, "Carbon nanotube electron sources and applications," Philosoph. Trans. of The Roy. Soc. A Math. Physical and Eng. Sci., vol 362, no. 1823, pp. 2239 – 2266, Nov. 2004.

[8] R. H. Fowler and L. W. Nordheim, "Electron emission in intense electric fields, "Proc. R. Soc. Lond. A, Math. Phys. Sci., vol. 119, no. 781, pp. 173– 181, May 1928.

[9] R. G. Forbes, "Physics of generalized Fowler-Nordheim-type equations," J. of Vacuum Sci. & Technology B: Microelectronics and Nanometer Structures, vol. 26, no. 2, pp. 788 – 793, 2008.

[10] X. Lu, Q. Yang, C. Xiao, and A. Hirose, "Nonlinear Fowler–Nordheim plots of the field electron emission from graphitic nanocones: Influence of non-uniform field enhancement factor," J. of Physics D: Appl. Physics, vol. 39, no. 15, pp. 3375–3379, Aug. 2006.

[11] R. Gao, Z. Pan and Z. L. Wang, " Work function at the tips of multiwalled carbon nanotubes," Appl. Physics Lett., vol. 78, pp. 1757-1759, 2001.

[12] P. Y. Chen, T. C. Cheng, J. H. Tsai, and Y. L. Shao, "Space charge effects in field emission nanodevices.," Nanotechnology, vol. 20, no. 40, p. 405202, Oct. 2009.

[13] J. Epstein, “Tungsten contacts on silicon substrates”, US Patent 3664874 A, Baltimore, MD, 1972.

[14] E. Lassner and W.D. Schubert, “Tungsten: Properties, chemistry, technology of the element, alloys, and chemical compounds”, Springer Science & Business Media, 2012.

[15] L.D. Locker and C.D. Capio, “Reaction kinetics of tungsten thin films on silicon (100) surfaces”, J. of Appl. Physics, vol. 44, no. 10, pp. 4366-4369, Oct. 1973.

Chapter 6

Conclusions and Future Work

6.1 Conclusions

We successfully fabricated randomly aligned multi-wall CNTs on ceramic substrates and characterized them using field emission tests, Fowler-Nordheim curves, AFM, SEM, and Raman spectroscopy. The results of this study show nanotubes on the ceramic substrates are very promising for the high temperature electronic device applications. They fill the gap of not having enough material varieties in high temperature electronics and are a strong alternative candidate to SiC (silicon carbide). In addition to our studies presented here, the ceramic substrates are being good electrical insulators, with the other studies in the literature that look into the substrate's specifications such as thermal expansion coefficient and strength [1], and the future work in lifetime aging/stress, and packaging technologies, CNTs on ceramic could take an important place in the industry for the aforementioned field.

Our research group has already demonstrated three applications, implementing MWCNTs that are fabricated in house. In the first application, the nanotubes are used as a cold cathode emitter of pseudospark switches. Pseudospark switch is a fast closing pulsed power switch with high hold-off voltage, low delay, and low jitter time [2]. Improved results with the CNT implementation achieved [3]. The switch triggered by the electrons emitted from CNTs that are accelerated in the electric field of the switch cavity and initiated plasma.

The other device is a CNT diode that consists a cathode formed by nanotubes [4] and acted as a radio frequency identification (RFID) tag [5]. We used an RF signal to initiate the field emission from the CNTs and then recorded the forward-bias current as the indication of the detected signal. The system includes passive elements such as a capacitor used as an RFID tag, a transmitting antenna and a receiving antenna that are both biconical shapes. It also consists a circuit with a pulse generator, the CNT diode, and a Pearson coil to measure the current that incorporates with the tag [4].

6.2 Future Work

It would be a great contribution to the literature to repeat our electrical characterization tests with different ceramic materials besides alumina (Al_2O_3) such as aluminum nitride (AlN) and silicon nitride (Si_3N_4) to investigate and see how the different ceramic substrates effect turn – on fields and emission current densities and if there is any correlations or patterns between those results. Furthermore, although our characterization results are very promising, larger number of samples would be useful to make firm conclusions towards how the field emission mechanism and field enhancement factor is affected with the different parameters such as different patterning, thin-film under layers, and substrate materials. It would also be interesting to see how high the elevated temperature field emission mechanism follows trend of decreasing turn-on voltage pattern beyond our $300^{O}C$. All these future works could contribute to the new application implementations of CNTs on ceramic substrates and put the promising properties of CNTs in use in multiple and broad range of high temperature electronic device applications at the technology market in the near future.

REFERENCES

[1] N. Chasserio, S. Guillemet-Fritsch, T. Lebey, S Dagdag, "Ceramic substrates for high-temperature electronic integration," J of Electronic Materials, vol. 38, no. 1, pp. 164-174, 2009. DOI: 10.1007/s11664-008-0571-8

[2] H. Zhao, "Design and construction of carbon nanotubes (CNTs) triggered pseudospark switch," Ph.D. dissertation, Dept. Elec. Eng., Auburn Univ., Auburn, AL, 2012.

[3] H. Zhao and H. Kirkici, "Carbon-Nanotube-Triggered Pseudospark Switch," IEEE Trans. Plasma Sci., vol. 40, no. 9, pp. 2225-2231, Sept. 2012.

[4] B. Yakupoglu and H. Kirkici, "Fabrication and operating characteristics of carbon nanotube diode," *2014 IEEE Int. Power Modulator and High Voltage Conf. (IPMHVC),* Santa Fe, NM, 2014, pp. 337-339.

[5] M. Jung, T. Baginski and H. Kirkici, "Test-bed of pulsed radio frequency (RF) signal used with a diode made of carbon nanotubes (CNTs)," *2014 IEEE Int. Power Modulator and High Voltage Conf. (IPMHVC),* Santa Fe, NM, 2014, pp. 599-602.